In Silico Screening and In Vitro Evaluation of GSK-3β Type I and II Inhibitors: Potential Treatment for Alzheimer's Disease?

by

Matthew Davies

A thesis submitted in partial fulfilment for the requirements for the degree of
MSc (by Research) at the University of Central Lancashire

April 2019

STUDENT DECLARATION FORM

Type of Award   **Master by research**

School   **School of Physical Sciences and Computing**

Concurrent registration for two or more academic awards

I declare that while registered as a candidate for the research degree, I have not been a registered candidate or enrolled student for another award of the University or other academic or professional institution

Material submitted for another award

I declare that no material contained in the thesis has been used in any other submission for an academic award and is solely my own work

Signature of Candidate _____

Print name: _____**Matthew Davies**_____

Abstract

Alzheimer's disease is a neurodegenerative disorder, and the most common form of dementia. The disease is becoming increasingly prevalent in our aging population, and as there are no effective methods of treating the condition, there is an increasing need for the development of new treatments. In this project, the *in silico* design, screening and *in vitro* validation of a selection of potential type I and type II inhibitors of GSK-3β as a possible pathway to a new treatment for Alzheimer's disease is presented. The screening of compounds for possible type I activity was carried out using a newly designed docking consensus scoring method, first employing a benchmarking database to assess various different combinations of docking algorithms to be used in a virtual screening of 157,238 compounds. The final consensus scoring method was a Simple Sum Rank combination of Glide-SP and –XP, AutoDock Vina and GOLD ASP, chosen based on its superior statistical metrics produced for EF (24), EF' (33) and BEDROC α=160.9 (0.345), all of which were higher than those of the individual programs. Pharmacophore models were applied to improve the overall accuracy of the results. Once the virtual screening had finished 10 diverse final compounds were selected fit for *in vitro* validation, based on a wide variety of different protein-ligand interactions. The best type I inhibitor compound **6** (ZINC000072152229) with an IC_{50} of 24.69 ± 0.73 µM. For the investigation of type II inhibition of GSK-3β, two different type II DFG-out models were developed for the virtual screening of a natural product database (27,286 Compounds). The first model was created using DOLPHIN docking, involving the deletion of 5 residues (201-205) to create the type II consistent binding site, and the second model was designed using a combination of Prime loop refinement, induced fit docking and molecular dynamics. Both models were validated using a selection of analogues of type II ligands with known experimental inhibition data. Both of the models produced experimentally consistent data, which indicated they were both accurate at predicting type II binding. Once the type II virtual screening was completed, the resultant ranks of the compounds for each model were combined into a simple sum consensus score, and 20 compounds were selected for biological validation. The three type II ligands that performed the best in the biological validation were Sorafenib (one of the known type II inhibitors) with an IC_{50} of 32.64 ± 0.76 µM, compound **2** (ZINC000008299930) with 26.96 ± 1.77 µM and compound **4** (ZINC000008297322) with 9.75 ± 2.2 µM, a promising result for the first ever screening of human GSK-3β for type II inhibition, validating such an approach in the future.

Acknowledgements

I would like to thank my project supervisor, Dr Joseph Hayes for his constant support. The completion of this project would not have been possible without his help and guidance, as well as the help of my other two supervisors Dr Jane Alder and Dr Phil Welsby.

In addition, without the work of the previous student who worked on this project, Raees Ahmed, this project would not have advanced as far as it has.

I would also like to thank Professor Ana Martinez, Paula and everyone else at the Consejo Superior de Investigaciones Ciencias for their help with the biological parts of my work on my Erasmus+ placement, and for giving me the opportunities for the amazing experiences I've had and the irreplaceable friends I've gained along the way.

Finally, I would like to thank everyone back home who supported me throughout my entire time at university, and everyone from the office, without whom this year would have been totally different.

List of Abbreviations

AD	Alzheimer's disease
PS AD	Presenile Alzheimer's disease
OD	Other dementia
CSF	Cerebrospinal fluid
DAT	Dementia of the Alzheimer's type
MID	Multi-infarct dementia
NIR	Near infra-red
NMDA	N-methyl-D-aspartic
GSK3-β	Glycogen Synthase Kinase-3 beta
CSIC	Consejo Superior de Investigaciones Cientificas
DOLPHIN	Deletion Of Loop PHe-gly-IN
Ph^+CML	Philadelphia-positive chronic myeloid leukaemia
FDA	Food and Drug Administration
MRS	Magnetic Resonance Spectroscopy
HBDs	Hydrogen Bond Donors
HBAs	Hydrogen Bond Acceptors
VdW	Van der Waals
QSAR	Quantitative Structure Activity Relationship
MD	Molecular Dynamics
SP	Standard Precision
XP	Extra Precision
DISE	Directed Sphere Exclusion
K_i	Inhibitory constant
ADME	Absorption, Distribution, Metabolism and Elimination
GUI	Graphical User Interface
EF	Enrichment Factor
EF'	Modified Enrichment Factor
ROC	Receiver Operator Characteristic
AU-ROC	Area Under the ROC Curve
BEDROC	Boltzmann-Enhanced Discrimination Receiver Operator Characteristic
CIB	Centro de Investigaciones Biologicas

Kinase-Glo   Luminescent Kinase Assay

RMSD   Root Mean Square Deviation

IFD   Induced Fit Docking

List of Figures

List of Tables

List of Equations

Contents

Chapter 1: Introduction

1.1 Introduction to Alzheimer's disease

Alzheimer's disease (AD) is the most common form of dementia, and is becoming increasingly prevalent due to advances in modern medicine allowing people to live much longer lives[1]. The noncommunicable disease begins in the hippocampus region of the brain, and then spreads to the rest of the organ over time[2]. This can manifest itself as the decline in thinking ability, motor skills, learning, memory and language skills in patients which is caused by the death of neurons, causing severe shrinkage to occur (shown in Figure 1.1).

Figure 1.1: A comparison of a healthy brain (left) and a brain afflicted with Alzheimer's disease (right) displaying severe shrinkage of multiple cortexes caused by the death of neurons. [3]

The disease was first observed by Alois Alzheimer in 1907, when he described the symptoms of a woman who had begun to develop anatomical characteristics that were inconsistent with recognised illnesses[4]. This coupled with a rapid loss of memory, and the other unusual symptoms the patient displayed, caused Alzheimer to describe the disease as a special illness[4]. The patient that Alzheimer had examined had a progressive form of presenile dementia[4], which would later become known as Alzheimer's disease. AD has two main pathological features that can cause the death of neurons, the formation of amyloid plaques, and neurofibrillary tangles[1]. Amyloid plaques, also known as senile plaques, are formed by the peptide amyloid beta (Figure 1.2 (a)) when it appears in the outside of neurons in dense fibrils[1]. This protein is a by-product of the amyloid precursor protein (APP), which is believed to be involved in neuronal development. The other main pathogenic feature of the disease that can cause the death of neurons is the formation of neurofibrillary tangles. These tangles are aggregated masses of hyperphosphorylated tau protein (Figure 1.2(b)) that accumulate as paired helical filaments, and can be expressed in neurons in patients of AD[1]. Tau protein acts in the body to stabilize the microtubules in the cytoskeleton of cells[1] and is

normally regulated by phosphorylation. However, when this process begins to fail, hyperphosphorylation starts to occur, beginning the formation of the tangles.
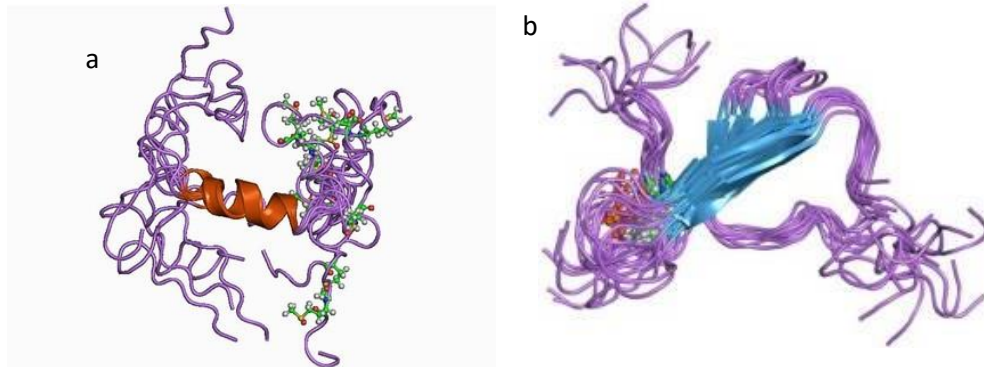
Figure 1.1: The structures of the two proteins amyloid beta(a) [5] and tau protein(b) [6]

There is an observed positive correlation between the amount of neurofibrillary tangles that are present in the brain and the severity of the dementia caused by AD, which is shown in Table 1.1 below[7].

Table 1.1: The levels of Hyperphosphorylated tau in patients of senile AD (S AD), presenile AD (PS AD) and other dementias (OD). A positive correlation between the amount of hyperphosphorylated tau protein and the severity of the dementia can be seen. [8]

Levels of CSF phosphotau (pg/ml)	
S AD	49.78(±36.09)
SP AD	44.06(±33.29)
OD	15.01(±27.05)

During Alois Alzheimer's initial investigation of the brain of the patient in 1907, he observed the presence of these two pathological features. In his paper he described tangles of fibrils that outlast the neuron itself, as well as small military foci caused by "the deposition of a special substance in the cortex"[4], which are the neurofibrillary tangles and the amyloid plaques respectively.

1.2 Symptoms and Diagnosis of Alzheimer's Disease

It is well established that subtle cognitive impairment can be displayed in patients years before the clinical diagnosis of probable AD[9]. This period, in-between the initial onset of the disease and the clinical diagnosis, where the patients begin show these early signs, is named the "preclinical phase" [10]. The first suggested sign of AD in clinical literature is memory loss for the majority of patients of the disease[11]. Disorientation also appears as an early sign of AD, due in part to its relation to the memory loss[11]. Due to the subtlety of these symptoms in the early stages, it can be difficult to detect the initial effects. In a

study by La Rue et al. [11], they investigated the ease at which different family members who accompanied patients to a dementia clinic for a diagnostic evaluation were able to detect and notice certain symptoms of the disease in its early stages. The figure below (Figure 1.3) shows the symptoms that the family members first recognised for patients with dementia of the Alzheimer type (DAT) compared with patients of Multi-Infarct dementia (MID) and Depression.

FIRST SYMPTOMS OF DEMENTIA
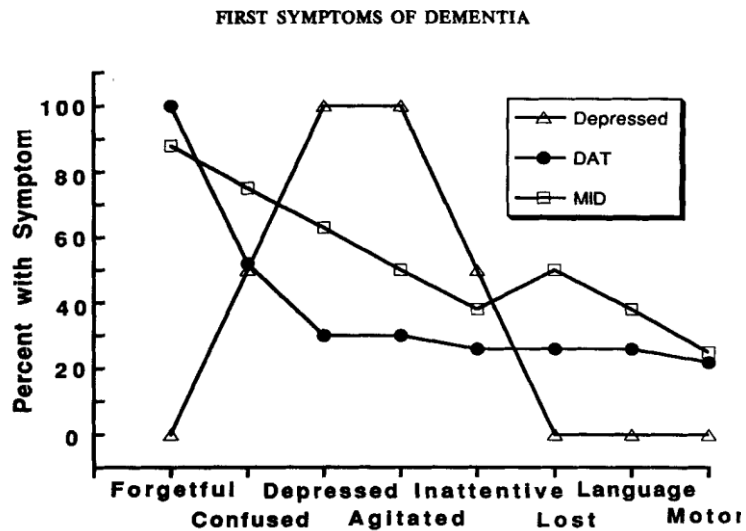
Figure 1.3: The first symptoms reported by family members for patients of each of the three categories, Depression, DAT and MID[11].

As can be seen in Figure 1.3, for DAT, forgetfulness was by far the most common first symptom noticed by the family members, with it being spotted in almost 100% of cases. The next most common was confusion, spotted in around 50% of cases, and then the rest of the symptoms are all clustered around 30%. For MID on the other hand, all other symptoms except memory loss were consistently more noticed by family members than for AD, however the forgetfulness was observed by just below 90%[11]. In general, available literature suggests that the preclinical phase of probable AD can be longer than a couple of years[10]. However, because of prohibitive high costs and low yield of prospective studies of AD, very few large-scale studies focus on the preclinical phase[10]. As a result, the length of the preclinical phase of probable AD, and the signs of onset present have not been firmly established[12]. In a paper by McKhann, G et al. [13] they outline the symptoms necessary for the diagnosis of Probable, Possible and Definite AD. For Probable AD, the patient needs to display deficits in two or more areas of their cognition, progressive worsening of their memory functions and an absence of symptoms of other brain disorders that could cause the cognitive loss of functions[13]. These diagnoses can also be supported by looking for symptoms such as progressive deterioration of specific cognitive functions, for example language, perception and motor skills. They also could display an impairment of their ability to carry out daily activities,

and that their patterns of behaviour have altered[13]. For a diagnosis of definite AD, along with the symptoms necessary for probable AD, histopathologic evidence obtained from a biopsy is of course also needed[13]. More recently, Paraskevaidi el al [14] recently applied NIR (near infra-red) spectroscopy to the detection of the various blood biomarkers of AD, and found that their model could differentiate between healthy patients and those with AD with an accuracy of 92.8%.

Prevalence

According to recent figures from the world health organisation, more than 50 million people currently are affected by dementia, including AD [15]. Data obtained from population based studies suggests that the prevalence of AD in Europe in people over the age of 65 is 4.4%, whereas in the US in over 70s the prevalence is 9.7%[16]. The graph below in Figure 1.4, shows the prevalence of AD increases rapidly as the age of the patient increases, suggesting that as the population ages, the disease will begin to rapidly gain prevalence. It also suggests that people in different areas, for example Brazil, can be more likely to have AD at an earlier age. This could be due to multiple possible reasons, one example being quality of healthcare.
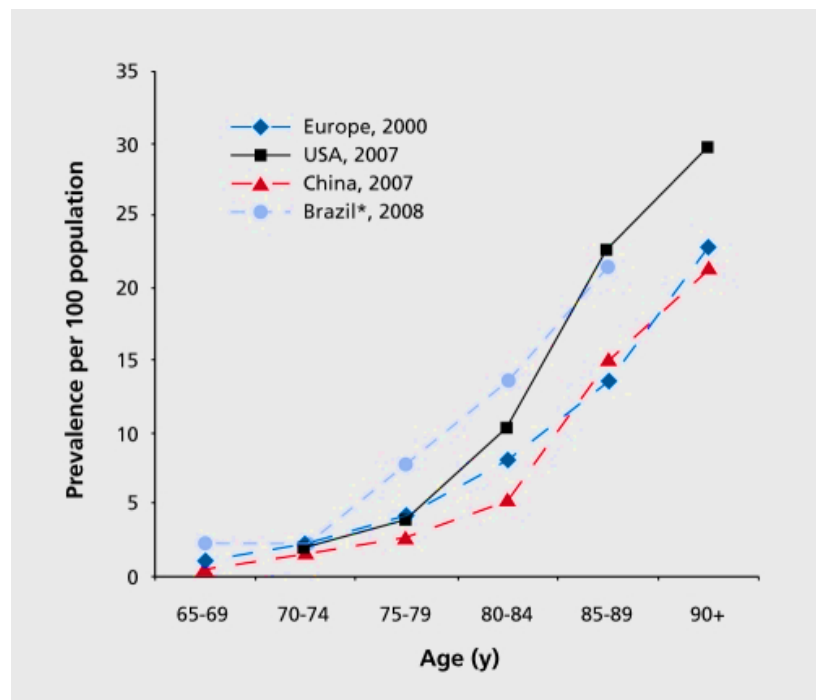
Figure 1.4: shows the prevalence of Alzheimer's disease per 100 people across various countries and continents[16].

1.3 Previous and Current Treatments of the Disease

There have been a few different drugs approved for treating AD throughout the years. However, for the most part they are used to alleviate the symptoms of the disease, to slow it's progression in patients, and to try to improve their quality of life. Three common types of treatments currently in use, or currently being investigated for combatting AD are acetylcholinesterase inhibitors[17], N-Methyl-D-aspartic acid (NMDA) receptor antagonists[17] and more recently GSK3-β inhibitors[18]. Neurons in AD have been found to express excessive amounts of the neurotransmitter glutamate, which can damage the already afflicted neurons further. Therefore prevention of this upregulated action of glutamate could serve to slow the progression of the disease that is caused by this additional damage[19]. To do this, some of the more frequently prescribed treatments for AD, NMDA receptor antagonists, are used to block the receptors that the glutamate interacts with. This returns the levels of the neurotransmitter the neuron receives back to normal, protects from damage. The National Institute of Health and Care Excellence recommends that these treatments are given to patients with moderate to severe symptoms, to alleviate the symptoms associated with the later stages of the disease. Danysz et al. [20] found that *in vivo* memantine (shown below in Figure 1.5), a NMDA receptor antagonist, provided protection from a variety of neuronal toxic conditions, for example the formation of amyloid plaques, inhibition of the mitochondrial function of neuronal cell, and inflammation. They then stated that as all three of these factors are implicated as pathological features of AD, a drug that can reduce all three should be effective as a therapeutic treatment for the disease[20].
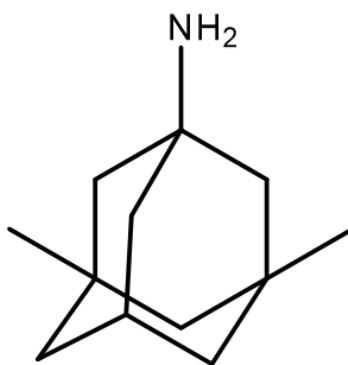
Figure 1.5: The structure of memantine

The second type of treatment that is used more commonly is acetylcholinesterase inhibitors. Through various investigations, it was found that patients of AD have lower levels of acetylcholine, a neurotransmitter involved in learning and the encoding of new memories[21]. Lower levels of this neurotransmitter has also been linked to the formation of amyloid plaques[20] and increases their density, which would cause an increase in the progression of neurone death[17]. Therefore, the inhibition of acetylcholinesterase would

serve to protect the neurotransmitter from the enzyme, preventing its breakdown and therefore raising its levels in the brains of patients. Some examples of different drug treatments currently employed that are acetylcholinesterase inhibitors are donepezil (Figure 1.6(a)) [22], rivastigmine(Figure 1.6(b)) [23] and galantamine (Figure 1.6(c)) [24]. These treatments act to return the levels of the neurotransmitter in the brain to normal, restoring the functionality of the neuronal communication, alleviating some of the milder symptoms[19].
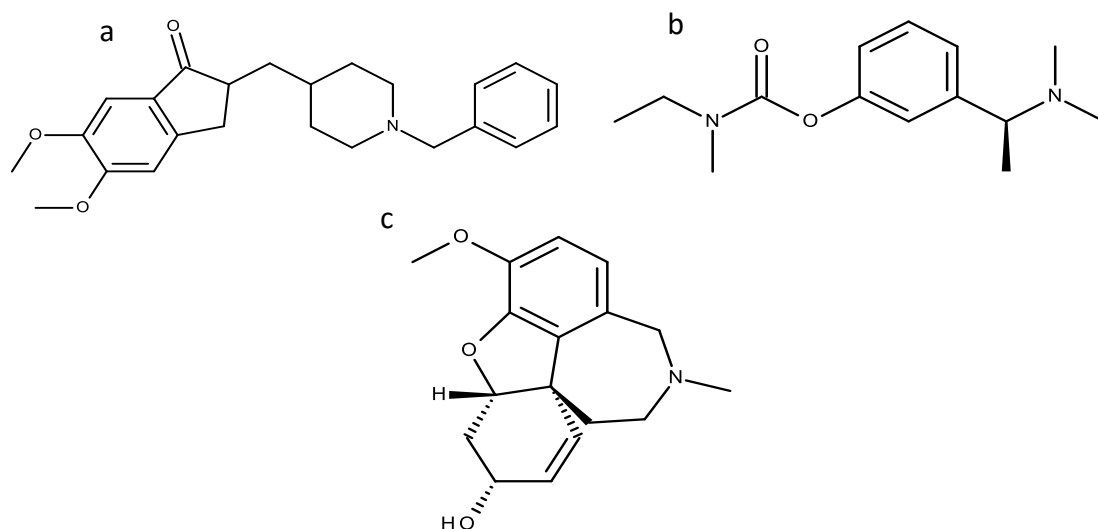
Figure 1.6: The structures of donepezil (a), rivastigmine (b) and galantamine (c)

Rogers et al. [22] reported the results of a 15 week, double blind study of the efficacy and safety of donepezil in patients with moderate to severe AD. Out of 468 patients, split into three groups (placebo, 5 mg/d and 10 mg/d), 56 patients withdrew with adverse effects being the most common reason, while the rest finished the trials. They found that patients that had received the drug demonstrated improvements in cognitive function superior to that of the patients that received the placebo [22]. The clinical improvement of the patients in the study are shown below in Figure 1.7.
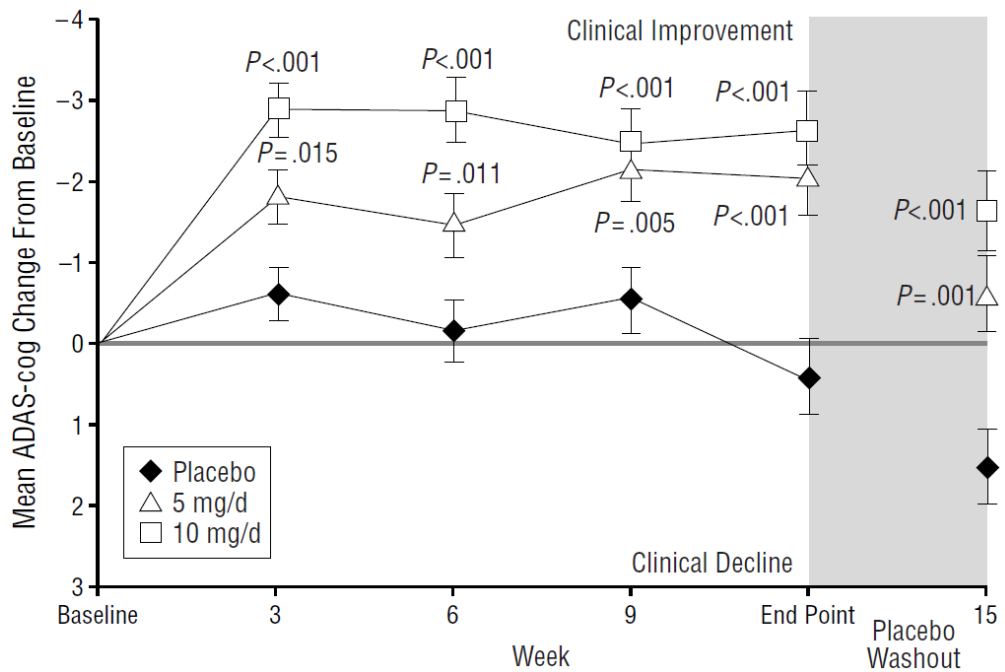
Figure 1.7: The least squares mean clinical improvement for cognition each of the 3 groups of patients with moderate to severe Alzheimer's disease experienced over a 15 week period[22].

Rosler et al. [23] investigated the acetylcholinesterase inhibitor rivastigmine by testing it in an international trial. Similar to the previously mentioned trial of donepezil, the patients were separated into three groups (placebo, low dose and high dose). The researchers found that by week 26, the difference in mean change in cognitive ability from the baseline based on scores on the progressive deterioration scale between the patients who took the placebo and those on the higher dose of rivastigmine was statistically significant (Figure 1.8). The authors conclude that the study provided evidence that Rivastigmine was alleviating the cognitive depreciation associated with moderate to severe AD, and that the effects were directly dose dependant[23].
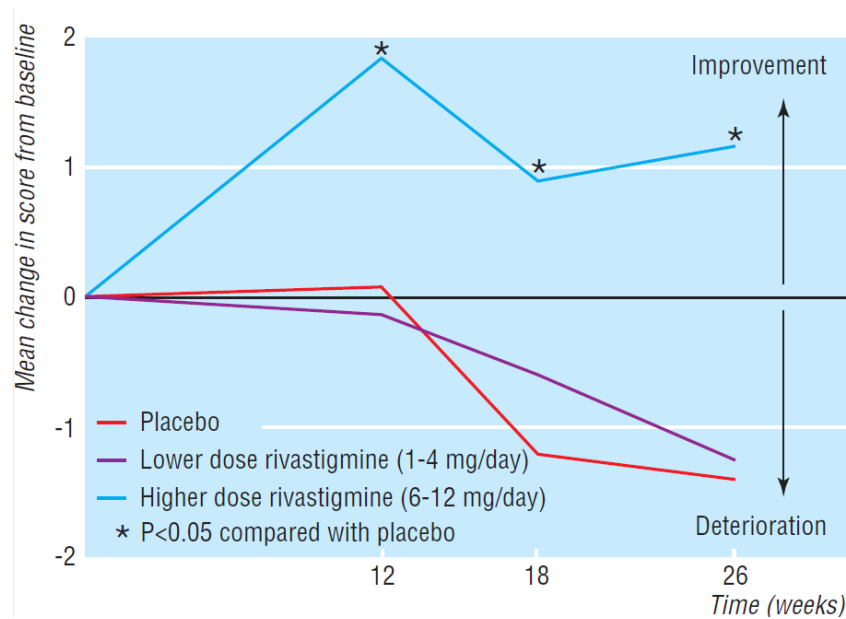
Figure 1.8: The mean change in baseline scores on the cognitive subscale of Alzheimer's disease assessment scale[23].

Raskind et al. [24] examined the effects of galantamine in a 6-month double-blind trial with patients split into three groups, one with a high dose one with a lower dose and a placebo control. This was followed by a 6-month Open label extension where all three groups were given the same 24 mg dose, The results of which are shown in Figure 1.9 below[24].
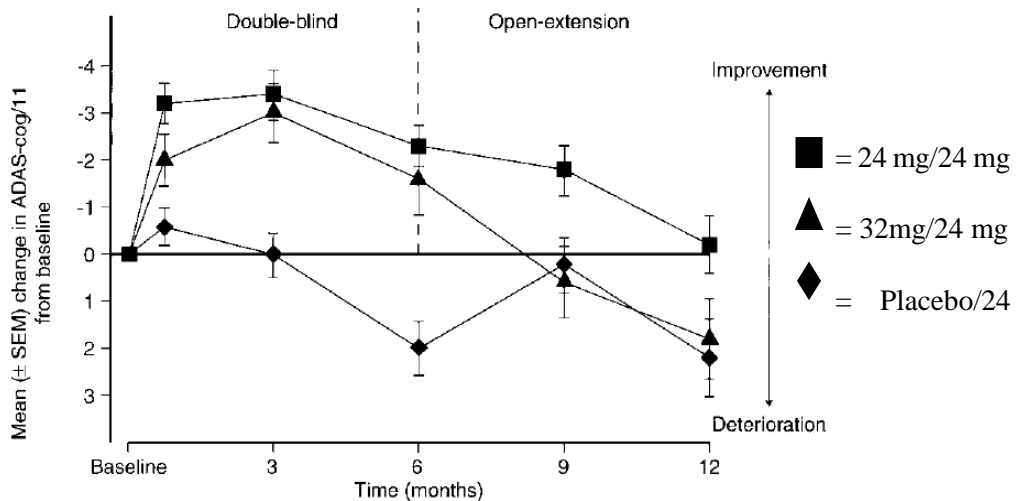
Figure 1.9: The mean change from the baseline assessment cognitive subscale scores over the first and second 6-month periods[24].

As can be seen from the graph above, while there is not much difference between the results of the two different doses of galantamine, they both show a large increase in cognitive function when compared to the placebo. It can also be observed that when the placebo group was given its dose at the start of the open-extension period their cognitive function improved noticeably. This led the authors to conclude that their study had

provided evidence that Galantamine helped alleviate some of the symptoms of moderate AD in patients[24].

Other treatments for this disease include the use of different drugs to combat symptoms, for example cerebrolsyn. This drug is a combination of different amino acids and small peptides, enzymatically cleaved from purified brain proteins[19]. They act by protecting the plasticity of the neurons[25] and protect and support the neurons during stressful conditions[26] to slightly improve the mental ability of patients. However, any methods the drug uses to exact its therapeutic effects are currently unknown. Some possible mechanisms that have been proposed by academic studies and research are interactions with the aforementioned amyloid peptides[27], neuroprotective proteins such as GSK-3β (glycogen synthase kinase-3) [28], and neurotransmitter receptors[29].

1.4 GSK3-β as a target for AD

While these drugs are being used widely to treat AD, there is a clear need for more effective forms of treatment. One such new possible treatment, and the target of this project, is the use of inhibitors for the enzyme Glycogen Synthase Kinase-3 beta (GSK-3β). The enzyme GSK-3β has been found to be a key component in many bodily processes and regulation pathways, some examples of this are cell cycle progression gene transcription and the insulin signalling cascade [30]. In a paper published in 2007 called 'The GSK-3 Hypothesis of Alzheimer's Disease'[18], the enzyme was linked to the pathways of formation of both the amyloid plaques and the neurofibrillary tangles[31]. It has also been found that in patients of AD, the enzyme is overexpressed, which is the hypothesised cause of the increased β-amyloid production and the hyperphosphorylation of the tau protein. It is also associated with local plaque associated microglial-mediated inflammatory responses, for example the production of neurotoxic cytokines[32], another typical symptom found in disease sufferers, and can lead to the death of neurones.

1.5 Objectives

1) To investigate and design novel type I (ATP binding site) and type II (activation loop out) inhibitors of GSK-3β.

2) To apply a consensus scoring method involving a virtual screening with 4 different programs, GOLD, Glide-SP, Glide-XP and AutoDock to a large database taken from the ZINC docking database website (www.ZINC15.org) [33].

3) To design two novel type II structures of GSK-3β, using different computational methods, molecular dynamics and DOLPHIN docking[34], and to use them to screen a database *in silico*. The results for these two models are to be combined using a consensus scoring method.

4) To select the top compounds from both the type I and type II screenings for transportation to the CSIC in Madrid on an Erasmus+ placement where they will have their IC$_{50}$ values tested *in vitro*

1.6 Synopsis

While chapter 1 mainly focused on background information about AD, current treatments, and the GSK-3β enzyme as a potential target, Chapter 2 of this thesis discusses GSK-3β in detail, focusing on the enzyme's known structural features. It describes in detail both of the different types of inhibition used in this project, Type I and Type II. Current inhibitors of the ATP binding site of GSK-3β are discussed also. The last section of Chapter 2 contains a discussion about inhibitors of Type I GSK-3β that have reached clinical trials;

Chapter 3 presents and describes the theoretical basis behind any computational programs and techniques used in this project, beginning with an initial overview of molecular modelling. This is followed by a detailed explanation of molecular docking, along with a description of any docking programs used and a subsequent description of Molecular Dynamics

Chapter 4 presents the results of this project for Type I inhibition. It begins with a short introduction of the topic and the work that I have done with Type I inhibitors. This is followed by a detailed explanation of the methodology used including the consensus method designed, and the biological experiments carried out at the CSIC. The results of each step are then reported and discussed in depth, followed by a conclusion.

Chapter 5 contains all of the work involving the design of Type II inhibitors and begins with a short introduction of the topic. This is followed by a detailed explanation of the methodology used in the design of the two different Type II models, the selection of ZINC database compounds, the *in silico* screening and biological validation experiments performed. The results of each step are then reported and discussed in depth, followed by a conclusion.

Chapter 6 presents the overall conclusion of the entire project as a whole, as well as an analysis of the progression of the project and any suggested future work that could be built around this research.

Chapter 2: Glycogen Synthase Kinase-3 beta

2.1 Introduction

The first reversible inhibitor of GSK-3β discovered was lithium in 1993, by Melton and Klein[35]. It was found to act in two different ways, direct inhibition of the enzyme and via increasing the inhibitory phosphorylation of the enzyme[31]. When administered, lithium was found to reduce the production of both hyperphosphorylated tau[36] and the primary component of amyloid plaques, β-amyloid[37]. Additionally, in a recent trial held in Japan, it was found to improve the cognitive function of the participants[38]. Unfortunately, lithium was found to inhibit many other kinases besides GSK-3β, causing it to have a high neurotoxicity due to it affecting the levels of many different neurotransmitters. Accordingly, the search for many different, potent and specific inhibitors of GSK-3β has continued, and has gained an unsurprisingly large amount of interest[30]. As upwards of 20 to 30 different crystal structures have been solved for GSK-3β, more and more structure based drug design techniques including virtual screening, molecular dynamics, and many others being increasingly employed in the search for new inhibitors that are more selective than lithium.

2.2 Structural features of GSK-3β

Like all other proteins, the structures of enzymes are incredibly important in relation to the functions that they carry out, and also how they interact with other molecules in the body. Therefore, knowledge about the structures of these enzymes is crucial for the study and design of potential inhibitors. GSK-3, a multifunctional Ser/Thr kinase, has many different roles in the human body and various diseases, including AD [39]. Currently, there are only two known members of the mammalian GSK-3 family, GSK-3α and GSK-3β. In this project, we will focus on the β form. The structure of GSK-3β consists of a coupled pair of domains, a carboxy-terminal α-helical domain and an amino-terminal β-sheet domain, which is shown below in Figure 2.1[40].
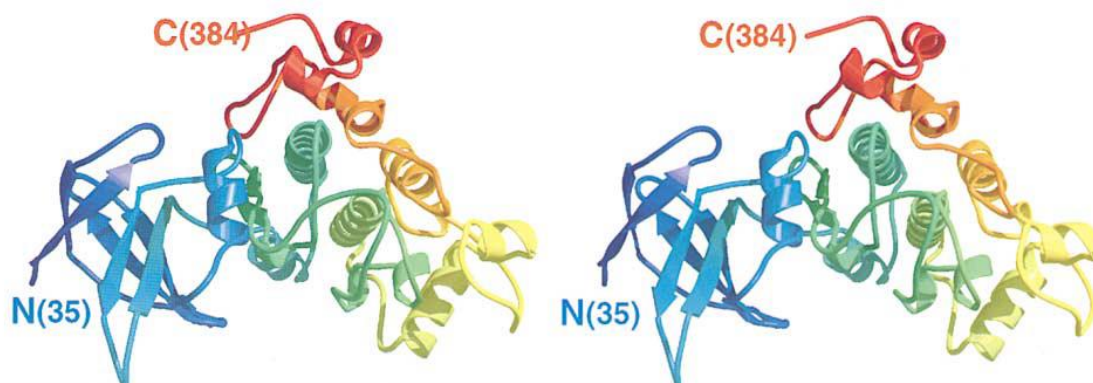
Figure 2.1: GSK-3β, the amino-terminal end of the enzyme (residue 35) is shown in blue and the carboxy-terminal end (residue 384) is shown in red [40].

GSK-3β has a molecular weight of 47 kDa is made up of 420 amino acid residues, however only 351 (35 to 386) have shown any clear electron density when studied[40]. Unusually, unlike most other similar kinases, the visible N terminal-β-sheet domain end of GSK-3β (residues 35-134) consists of a closed orthogonal β barrel formed from a seven-stranded β-sheet. Moreover, between residues 4 and 104, the 5th and 6th strands of the β-sheet are connected by a small α-helix, which is shorter than that of other kinases, with only 2 turns. After the N terminal section, the residues between 138 and 149 form an α helix connecting the N terminal section to the rest of the molecule. Residues 152 to to 342, form the main section of the α-helical domain, similar to that of some MAP (mitogen activated protein) kinases[41]. One major difference however, is the absence of a second α-helical domain located between residues 276 and 293[42]. The next noteworthy structural feature appears between residues 342 and 386 in the form of a series of short loops and helices, pressed against the long helix located between residues 155 and 175. This feature, unlike the α-helical domain, is atypical compared to most other MAP kinases, as this region would normally snake back and re-join the N terminal end of the enzyme[40]. The other end of the protein, the C terminal, begins at residue 384. GSK-3β has a pair of phosphorylation sites, the first being residue Ser9, the phosphorylation site for AKT (another Ser/Thr kinase) and the second being residue Tyr216, which increases the catalytic activity of the enzyme[43]. It also has an Axin binding channel (Axin being a protein with importance in the Wnt signalling pathway), located between residues 262 and 273, that is formed by an α-helix[44].

2.3 ATP binding site

GSK-3β, like all other kinases, uses ATP molecules to phosphorylate substrate molecules, and to activate the kinase activity that takes place in its active site. Therefore, the ATP binding site is located in the cleft between the N-terminal domain and the C-terminal domain, inside the "activation segment" of the active site of the enzyme [45]. When this Tyr216 is phosphorylated, it creates a conformation of the activation segment that correctly forms and aligns the catalytic and substrate binding sites, largely increasing enzymatic activity[45]. When ATP enters the binding site, the enzyme removes one of its phosphate groups and transfers it to either a threonine or serine residue of the enzyme's various substrates[46]. Another important region of the ATP binding site is the hinge region. This region, containing the residues Asp133, Tyr134 and Val135 is very important for the binding of inhibitor molecules to the ATP binding site[45][47][42]. The ATP binding site also contains the activation loop, or DFG loop (Asp200-Phe201-Gly202). This loop can have two formations, the DFG-in active conformation where the phenyl sidechain of

the phenylalanine residue is positioned on the inside of the loop, and the DFG-out inactive conformation, where the phenyl group is flipped outside the loop[48].

Inhibition of the ATP binding site of a kinase with the activation loop in the DFG–in conformation is known as Type I inhibition[48]. This is the most commonly explored type of inhibition for most kinases, including GSK-3 β, due to the fact that it mostly acts by substrate phosphorylation from the ATP binding site. The first groups of molecules with already known inhibitory activity against other kinases to be tested against GSK-3β were the paullones, indirubines and bisindol-malemides[31][49]. All of these compounds were shown to be competitive with ATP for its binding site. Some well-known and studied type I inhibitors are shown in Figure 2.2, along with their inhibition data.
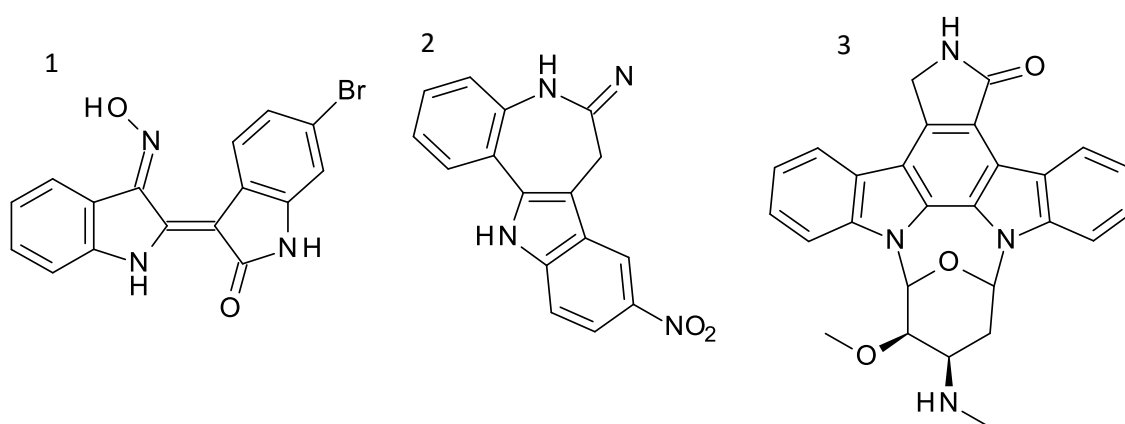
Figure 2.2: Three well known inhibitors of GSK-3β, 1) 6BIO (5 nM), 2) alsterpaullone (0.8 nM) and 3) staurosporine (15 nM)

While inhibition of the ATP binding site is the most straightforward way to inhibit a kinase, it is ATP competitive, which as discussed in chapter one may have kinase selectivity problems. One of the earlier groups of ATP binding site inhibitors discovered for GSK-3β are the derivatives of the malemide family of compounds. In the complex of GSK-3β with a malemide derivative, shown below in Figure 2.3, two hydrogen bond interactions are formed with the hinge region, one from the NH of the malemide derivative to the carbonyl oxygen of the backbone of Asp133, and the other between the adjacent carbonyl on the inhibitor to the backbone NH of Val135[47]. The IC_{50} values for the malemide compounds range between 4nM and 34nM, making them strongly potent inhibitors. Two other hydrogen bond interactions can be observed, with Arg141 and Gln185, which can serve to hold the inhibitor in place.
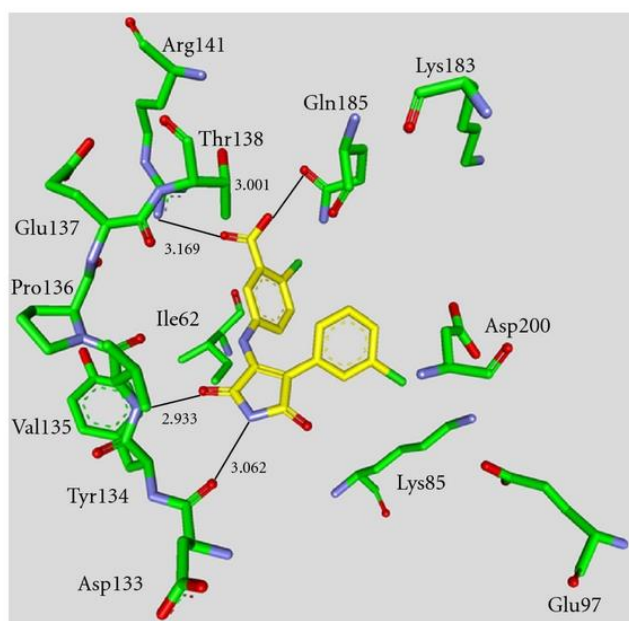
Figure 2.3: The complex between GSK-3β and a malemide derivative bound at the ATP binding site [47]

A second example of an ATP competitive type I inhibitor is staurosporine, a natural molecule synthesised by the bacterium *Streptomyces staurosporeus* [50]. The interactions it forms with the ATP binding site are very similar to those formed by the malemides, as it forms two hydrogen bond interactions with the hinge region, one with the Asp133 carbonyl and one with the Val135 NH. While these are the only direct bonds the molecule forms with the site, it has also been reported to have polar interactions as well[45]. The reported IC_{50} value for staurosporine was of 15 nM [51], making it as equally potent as the malemides. A third group of molecules that inhibit GSK-3β at the ATP binding site are the paullones[52]. One example from this family of compounds is 9-nitro-paullone, more commonly known as alsterpaullone, shown below in complex with GSK-3β (Figure 2.4). These compound are some of the most potent inhibitors of GSK-3β to have been found to date, with the IC_{50} of alsterpaullone being 0.8 nm[53], and it has been observed that derivatisation can increase its potency by a magnitude of up to 150 times[47]. Alsterpaullone can be seen to also form two hydrogen bond interactions with the hinge region; however, these are both formed with Val135, one to its backbone carbonyl and one with the backbone NH, as well as a polar interaction with the sidechain of Lys85.
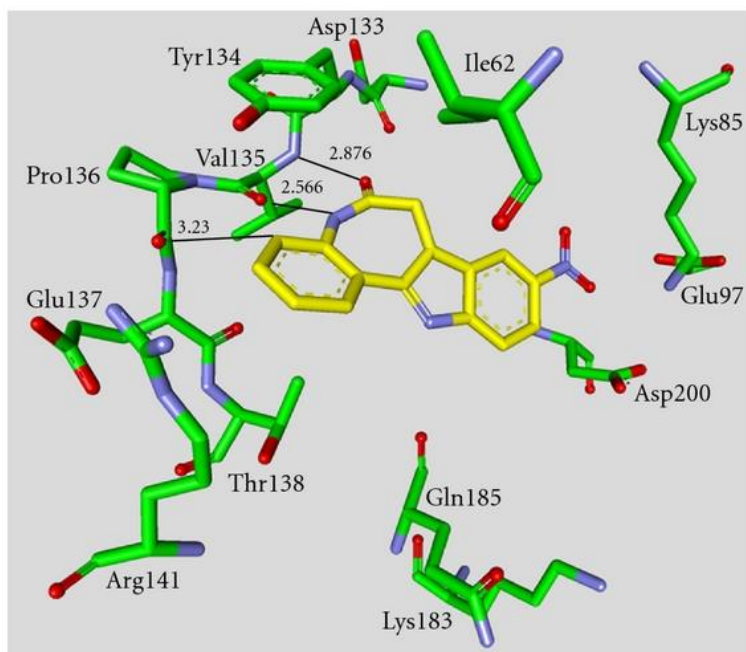
Figure 2.4: Alsterpaullone (in yellow), interacting with the ATP binding site of GSK-3β [47].

Another family of derivatives that can inhibit GSK-3β in a type I manner are the indoles[47], a group of compounds made from naturally occurring indigo dyes. One good example of a subgroup of this family that show strong inhibition are the indirubins. 6-bromoindirubin-3-oxime, more commonly known as 6-BIO (shown in complex with GSK-3β in Figure 2.5), has an IC_{50} of 5nM[42].
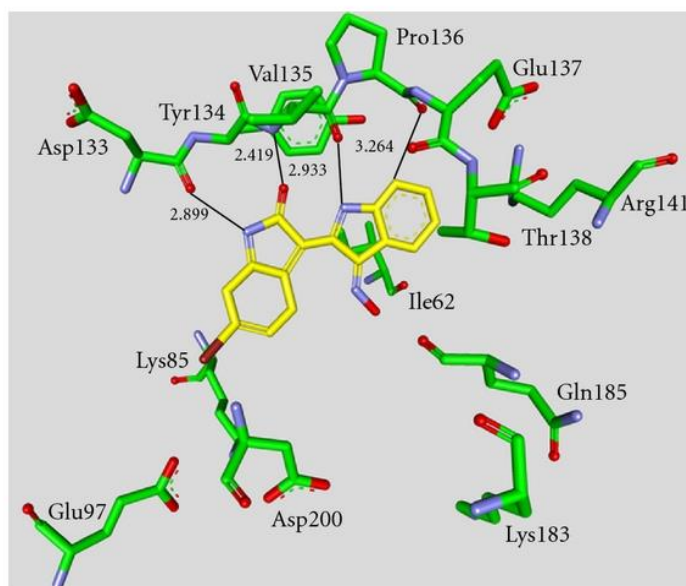
Figure 2.5: The structure of 6-bromoindirubin-3-oxime interacting with the ATP binding site of GSK-3β [47]

6-BIO interacts with the ATP binding site similarly to the previous molecules. It has the interaction between a NH on one of its rings with the backbone carbonyl of Asp133, and

the carbonyl oxygen on the same ring of the inhibitor interacts via a hydrogen bond with the NH of Val135. The NH of the other fused ring system of 6-BIO also interacts with Val135 via hydrogen bonding, this time with the backbone carbonyl. Once again, this strong binding molecule displays multiple hinge region interactions, which serves to explain why these interactions are highly sought in the design of new inhibitors, and why binding to this region has been explored in great depth. Another group of inhibitors of GSK-3β are the oxidiazole derivatives, the best of which has an IC_{50} of around 2.3 nM[54]. These compounds were also found to be selective for GSK-3β, an uncommon trait for ATP binding site inhibitors to have. They also bind by forming two hydrogen bonds with Val135, but they also form a unique hydrogen bond relay network between the nitrogen atoms of the oxidiazole, Lys85, Glu97 and Asp200 via two water molecules [47].

2.4 Overview of Type II Inhibition in Kinases

This section presents a brief overview of the general features for type II inhibition in kinases, whereas the next section will specifically address the features for GSK-3β .Type II inhibition involves the binding of inhibitors to the enzyme while the activation loop is in the DFG-out position. This allows the inhibitor to extend past the loop from the ATP binding site into the allosteric site that is opened by the removal of the phenyl group of the phenylalanine from its entrance [48]. This flipping of the loop is shown below in Figure 2.6.
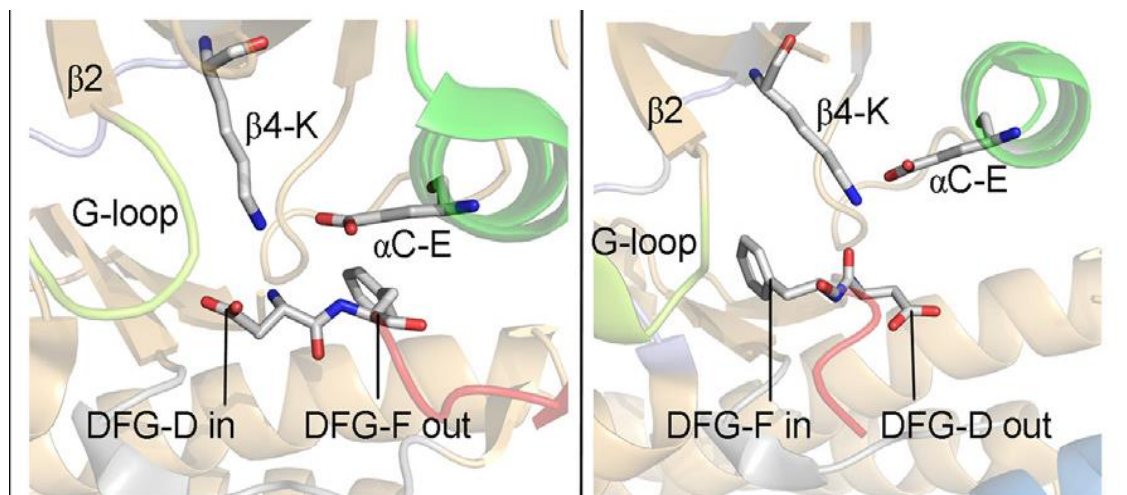
Figure 2.6: A comparison of a DFG-out conformation (left) and a DFG-in conformation (right)[48]. The inactive conformation of a kinase is produced by the DFG-F out position, and this will be referred to as DFG out in the rest of this thesis.

As can be seen from the figure above, the backbone of the DFG loop rotates, flipping the side chain of the phenylalanine outside of the loop and opening up the entrance to the allosteric site cavity, whereas the side chain of the aspartic acid is flipped inside. Importantly, this does not restrict the entrance to the cavity, as the ASP sidechain is much smaller than the phenyl ring, and is tucked more towards the side of the pocket.

The rotation of the backbone also positions the backbone NH of the aspartic acid close to the entrance of the pocket, which creates a site for a hydrogen bond interaction. This interaction with the backbone NH is actually one of the classical interactions of a type II complex[34] along with one or two hydrogen bonds with the glutamic acid of the αC-helix and a hydrogen bond with the hinge region. These interactions are shown below in Figure 2.7. As well as these three interactions, another important factor in a kinases ability to form a type II complex is the gatekeeper residue[48]. This residue, if too large, can block the space between the hinge and the allosteric pocket that the hinge end part of the inhibitor would occupy, preventing the molecule from binding in that region, which as previously discussed is an important interaction for type II inhibitors.
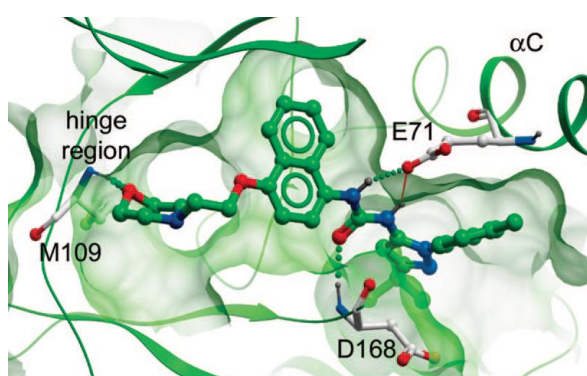
Figure 2.7: The ligand BIRB-796 (ball and stick molecule) docked into a complex in a type II conformation, with the classical interactions displayed[34].

It is hypothesised that type II inhibitors have the potential to be much more selective than type I, owing to the uniqueness of inactive kinase conformations[48]. The first FDA approved type II inhibitor was a molecule named imatinib[55]. It is used to inhibit ABL Kinase for the treatment of Philadelphia-positive chronic myeloid leukaemia (Ph$^+$CML). Imatinib displays all three classical type II interactions, and even an advantageous hydrogen bond with the side chain of the Thr315 gatekeeper residue[48]. Another type II inhibitor that has achieved FDA approval is sorafenib[48][56]. The molecule is an inhibitor of multiple protein kinases, including CDK8 serine/threonine kinases and is currently treatment of hepatocellular, renal cell, and differentiated thyroid carcinomas. As sorafenib binds to the inactive conformation, it also forms all of the classical interactions expected of a type II inhibitor, however, in this case the two NH urea groups of Sorafenib can exploit two hydrogen bonds with the αC glutamic acid. A third and final example of a type II inhibitor is nilotinib[48]. Nilotinib is also an inhibitor of ABL, for the treatment of Ph$^+$CML, and was developed as a second-line medication for CML that has become imatinib resistant through mutations. It has a similar core structure to imatinib, and therefore shares its 3 classical hydrogen bond interactions, as well as the hydrogen bond with the gatekeeper residue[48]. Nilotinib is effective against most mutant versions of ABL,

the biggest exclusion to this being the common T351 gatekeeper mutation to isoleucine, a residue bulky enough to block type II activity.

2.5 Type II of GSK3-β Inhibition

While type II inhibition could prove highly selective and therefore much more specialised than type I inhibition, it has not yet been proven that this type of inhibition can occur for GSK-3β. However, a paper by Grütter et al[56] showed the *Ustilago Maydis* form of GSK-3β undergoes type II inhibition with analogues of the previously mentioned known type II inhibitors, sorafenib and BIRB-796. The structures of these two inhibitors are shown below in Figure 2.8.
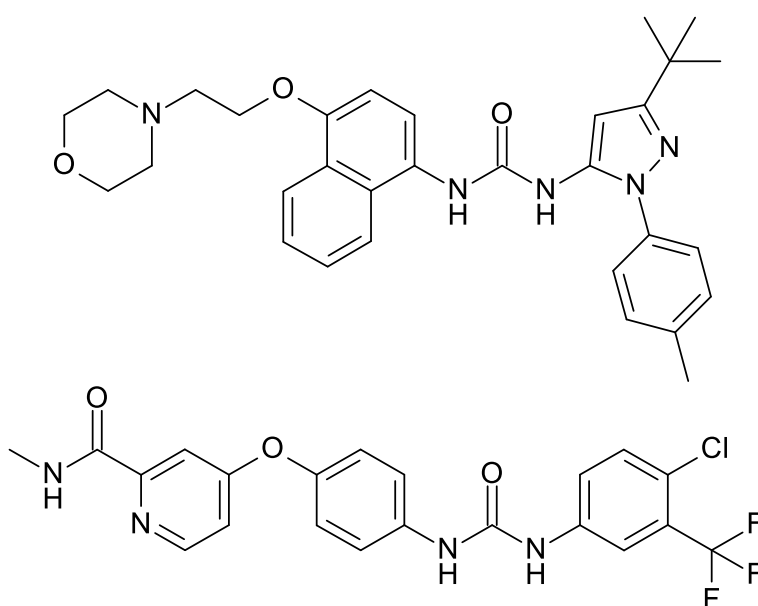
Figure 2.8: The structure of BIRB-796 (above) and sorafenib (below), known type II inhibitors.

As well as this, the paper also showed the analogues of these two compounds having activity, although lower, with the human form of the enzyme with an IC_{50} of 8.1 mM. This could be evidence that the human form can also transition to a DFG-out conformation and therefore undergo type II inhibition. If this is the case, combined with the gatekeeper residue of GSK-3β being Leu132, a relatively small residue that would not block type II activity, then there is the potential for the design of novel type II inhibitors to be used as treatments for AD. If possible, these would be have the potential to be much more selective than ATP binding site inhibitors that are much more commonly investigated for the enzyme. The biggest difference between the human form and the *Ustilago Maydis* form around the area containing the DFG loop is that the former contains a salt bridge between the residues Gln206, Phe175 and Lys103[56] shown below in Figure 2.9. As this is the only real difference in this area, it is possible that the reason the type II inhibitors received a lower IC_{50} with the human form due to the salt bridge needing to be broken

before the loop can enter the DFG-out conformation. The IC_{50} values for the derivatives of sorafenib are shown below in Figure 2.10, which clearly display that the general shape of a these compounds is conducive to type II interaction.
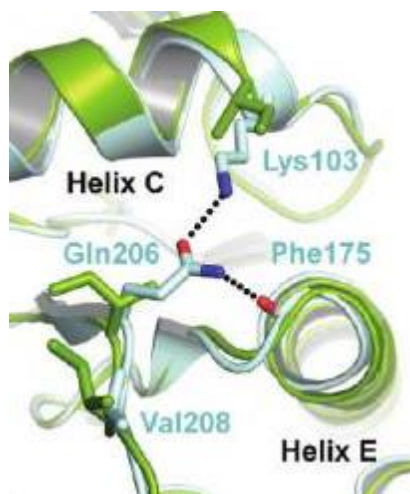
Figure 2.9: The salt bridge formed in the human GSK-3β(blue), super imposed on the *Ustilago Maydis* Form(green)[56].
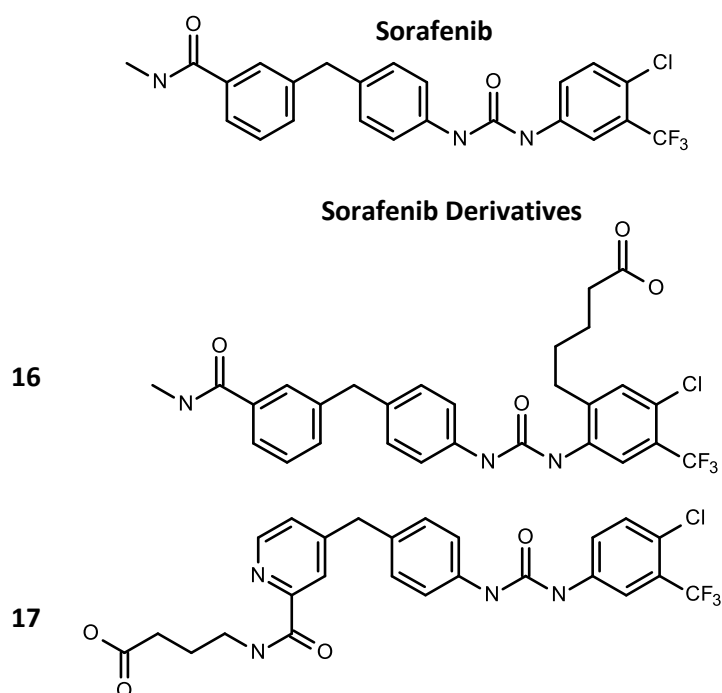
Compound	IC_{50} *UM*GSK3	IC_{50} *Hs*GSK3β
Sorafenib	0.71± 0.21	8.3 ± 0.8
16 (sorafenib derivative)	0.057 ± 0.011	0.86 ± 0.18
17 (sorafenib derivative)	0.154 ± 0.103	3.3 ± 0.6

Figure 2.10: The structures of the sorafenib derivatives and their IC_{50} values with both forms of GSK-3β[56].

2.6 GSK-3β Inhibitors in clinical trials

Before new treatments can be administered to, and distributed among, the general public, they must successfully undergo clinical trials, which typically involve 3 phases (1-3), but can have up to 4, (0-4). Phase 0 and Phase 1 trials tests small doses the drug on minimal selections of people, to investigate and responses that occur in the bodies of the participants, any side effects that may occur, and the range for safe doses. Phase 2 trials are more focused on administering the drug to larger groups of people to further investigate the optimization of the dosage of the drug necessary for the best therapeutic effect. Drugs that pass this stage progress to the next phase of trials, phase 3, which is used to compare the therapeutic effects achieved with the new drug treatment to those of other treatments that are currently available. If the drugs then pass phase 3 trials may then be moved on to the phase 4 trials, which are performed after a drug has been given a licence, are carried out to observe any long term effects the drugs might have, and how well it works when it is used more widely. Due to the current academic interest in the use of GSK-3 β inhibitors to combat AD, a number of these inhibitors have now reached human clinical trials. One example of an inhibitor of GSK-3 β involved in a clinical trial is a 2 phase trial titled "Safety Study of a Glycogen Synthase Kinase 3 (GSK3) Inhibitor in Patients with AD" [57]. The trial aimed to determine the safest oral dose of NP031112, a GSK-3β inhibitor (Figure 2.11), for patients with mild to moderate AD [57]. The trial took a selection of males and females aged between 60-85, and administered either four escalating oral doses of the drug or a placebo, to investigate any side effects. As of the September 2018, Clinical trials.gov [58] and the World Health Organisation [57] have not received the results from this trial, however, it is stated that the trial has ended on both websites. In a second example, the GSK-3β inhibitor AZD1080 (Figure 2.11), reached phase one clinical trials in 2013 [59]. However, as these trials proved unsuccessful, they were eventually were discontinued and discarded[60]. The first group of none ATP competitive inhibitors of GSK-3β to be found were the thiadiazolidinones [61] and since their discovery many other non ATP inhibitors have also been found. Through studies the thiadiazolidinones were shown to decrease levels of tau hyperphosphorylation and amyloid plaques, with a second generation thiadiazolidinone family drug recently reaching clinical trials, showing that these compounds have great promise as inhibitors for the enzyme[62]. There are many differing derivatives of the thiadiazolidinones, for example TDZD-8 (Figure 2.11), which are still being synthesised and modified to test their inhibitory activity, and the family of molecules has remained largely relevant in the field of GSK-3β inhibition and AD research.
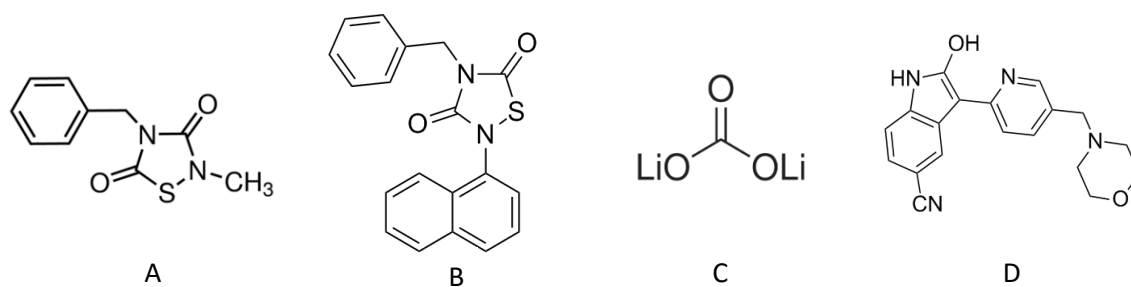
Figure 2.11: Drugs used in some of the aforementioned clinical trials: A is TDZD-8, a derivative of thiadiazolidinone and a known selective inhibitor of GSK-3β. [63] Drug B is NP031112 [64], C is lithium carbonate [65] and D is AZD1080 [66].

Another example of a clinical trial involving an inhibitor of GSK-3 β is a 3 phase trial titled "Evaluation of Lithium as a Glycogen-Synthase-Kinase-3 (GSK-3) Inhibitor in Mild Cognitive Impairment" [67]. This trial aims to create information designed to justify a much larger study of lithium as a GSK-3 β inhibitor, as well as technical data for use in Magnetic Resonance Spectroscopy (MRS) with the aim of detecting early brain changes in patients of AD. The secondary objective of the study, is to investigate if blood amounts of GSK-3 relate to GSK-3 activity in the brain[64]. According to the description, the first phase of the trial, rats will be used to help create a reliable method to measure the brain biomarker activity levels. In phase 2 of the trial, they intend to investigate the difference in GSK-3 β activity between people with AD and people without the disease. In the third and final phase of the trial, lithium carbonate (Figure 2.10) will be administered to 20 people to establish the minimum dose required to inhibit the activity of GSK-3 β [67]. As of September 2018, this trial has not begun recruiting participants. An American company ChemDiv [68] published an online library called GSK3β-Targeted Library. In the literature [39] they provide alongside this library, a table (p9-10 [39]) with examples of GSK-3 β inhibitors currently undergoing clinical trials. One example from the table is LY-2090314, which moved into phase 2 trials, with a good clearance time, however the creators of the drug did not report its therapeutic effects [46]. Another example shown in the table [39] is indirubin, which was produced by the Chinese Academy of Sciences and was entering clinical trials as the paper [39] was produced. A final inhibitor that made it into trials is tideglusib, which advanced to stage 2 trials and is one of the more widely known inhibitors that made it to clinical trials, however, it was found in multiple trials to have no long term clinical benefit, despite it being safe to take [69].

2.7 Conclusion

As can be seen in this chapter, the type I inhibition of GSK-3β has been explored in great depth, meaning that there is a lot of data available that can greatly aid researchers in the hunt for new, potent and selective inhibitor molecules. However, to date virtually none of the GSK-3β inhibitors trialled have successfully passed through clinical trials, meaning that there is still more work needed in this area in terms of potential treatments for Alzheimer's disease. Type II on the other-hand, a much less common form of inhibition, is entirely novel and unexplored with GSK-3β, and a breakthrough in this area of research could potentially lead to much more selective inhibitors.

Chapter 3: Molecular Modelling

3.1 Introduction

Molecular modelling techniques have become an integral and important part of many research areas. A rapid increase in prevalence can be in part attributed to advancements in software and hardware that can be used by researchers, as new computational techniques are constantly being developed [70]. These advances have enabled researchers to more easily carry out a plethora of complex simulations, calculations and predictions, allowing them to study, for example, complex biological structures in depth. As well as this, there has been a considerable increase in accessible structural data for enzymes and other proteins (www.pdb.org), through NMR, X-ray crystallography and electron microscope studies [70] (Figure 3.1). This structural data can then be used to predict many possible interactions that the proteins could have, as well as structure based drug design (SBDD) efforts and it has led to computational techniques to becoming more widely used.
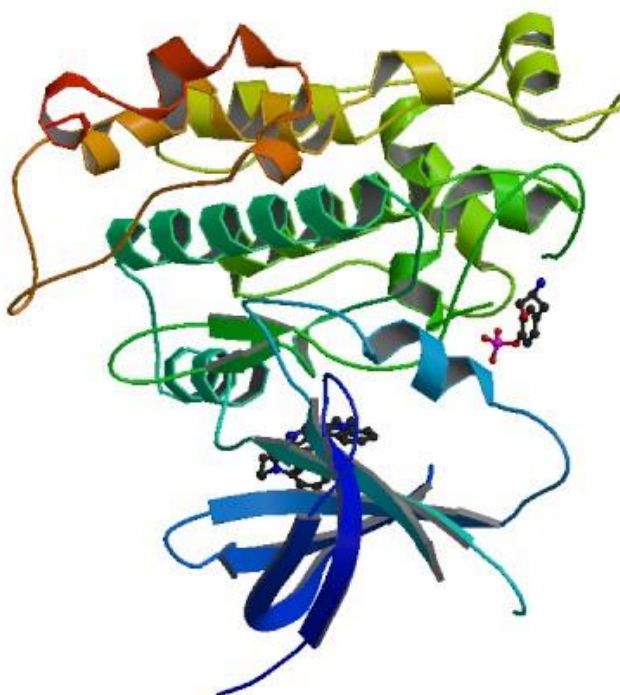
Figure 3.1: GSK-3β solved with x-ray crystallography [71] (PDB: 2OW3). The larger ligand shown is 2OW3, the smaller ligand indicates the location of the allosteric binding site.

One of the most widely used techniques that uses molecular modelling is virtual screening. This technique involves the use of use of a variety of docking programs, which will be discussed in depth in Section 3.2, and other computational procedures to screen a large database of organic molecules for any compounds that show possible activity

with a certain protein [72]. The initial step of a virtual screening is the design a computational screening method that can recognise and select already known active compounds from a large database that contains both known active compounds and decoy molecules similar in structure to the active compounds. Once developed, this method can then be used to screen large databases, selecting any compounds with scores similar to those of the actives used to create the method to be investigated in a lab study.

This chapter will give a brief overview of some common techniques used, with an emphasis on methods relevant to this thesis.

3.2 Biological Structure Prediction and Analysis

One of the most common applications in molecular modelling currently is the investigation of large biological molecules and their structures. There are more than 40511 distinct protein sequences available[73], and the amount of sequenced genomes growing exponentially. While it would take inordinately long amounts of research time to even begin to sort through all of this structural data manually, all of the recent technological advances and new computational techniques allow for the data to be fully processed quickly and easily. This means any generated information can be effectively incorporated in hypothesis driven biological research, as well as medicinal chemistry research [70].

Sequence analysis is one example of a technique that can be used to investigate biological structures. The structure and amino acid sequences of a protein have great importance in relation to its function. For example, using the hydrophobicity of an amino acid in a sequence, its location and orientation can be discerned using sequence analysis [70]. From this positional information, a secondary structure can be predicted. This is useful for finding 3D structural features, for example structural folds, by comparing the secondary structure with that of other similar proteins, as obtaining of a 3D structure is extremely helpful for the researchers that use molecular modelling techniques. There are quite a few varied molecular modelling techniques that can be used to find the 3D structures of proteins. A first example of this is threading [70], which threads the sequence through a database, trying all the possible conformations while scoring them. Another technique is *Ab initio* modelling [75], which involves using statistical analysis and energy functions based on physics to predict any possible folds for newly acquired sequences. A third technique, homology modelling [74], uses homologues, a type of structural template, which must be chosen after thorough analysis. These produced models can then, during structure validation, be analysed further, to produce a Z score to show if the structure is accurate [70]. Homologues must also be validated as it would be would be useful to compare them.

3.3 Pharmacophore and QSAR Methods

Another example of a type of molecular modelling technique that is regularly employed in drug design is pharmacophore modelling. Pharmacophore modelling is mainly used to find molecules with similar structural features to a known active for an enzyme. This involves the creation of a set of pharmacophore templates, which are created using a selection of known active compounds, mapping the geometric locations of their functional groups that form interactions, and then comparing the geometry of different molecules to find any that have similar groups in the same areas [76]. Groups that can be used when creating pharmacophore templates are Hydrogen Bond Acceptors (HBAs), Hydrogen Bond Donors (HBDs), and large VdW force exerting groups, like aromatics.

Molecular modelling can also be used to make predictions for the various drug like properties of small organic molecules using QSAR and 3D QSAR. QSAR, which stands for Quantitative Structure Activity Relationship [77], is used to relate any structural and physiochemical features of a small organic molecule to its interactive activity, in a predicted mathematical fashion. The main physiochemical properties that can be used to calculate the potentials for biological activity are; the hydrophobicity of the molecule and its substituents and the electronic properties and steric properties of the substituents[78]. The equation used for this is the Hansch equation, which is shown in Equation 3.1. C and LogP are the molar concentration and the hydrophobicity respectively, π covers the steric factors and σ involves any electronic factors

$$Log \frac{1}{C} = -0.015(logP^2) + 0.14\, logP \qquad \textbf{Eq. 3.1}$$

$$+0.27 \sum \pi_x + 0.40 \sum \pi_y + 0.65 \sum \sigma_x + 0.88 \sum \sigma_y + 2.34$$

On the other hand, 3D QSAR employs the use of pharmacophore models to help predict possible biological activity, and does this by positioning both the molecule and the pharmacophore into a three dimensional grid. At each point of this grid a probe atom is placed, and this probe atom is used to measure any possible steric and electronic interactions that the molecule can have at that point in the 3D grid. This information is then used to create a 3D interaction model that can then be used to predict the biological activity of the molecule using regular QSAR.

3.4 Molecular mechanics

A further important aspect of molecular modelling is the use of molecular mechanics. Molecular mechanics potentials are used in molecular modelling to determine the forces acting on atoms in the calculation in the form of forcefields. These forcefields can be used to predict values for 2 classes of interactions, non-bonded interactions, for example van der Waals forces and bonded interactions, for example bond angle bending, bond stretching and bond torsion. Each of the different interactions has their own term in the full equation for a forcefield, an example of which is shown below in equation 3.2 [70].

$$U = \sum_{\text{bonds}} k_b(b - b_o)^2 + \sum_{\text{angles}} k_\theta(\theta - \theta_o)^2$$

$$+ \sum_{\text{diherdrals}} A(1 - \cos(n\pi - \phi)) + \sum_{\text{charges}} \frac{q_i q_j}{\varepsilon r_{ij}} + \sum_{\text{atoms}} \left(\frac{C_{12}}{r_{ij}^{12}} - \frac{C_6}{r_{ij}^6} \right) \qquad \textbf{Eq. 3.2}$$

Where, for the bonds term; k_d is the force constant of the bond, d is the bond length, d_0 is the reference bond length. This term is used to simulate and calculate the potential bond-lengths for a molecule. For the angles term, which predicts the angles of all of the molecules' bonds ((a) Figure 3.2), k_θ is the force constant of the bond angle, θ is the size of the predicted bond angle and θ_0 is the reference angle size. For the prediction of the angles of dihedrals in a molecule ((b) Figure 3.2), the dihedrals term is used, in which A is the summation coefficient, π is the torsional angle, n is the multiplicity of the function and ϕ is the phase shift. Non bonded interactions, both the columbic interactions (charges) and atoms terms, are shown between pairs of atoms (i and j). In these terms; q_i is the partial atomic charge for atom i, ε is the coulombic potential, C is the Van der Waals radius multiplied by the Lennard-Jones well-depth, r is the distance between 2 atoms.
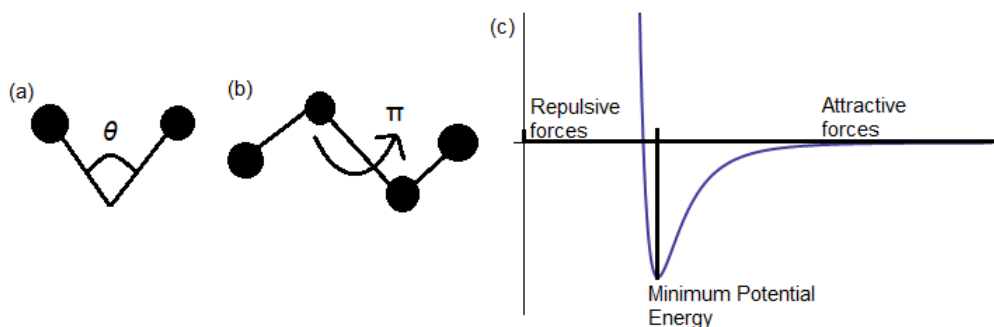
Figure 3.2: 3 diagrams related to the equation above (Eq. 3.2). In this figure: (a) visually represents θ in the angles term, (b) represents π in the dihedral term and (c) displays a graph of a Lennard jones potential.

The atoms term calculates the relationship between the attractive and repulsive energies that the simulated molecule experiences through the calculation of a Lennard Jones potential ((c) Figure 3.2). This is done by plotting the bonding potential energy against distance of separation for two atoms or molecules based on the Pauli repulsion energies, a summation of the repulsive forces acting on the particles, and the summation of the Van der Waals forces acting on the particles when they are moved closer together. When the molecules are too far apart to affect each other the potential energy between them is 0, this increases as they get closer. At the point at which the two particles are close enough to bind together, the potential energy decreases to a negative value, until they reach equilibrium and the minimum potential energy is achieved. However when these molecules are pushed even closer, the repulsive forces begin to exact a stronger effect, and the potential energy rises again sharply. As the distance is plotted starting from 0, the effects of the repulsion on the potential energy, and then the lessening of the effects are seen in reverse, which creates the Lennard-Jones function.

3.5 Docking Methods

Another of the more prevalent uses of molecular modelling techniques, and the one being used the most in this project, is molecular docking. Docking is mainly used in the prediction and ranking of binding affinities (and binding geometry) for ligands, drugs and other small molecule compounds with protein complexes, but is not limited to such [70]. Docking programs have two main parts, a search algorithm and an energy scoring function [79]. A search algorithm is the mathematical equation with which a docking program searches for conformations of ligand molecules and their subsequent docking poses. Currently there are 2 main search algorithm classes that are regularly used by modern docking programs, and these are rigid and flexible docking. Used mainly by older programs, for example DOCK, rigid docking treats the ligand as a rigid structure meaning that the conformations for the ligands are generated before the docking begins, and then docked separately into the protein to create the poses [80]. On the other hand, flexible docking treats the ligand as flexible, generating ligand conformations once the ligand is already inside the active site "on the fly" while the docking is taking place. This allows it to avoid using conformations that do not fit into the site while taking into account the geometry of the protein, and allows more exhaustive searching for the best conformation [80]. Flexible docking is the most common type of search algorithm used today, and has subtypes of its own. The first major example of a type of a flexible docking search algorithm is a Genetic algorithm, a diagram of which is shown in Figure 3.3. Genetic algorithms use Darwinian evolution to search for the best ligand binding conformations, which means a set of conformations in the binding site first, and the best interactive features these different conformations have are then combined to generate a "child"

generation of conformations. These new conformations may then be randomly mutated, making changes to certain features. This is then repeated until there is no significant improvement in the score produced by the next generation of conformations.
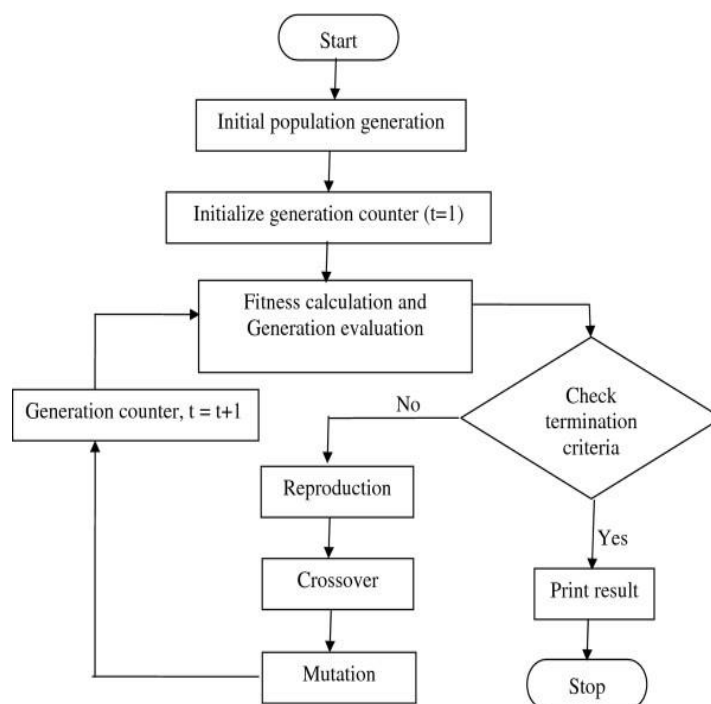
Figure 3.3: A diagram showing the processes used in a Genetic search algorithm [81]

An example of a program that uses this type of algorithm is GOLD [82] which is a product of the Cambridge Crystallographic Data Centre (CCDC), and is also one of the more commonly used docking programs. GOLD uses a Genetic flexible search algorithm, and it also offers a wide variety of scoring functions, example being Chemscore and ChemPLP, which are empirical based scoring functions, ASP, a knowledge based scoring function and Goldscore, a force field based scoring function. This range of scoring functions allows for the researcher to use a variety of different methods when investigating ligand molecules within the same program. While the GUI was found to be a little bare, the wizard provided for setting up docking calculations greatly increases the ease at which GOLD can be used. In one paper, D. Kitchen et al [82] investigated the accuracy of GOLD and found that the ligand poses it produced compare well with the X-ray conformations, stating that any poses that were produced were satisfactory and comparable to those produced by other competitor programs such as Glide.

Another type of flexible docking search algorithm commonly used today is called a hierarchical search algorithm shown in Figure 3.4. In this type of search algorithm, individual ligand features are selected and filtered one at a time, for example its diameter, how well it can rotate around its diameter in the active site, its ability to make H-bonds and other similar features. Once these filters have been applied, the search algorithm minimizes the ligand, rescoring it using the full scoring function. This type of algorithm is

used by Schrödinger's Glide [83]. Glide, a commercial docking program created by the company Schrödinger, is arguably the most popular docking program currently in use, and is incorporated into the GUI Maestro [84]. Glide uses a flexible docking hierarchical search algorithm, and the scoring functions it uses, standard-precision (SP) and extra-precision (XP) are empirical based scoring functions. One study about Glide docking claimed the software was almost twice as accurate as other available docking programs [85]. Its GUI is intuitive and easier to use than many other similarly advanced and specialised software, and due to never releasing its exact details, their search algorithm is unique.

Critical to the accuracy of docking programs is the scoring function. This is used by the program to score the ligands' poses, and there are 3 main types [86]. The first type is an Empirical scoring function, some examples in use today being -SP/-XP with Glide and ChemPLP with GOLD. This type of scoring function acts by parameterising the ligand binding mode against documented experimental binding affinities, incorporating important interactions such as H-bonding, lipophilic interactions, ionic interactions and any loss of internal conformational freedom experienced by the ligand [87]. A knowledge based scoring function is the second type, one example being ASP. These score ligands based on statistical analysis of known interactions. The final common type of scoring function is a force-field based scoring function, which is based on the values obtained by molecular mechanics force fields like those discussed in Section 3.4. Examples of programs that use this type of scoring function are AutoDock and DOCK.
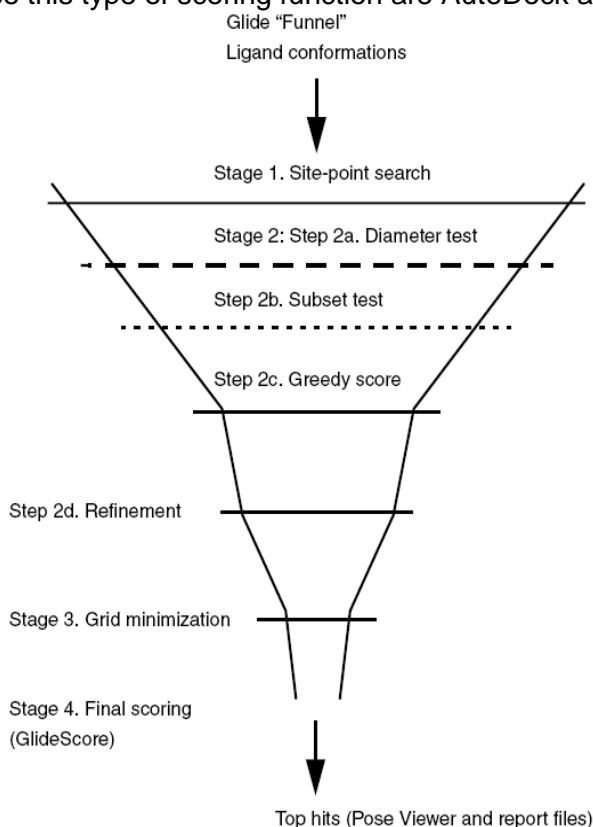
Figure 3.4: A diagram showing the processes used in a Hierarchical search algorithm.

3.6 Molecular Dynamics

Molecular Dynamics (MD) simulations, including the aforementioned molecular mechanics, can be used to simulate a chemical system over time, and to accurately calculate macroscopic properties of these systems, in an attempt to surpass current technological restrictions. This sometimes done via the creation of a simulation cell. Simulation cells are an orthorhombic box, or in the case of this project cubic, around the simulation system containing solvent molecules, and therefore cannot accurately represent the bulk properties of a real solvent liquid. This is overcome through the introduction of periodic boundary conditions (PBC), in which if an atom leaves the cell through its right side, it will enter at the same time through the left (Figure 3.5).
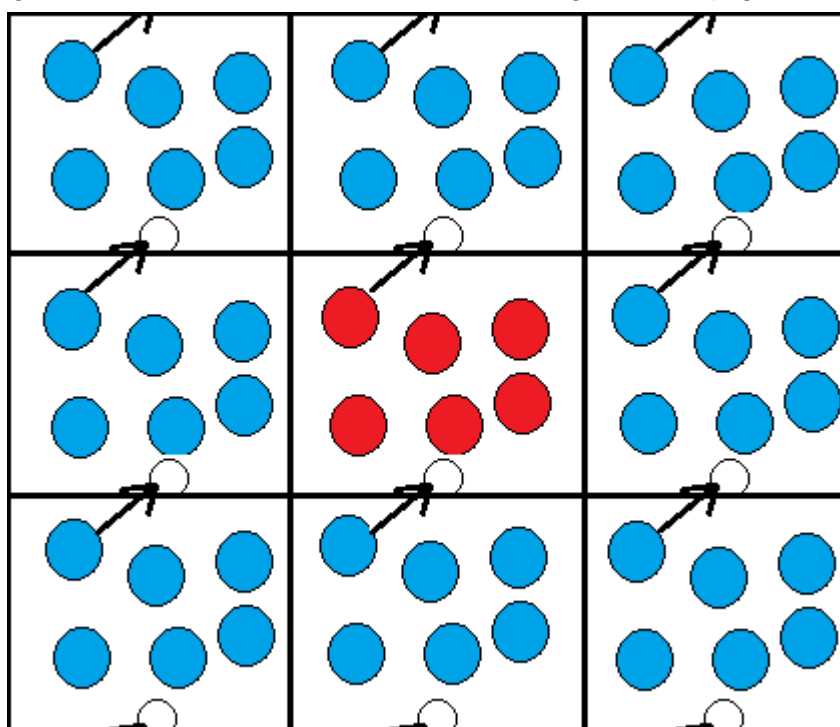
Figure 3.5: A 2 dimensional system with periodic boundary conditions, with the centre box being replicated multiple times to form an infinite lattice.

Statistical mechanics is employed in these simulations to link macroscopic and microscopic properties, and it does so by constraining certain parameters in the macroscopic state, the trajectory of the space points will move on a surface of phase space. The constraint parameters that control the thermodynamic state of the macroscopic system define this surface. According to ergodic theorem [88], this works with the assumption that, in a system time will follow a trajectory, eventually visiting all microscopic states consistent with the imposed external constraints. This fundamental concept of the ergodic theorem gives us a connection between the macroscopic property, G and the time average of this property over all microscopic states, G_t, which is shown in the equation below;

$$G = G_t = \langle G_i \rangle_{time} = \frac{1}{M} \sum_{t=1}^{M} G_i \qquad \textbf{Eq. 3.3}$$

In this equation, G_i is the value of the ith state, and M is the number of states. When a system is in equilibrium, G_i fluctuates around the equilibrium value, $\langle G_i \rangle$. This instantaneous fluctuation δG, at time t is described using the equation;

$$\delta G_i(t) = G_i(t) - \langle G_i \rangle \qquad \textbf{Eq. 3.4}$$

The general concept of MD is the solving of the classical Newton's equations for motion of a system of atoms interacting, according to the potential energy forcefields, as discussed previously with molecular mechanics. As with earlier, these forcefields work with the idea that the solution for the equations of motion of a molecule represent the time evolution of the trajectory, again with Newton's law of motion:

$$\vec{F}_i = m_i \vec{a}_i \qquad \textbf{Eq. 3.5}$$

where F_i is the force, m is the mass and a is the acceleration of atom i. This equation can be integrated numerically, allowing for the prediction of where these atoms will move over a short period of time. By repeating this process in succession, the full time dependant trajectory can be created for the whole system which represents the molecular motions. The main advantage of MD over molecular mechanics is that it does not restrict the system to harmonic motion around a single minima, but instead allows for the crossing of energy maxima to explore other stable conformations of the system.

This solving of the law of motion (Eq. 3.5) can be computed directly as a derivative of the potential energy V, with respect to the atomic coordinates r_i, using the equation shown below:

$$-\frac{\partial V}{\partial r_i} = m_i \frac{\partial^2 \vec{r_i}}{\partial t^2} \qquad \textbf{Eq. 3.6}$$

Then, from this equation, the force acting on atom i can be obtained. The standard numerical method for the solving of this equation for future positions is the finite difference method, by expressing the motion of a particular particle can be expressed in a Taylor series.

If the position at time t is written as $\vec{r}(t)$ then the position of the particle after a short interval of time, the (timestop) δt is:

$$\vec{r}(t + \delta t) = \vec{r}(t) + \frac{\partial \vec{r}}{\partial t} \delta t + \frac{\partial^2 \vec{r_i}}{\partial t^2} \frac{\delta t^2}{2} + o(\delta t^3) \qquad \textbf{Eq. 3.7}$$

The terms in this equation stand for; the position $\vec{r}(t)$, the velocity $\frac{\partial \vec{r}}{\partial t}$ and the acceleration $\frac{\partial^2 \vec{r_i}}{\partial t^2}$. Knowledge of the values of these three parameters is needed for the calculation. The general process of a dynamics calculation is carried out as follows;

- The input coordinates $\vec{r}(t = 0)$ are required, and the initial velocities and acceleration are obtained from the potential energy equation.
- $\vec{r}(t + \delta t)$ is then estimated and new coordinates are obtained
- The equation then updates the velocity and acceleration values

This process is repeated until the simulation is complete. In molecular dynamics, the integration algorithms that can be used to solve the motion equation can be based around the Leapfrog Verlet scheme[89], which comes with a variety of ensembles, for example NPT and NVT.

3.7 Conclusion

As seen throughout this chapter, there are a multitude of different applications for molecular modelling in chemistry, the investigation of biological and organic molecules and drug design. It is little surprise, therefore, that many researchers in medicinal chemistry are turning to these methods to speed up and aid with selection of new possible hit and lead compounds. The range of pharmacokinetics and pharmacodynamics data able to be predicted with computational calculations, and the speed and inexpensive way by which they can be calculated, make them almost indispensable in the search for new treatments for various diseases. Also, due to the large selection of different programs tackling similar processes in a different manner, a good example of this being the different search algorithms and scoring functions of the different docking software, and this allows different methods to be compared, to find the best one for a particular project. As also discussed in Section 3.1, the resources available to researchers are ever increasing and improving, with the databases that can be used holding hundreds of millions of compounds, and with thousands of freely accessible solved protein structures. In conclusion computational chemistry is a vital asset and provides more targeted grounds on which to build new research. It will also serve to speed up the drug design process exponentially as advancements in all fields continue, especially in projects such as the current.

Chapter 4: *In Silico* Screening and Experimental Validation of GSK-3β Type I Inhibitors

4.1 Introduction

Alzheimer's disease (AD) is a neurodegenerative disease characterised by a loss of memory ability and cognitive function. This is caused in part by the formation of pathological features, mainly amyloid plaques and neurofibrillary tangles that cause the death of neurons. The progressive death of neurons causes the lobes of the brain in a sufferer of AD to shrink, triggering the decline in function. In 2007, Hooper et al. [18] published a paper called 'The GSK-3 Hypothesis of Alzheimer's Disease', which contained a summary of all the evidence implicating the over action of the enzyme Glycogen Synthase Kinase-3 beta (GSK-3β), a Ser/Thr kinase, in the formation pathways of both the amyloid plaques and the neurofibrillary tangles. Therefore, the inhibition of GSK-3β could serve to reduce the formation of the two pathological features, potentially providing a new form of effective treatment for AD that is sorely needed. The most common way that a kinase of this type is inhibited is through type I ATP binding site inhibition, as all kinases use ATP to enact their functions. Therefore, while not necessarily highly selective, ATP competitive inhibitors have the potential to be highly potent and selectivity has previously been achieved[90]. The ATP binding site of GSK-3β is located in the cleft between the N-terminal β-sheet domain and the C-terminal α-helical domain of the enzyme, and area called the "activation segment". In this chapter, we present the screening of large database of compounds for type I inhibitory activity with GSK-3β, and the biological validation of the results. For the design of the virtual screening, a series of benchmarking studies using a designed training set of ligands, containing 30 known active inhibitors and 2089 inactive and decoy inactive molecules, were used to develop a reliable consensus scoring method for the virtual screening. This was done using multiple programs Glide-SP and -XP, GOLD[91] and Autodock[92]. This consensus method was then applied to the large database of compounds that was obtained from the ZINC15[33] database, and the virtual screening was carried out. Upon the completion of the virtual screening, a selection of sorting methods, including consensus binding based sorting methods and pharmacophores were investigated for use in the selection of compounds from the results of the screening for biological validation. The final selected molecules were taken to the Consejo Superior De Investigaciones Cientificas (CSIC) the Spanish national research institute, for *in vitro* validation binding assays of enzyme inhibition.

4.2 Aim

To design and implement a consensus scoring *in silico* virtual screening method for the selection of novel type I inhibitors of the enzyme GSK-3β from a large database of drug-like biological molecules for the possible treatment of Alzheimer's disease. Biological screening of selected compounds.

4.2.1 Specific Objectives

- Benchmarking study: to design an *in silico* method combining the results of multiple docking programs using a consensus scoring method

- To apply the screening protocol to a downloaded database of ZINC purchasable compounds to screen for potential activity with GSK-3β

- To select a set of compounds from the results of the *in silico* screening for purchase following further analysis of their binding potential

- To validate the results of the virtual screening using biological *in vitro* assays for the purchased compounds

4.3 Computational methods

4.3.1 Creation of an Active/Decoy Ligand Set
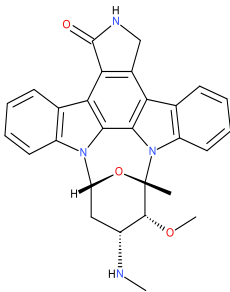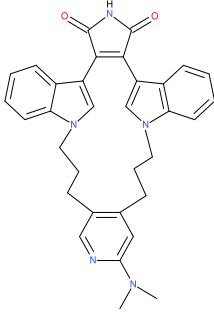
The active and inactive ligands used in the benchmarking study were all extracted from the ChEMBL[93] database (www.ebi.ac.uk/chembl)[94]. This is a chemical database fully available to the public containing bioactive molecules with drug-like properties. The best range of ligands with known binding affinities to select the active compounds from was determined using their IC_{50} (1-50 nM, 432 compounds) and inhibitory constant (K_i) values (1-50 nM, 143 molecules). These molecules were then prepared with Schrödinger`s LigPrep[95], converting their 2D structures to 3D based on stereochemical, tautomeric and ionization variations[94]. The forcefield used for the minimization was the OPLS3 (Harder et al.[422]) forcefield, as it is to date the most accurate and covers the chemical space in the most comprehensive manner[96]. After this, the ionisation states of the ligands were then generated with possible states at target pH 6 to 8, with the chiralities set to be determined using the 3D structure. [94]

In total 576 ligands were downloaded, which were then clustered. The representatives of these clusters would form the final `actives` that will be employed throughout the benchmarking docking calculations. The software used to cluster the ligands was Schrödinger`s Canvas[97] using a DISE (directed sphere exclusion) diversity based selection method. The type of binary fingerprint of the structures selected for use was
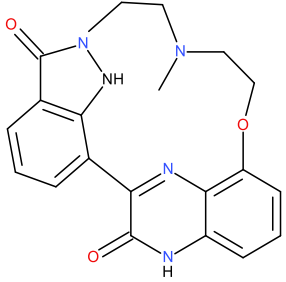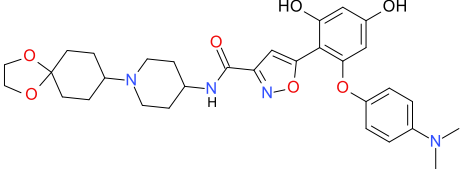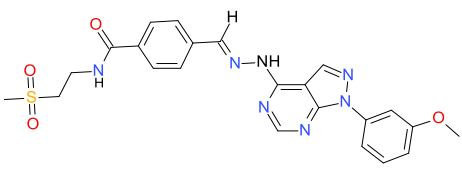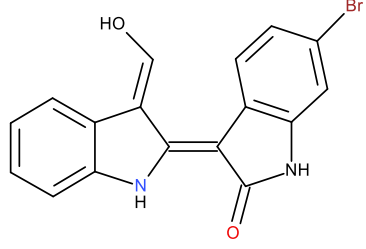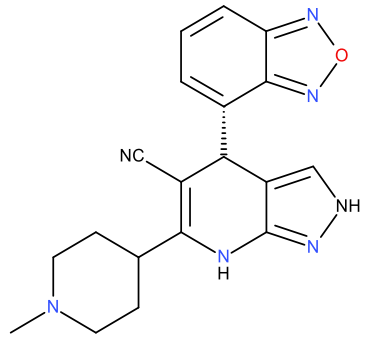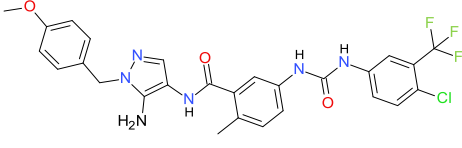
'radial'. The size of the subset of clusters was set to 30, producing a set of 30 structurally diverse active ligands for use in the active/decoy benchmarking study. [94]
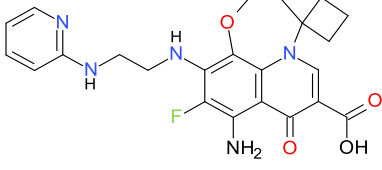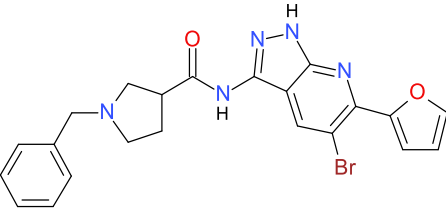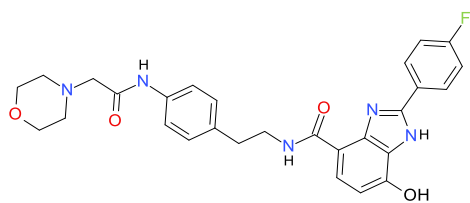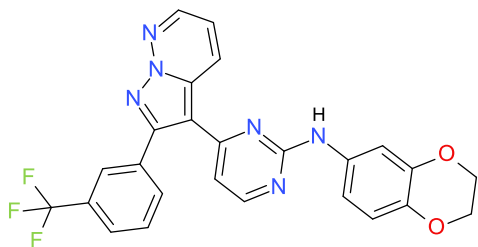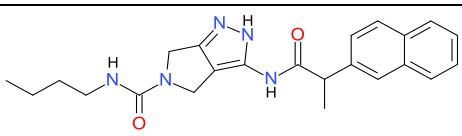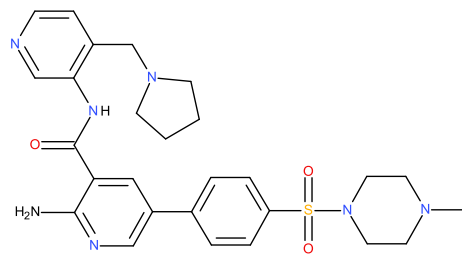
Once the set of 30 active ligands was obtained, the next step was the generation of decoys (presumed inactives), performed using the DUD-E decoy generator[98] [94]. The generator acts by processing the selected active compounds, and then outputting a maximum of 50 compounds with similar, each having similar physico-chemical properties but with dissimilar 2D topology.[99] Similarly to the active and inactive ligands, the decoys also needed preparation with LigPrep before use (using the same settings as described above). [94] The final database contained the 30 known active ligands shown in Table 4.1 below, along with 189 real inactive molecules (from ChEMBL with IC_{50} and K_i's > 50 μM), and the 1900 DUD-E decoys that were generated. The total number of molecules including tautomeric/ionization states was 3102 ligand structures. [94]
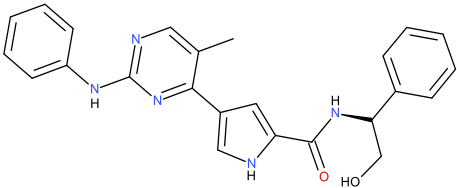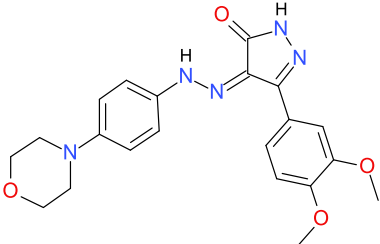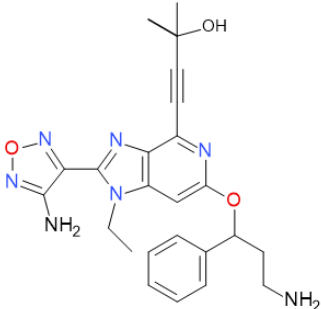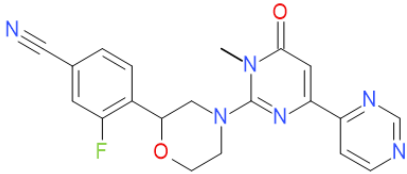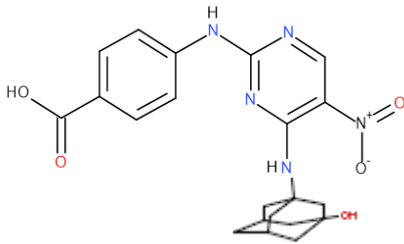
Table 4.1: The 30 active molecules obtained from ChEMBL[94] together with their GSK-3β inhibition data
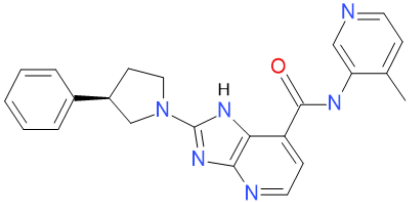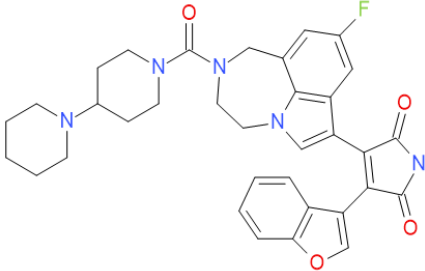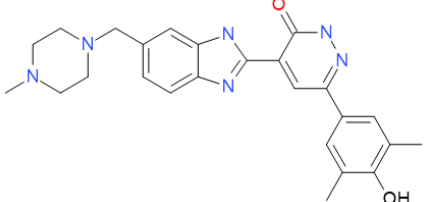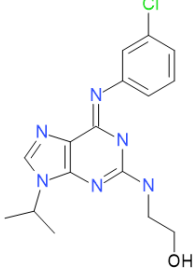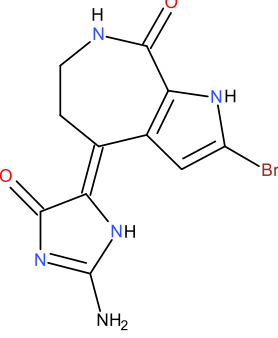
Entry No.	2D Active Ligand Structure	Scaffold Type	K_i/IC_{50} Affinity (nM)	Reference
1	**CHEMBL388978**	Staurosporine	IC_{50} = 15 nM K_i = 22 nM	Eur. J. Med. Chem., (2009) 44:6:2361 Bioorg. Med. Chem. Lett., (2010) 20:5:1661
2	**CHEMBL1087499**	Maleimide	IC_{50} = 3 nM	Bioorg Med Chem Lett 2007; 17: 2863-8.
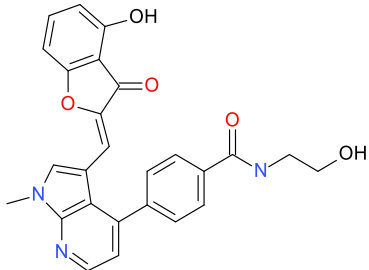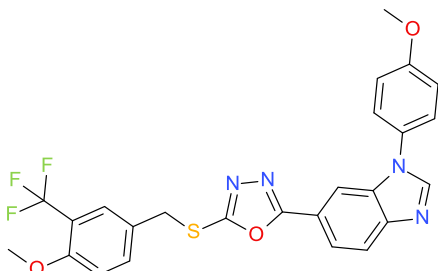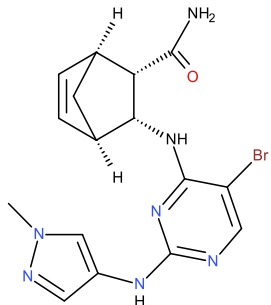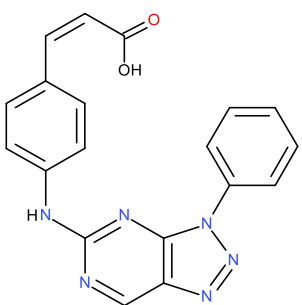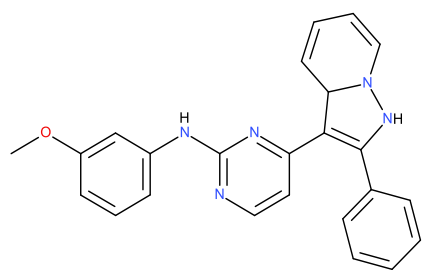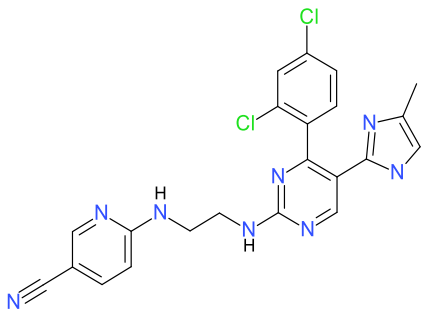
3	CHEMBL215803	Quinoxalinone-2-one Macrocyclic	IC$_{50}$ = 13 nM	Bioorg. Med. Chem. Lett., (2006) 16:19:5122
4	CHEMBL2443026	Isoxazole	IC$_{50}$ = 10 nM	Bioorg. Med. Chem., (2013) 21:22:7047
5	CHEMBL65987	Pyrimidine Pyrazole	IC$_{50}$ = 7.94 nM	Bioorg. Med. Chem. Lett., (2004) 14:9:2121
6	CHEMBL3125370	6-bromoindirubin-3-oxime	IC$_{50}$ = 5 nM	Bioorg. Med. Chem. Lett., (2014) 24:6:1532
7	CHEMBL3085387	Oxadiazole	IC$_{50}$ = 2.5 nM	Bioorg. Med. Chem., (2008) 16:2:636
8		Amino-pyrazole		Bioorg. Med. Chem.,

	CHEMBL1684800		**IC$_{50}$ =** 2.73 nM	(2011) 19:6:1915
9	**CHEMBL1940907**	Quinolone	**IC$_{50}$ =** 10 nM	Bioorg. Med. Chem., (2012) 20:3:1188
10	**CHEMBL317657**	Pyrazolo-pyridine	**IC$_{50}$ =** 14 nM	J. Med. Chem., (2008) 51:7:2062
11	**CHEMBL562089**	Benzimidazole	**IC$_{50}$ =** 40 nM	Eur. J. Med. Chem., (2009) 44:6:2361
12	**CHEMBL362155**	Pyrazolo-Pyridazine	**Ki** = 50 nM	J. Med. Chem., (2004) 47:19:4716
13	**CHEMBL380946**	Pyrazole	**IC$_{50}$ =** 50 nM	Bioorg. Med. Chem. Lett., (2006) 16:4:1084
14		Pyrazolone	**Ki** = 0.22 nM	J. Med. Chem., (2012) 55:21:9107

15	3I4B[e]	Pyrimidyl Pyrole	IC$_{50}$ = 29 nM	J Med Chem 2009; 52: 6362-8.
16	CHEMBL1086735	Pyrazolone	Ki = 3 nM	Bioorg. Med. Chem. Lett., (2010) 20:5:1661
17	CHEMBL1099297	Amino-furazan (Oxadiazole)	IC$_{50}$ = 41 nM	Bioorg. Med. Chem. Lett., (2009) 19:5:1508
18	CHEMBL3091543	Pyrimidone	IC$_{50}$ = 6.5 nM	Bioorg. Med. Chem. Lett., (2013) 23:24:6933
19	CHEMBL402902	Pyrimidine	IC$_{50}$ = 3 nM	Bioorg. Med. Chem. Lett., (2008) 18:12:3578

20	**CHEMBL2048675**	Imidazo-pyridine	**IC$_{50}$ =** 30 nM	Bioorg. Med. Chem. Lett., (2012) 22:13:4221
21	**CHEMBL2386093**	Maleimide	**IC$_{50}$ =** 0.53 nM	J. Med. Chem., (2013) 56:12:5115
22	**CHEMBL270473**	Benzimidazole	**IC$_{50}$ =** 1.5 nM	Bioorg. Med. Chem., (2008) 16:2:636
23	**CHEMBL311228**	Purine	**IC$_{50}$ =** 30 nM	Proc. Natl. Acad. Sci. U.S.A., (2007) 104:51:2052 3
24	**CHEMBL361708**	Hymenialdisine Paullone	**IC$_{50}$ =** 10 nM	Eur. J. Med. Chem., (2009) 44:6:2361 Trends Pharmacol. Sci., (2004) 25:9:471

25	 **CHEMBL1092754**	Benzofuranone	**IC$_{50}$** = 5.9 nM	Bioorg. Med. Chem. Lett., (2010) 20:7:2321
26	 **CHEMBL472043**	Oxadiazole	**IC$_{50}$** = 8.6 nM	Bioorg. Med. Chem., (2009) 17:5:2017
27	 **CHEMBL2071201**	Pyrimidine Pyrazole	**IC$_{50}$** = 34 nM	Bioorg. Med. Chem. Lett., (2012) 22:14:4750
28	 **CHEMBL255735**	Azapurine Pyrimidine	**IC$_{50}$** = 7 nM	Bioorg. Med. Chem. Lett., (2008) 18:12:3578
29		Pyrimidine	**IC$_{50}$** = 30 nM	Bioorg. Med. Chem. Lett., (2008) 18:2:653

		CHEMBL403405			
30		Pyrimidine	IC_{50} = 7 nM	Trends Pharmacol. Sci., (2004) 25:9:471	
		CHEMBL412142			

4.3.2 Creation of the *In Silico* Screening Database

The full preparation of the database for the *in silico* screening, in terms of processes applied and the amounts of compounds left after each step is summarised below in Figure 4.1. The tool used to obtain the initial compounds library for the actual virtual screening was the tranche browser of ZINC15 [33] (www.ZINC15.org), which allows the user to filter the entire ZINC database based on chemical properties such as molecular weight and LogP. The subset of compounds selected was the "drug like" subset, which contained a total of 123,547,009 compounds, defined by a molecular weight range of 200-500 Da, and LogP values between -1 and 5. [100] We increased the maximum molecular weight of the compounds to be downloaded to include the above 500 Da section, as there are known inhibitors of GSK-3β above this molecular weight and also because we planned to subsequently apply our own filters for maximum molecular weight and other properties. This increased the total to 123,557,117 ligands, downloaded in .smi format. [100]

```
┌─────────────────────────────────────┐
│   Downloaded database: 123,557,117   │
└─────────────────────────────────────┘
                  ↓
┌─────────────────────────────────────┐
│     Shuffled to obtain: 500,000      │
└─────────────────────────────────────┘
                  ↓
┌─────────────────────────────────────┐
│     Filtered to obtain: 157,238      │
└─────────────────────────────────────┘
                  ↓
┌─────────────────────────────────────┐
│    LigPrepped to obtain final        │
│    database of: 202,856              │
└─────────────────────────────────────┘
```
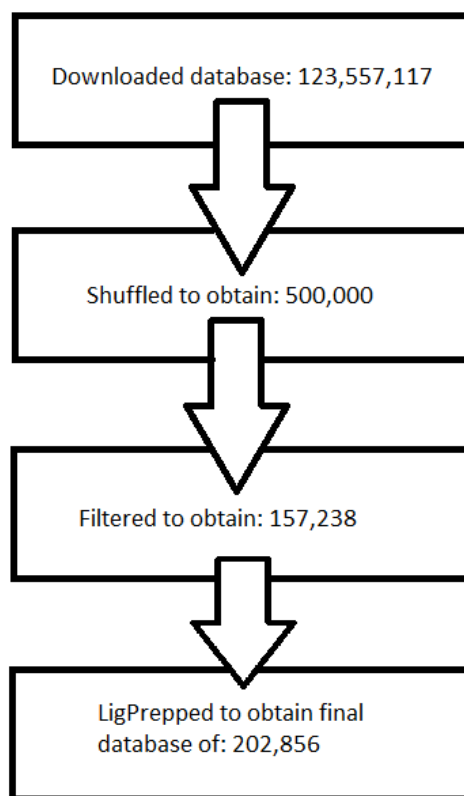
Figure 4.1: The creation of the benchmarking database, including the ligand counts at each step

With the resources available here, this number of ligands is far too large to be screened in a reasonable time period. Therefore, the shuffle command (*c.f.* appendix), was used to obtain a selection of 500,000 diverse ligands from the downloaded compounds to be imported for the 3D minimization. [100] As the SMILES all contained defined chiralities, they were imported into Schrödinger's Canvas [101] and then converted to 3D structures. These were then minimized using MacroModel [102] For the MacroModel minimization, the force field employed was OPLS3[100], as this was used in the preparation of the benchmarking database[94]. The method used for the minimization was the Truncated Newton Conjugate Gradient (TCNG), and the maximum iterations used was 300. All other settings were left as default. [100]

QikProp[103] from Schrödinger was used for ADME (Absorption, Distribution, Metabolism, Elimination) properties predictions allowing us to further sort and filter the ligands in the screening database. All settings for this were left as default. Filter rules were mainly based on Lipinski's rule of 5 [104], as well as [100] another paper containing recommendations for increasing a drugs blood-brain barrier permeability by Ghose et al. [105] The filter rules are shown below

- Molecular weight ≥ 200 and ≤ 650. This was based on Lipinski's rule of 5, increased to 650 to incorporate the full molecular weight range of the 30 known actives.

- LogP O/W between and including 0 and 5. This too was based on the rule of 5, and left unmodified.

- The amount of Hydrogen Bond Acceptors (HBAs) on the molecule ≥ 0 and ≤ 10, also from Lipinski's rules. This was already applied by the drug like subset with which it was downloaded.

- The amount of Hydrogen Bond Donors (HBDs) on the molecule ≥ 0 and ≤ 5. Similarly to the HBA's, this was both applied during the download from ZINC and also part of Lipinski's rules.

- The number of rotatable bonds must be less than or equal to 8. Included from Verbers Parameters [106] and modified on the recommendations of Ghose et al.

- A predicted CNS of 0 or above. This parameter was taken straight from the recommendations of Ghose et al[105], but modified to include compounds with a CNS of 0.

These filters were applied leaving 157,238 compounds. The filtered compounds were then prepared using Schrödinger's LigPrep, using the same settings as those of the benchmarking database[100] producing 202856 compounds including tautomers and ionisation states.

4.3.3 Protein Preparation for Docking

The PDB selected for docking was 2OW3 (Figure 4.2). This selection was based of the work of Doerksen [107] and collaborators in which they docked 24 diverse ligands into 13 different crystal structures of GSK-3β. 2OW3 was the PDB that recovered the highest percentage of actives, and therefore was chosen for this project. The preparation of the protein was carried out using Schrödinger`s Protein Preparation Wizard. Water molecules more than 5Å from het groups were removed, and, the bond orders were assigned and all missing hydrogen atoms were added [94]. The system was then refined using a restrained minimisation with the OPLS3 forcefield, with heavy atom convergence set to an RMSD of 0.3 Å to remove steric clashes.[94] The rest of the water molecules were then removed for subsequent docking. The co-crystalised ligand was modified to a pH of 7.0 ± 3.0, to generate a tautomer with the lowest state penalty.
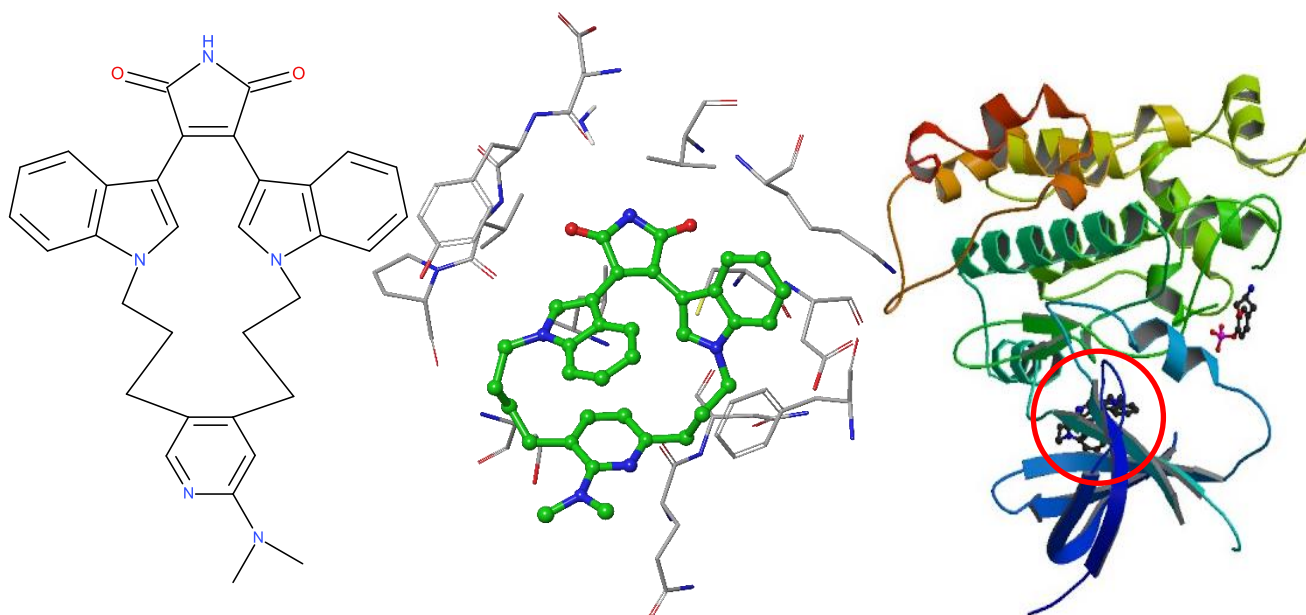
Figure 4.2: The 3D structure of the 2OW3 PDB, with a 2D structure of the bis-(indole)malemide pyridinophane inhibitor used to solve the crystal structure which can also be seen in the 3D model (circled in red).

4.3.4 Glide Docking Details

During docking, the shape and properties of the protein are mapped onto a grid with co-ordinates (X= -36.94, Y=-2.52, Z=69.5), that contains several sets of fields to accurately score ligands. This grid was generated using Glide`s Receptor Grid Generation feature. [94] The crystal ligand structure that was already bound within the ATP binding site used as the centre of the grid. In both the Glide-SP and -XP docking calculations, OPLS3 was used as the forcefield, the van der Waals radii factor was left at 0.80 and partial charge cut off was left at 0.15. Nitrogen inversion sampling, flexible ligand sampling and the sampling of ring conformations including input ring conformations were all also selected. For results output after the calculation, post docking minimization was selected to minimise the produced poses, minimising the ligand within the receptor field and allowing for more accurate poses. Strain correction terms were also selected, to optimise each ligand pose produced. [100]. Ligands were ranked by Glidescore, with one pose saved per ligand

4.3.5 GOLD Docking Details

The protein, taken directly from the previous protein preparation calculations (4.3.3), was selected in the GOLD wizard, the centroid of the co-crystallised ligand was used to define the site. Then, the distance from this centre point in which atoms can be selected to make interactions with the docked ligands was set to 10 Å. After this the detect cavity setting was also used, which restricts the selection of atoms for interactions to the solvent accessible surface of the site. Force all H bond donors/acceptors to be treated as solvent accessible was also selected. The search efficiency was set to 100% for all of the scoring functions, as this is the default setting. The ligands were also selected unmodified from Maestro, in .mol2 format. For the output, GOLD was set to only keep the best solution for each ligand [100]. GOLD calculations were initially performed using the ChemPLP and ASP scoring functions.

4.3.6 Autodock Docking Details

The ligand files were converted to .sdf in Maestro, for use in Autodock (version 4.2). [94] This is done using the chemical toolbox `Open Babel`. As .sdf files store the structures in 2D, energy minimisations were performed to acquire 3D structures. One of the parameters used for this is the Universal Force Field (UFF), which contains parameters for every atom. Another is a conjugate gradient optimisation algorithm. The number of minimisation steps used was set to 200. [94] The files were then converted to the .pdbqt format. This file format is able to store partial charges, atomic coordinates and AutoDock receptor and ligand atom types [94]. The unedited protein structure can be imported to PyRx (the GUI for Autodock), where it is instantly converted to the .pdbqt format. The co-ordinates and search space dimensions (Å) were obtained from the glide grid generated for docking [94]. The docking algorithm selected for use was the Lamarckian Algorithm (LA), as it was the most accurate algorithm available[94].

4.3.7 Consensus scoring

As consensus scoring can be used to potentially vastly increase the accuracy of a virtual screening[72], two main types of consensus scoring involving the ranks produced by each program were investigated. These were:

- Simple sum rank consensus scoring. The simple sum rank is obtained by calculating the sum of all the ranks obtained from all the programs, giving an overall consensus rank.

  i.e.: **(Glide ranks + GOLD Ranks + AutoDock ranks) = Ligand Simple Sum Rank**

- Deprecated sum ranked consensus scoring. This form of consensus scoring is initially the same as the simple sum rank, however, the worst scoring rank for each ligand is removed for the equation before the consensus rank is calculated.

  i.e.: **(Glide ranks + GOLD ranks + AutoDock ranks) – Worst Score = Ligand Deprecated Sum Rank**

As each docking program used did not score and return every ligand in the database, with some ligands rejected due to structural problems or other computational issues, a method was needed to match each of the ranks from the four different programs with their identifier codes into a single database. This was done using the KNIME analytics platform. KNIME uses a workflow of editable nodes as a replacement for code, allowing the user to perform similar data processing tasks without the need for knowledge of the intricacies of any coding languages. As well as this, it also contains nodes that can be edited using python, allowing for more complex coding to be included. The results of each of the screenings were exported from Maestro in the form of .csv files. The data from the .csv files for each docking method were sorted using the workflow shown in Figure 4.3 below. The data for each .csv file is first read by the csv reader nodes, which then pass the data to the column filter nodes, which select the columns that are needed. This data is then combined with the data of the previous .csv files using the joiner node, and finally the compounds missing a value are all given the highest rank for the respective program. This was then all written to a final consensus .csv file. KNIME was found to be extremely effective and intuitive and could be very easily applied to future screening projects as well.
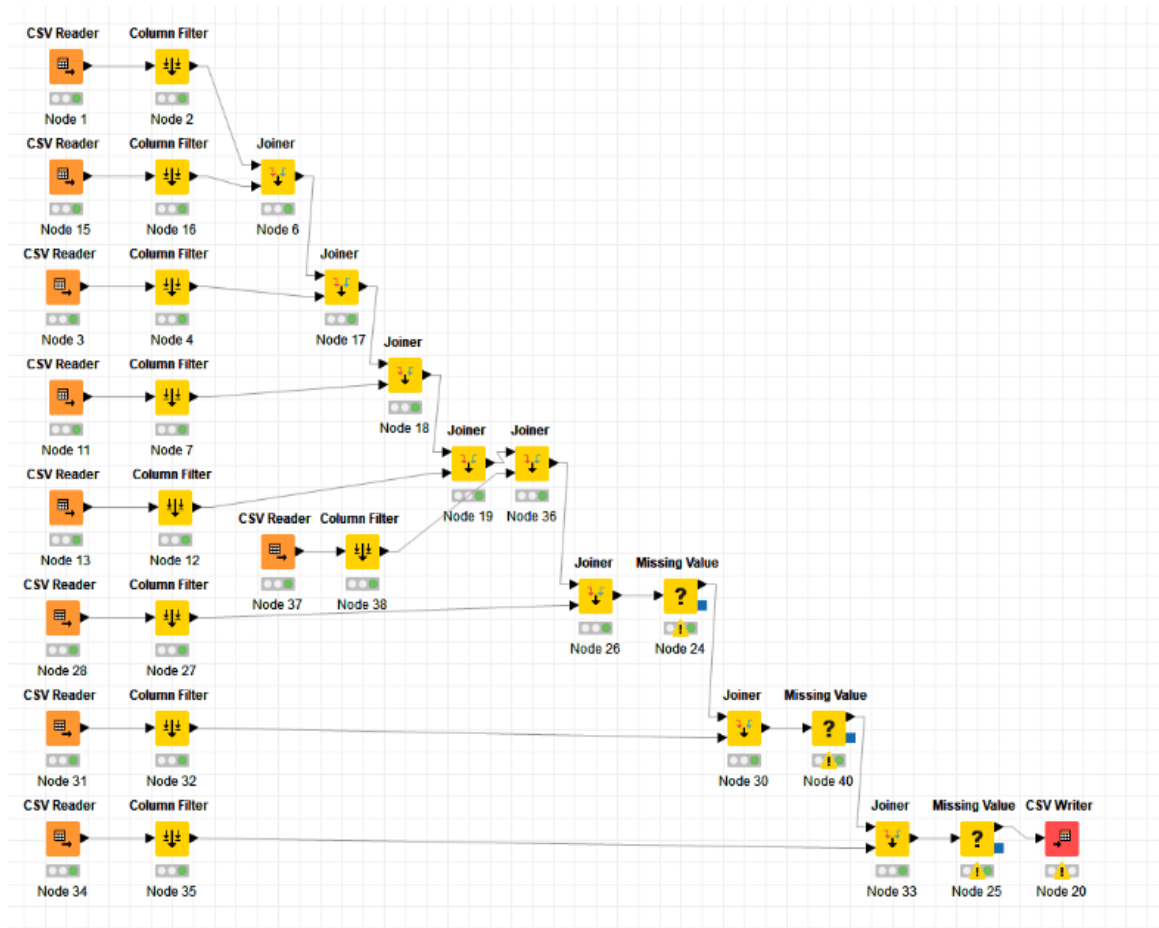
Figure 4.3: The KNIME workflow used to merge the .csv files containing the results from each of the docking programs into the final consensus score.

4.3.8   Statistical Analysis of Performance

Once the various docking calculations were finished and results imported into Maestro, they were then sorted by their scores to obtain ranks. For GOLD, the higher the fitness rating the better, and for Glide and Autodock the lower the score the better. The best score each ligand received was retained considering the tautomeric and ionisation states. Some statistical parameters that provide a much clearer view of the results of the docking performance were then calculated using the post process Enrichment Calculator available in Maestro[100], more specifically:

- The Enrichment Factor (**EF**): measures the Number of actives recovered in a database, relating the how many were recovered in the subset to the amount in the whole database. The enrichment factor is calculated using the following equation:

$$EF_{X\%} = \frac{n_a \div N_{x\%}}{\frac{n}{N}}$$

Eq. 4.1

$EF_{x\%}$ is the enrichment factor, (n_a) is the amount of actives received in a subset and ($N_{x\%}$) is the subset size. (n) is the total number of actives and N is the total number of compounds in the database.

- The modified enrichment factor **(EF'):** not only measures the number of actives recovered in a certain subset of the database, but how early they were returned in that subset The equation used for the calculation of **EF'** is:

$$EF' = \frac{50\%/APR_a}{n_a \div N_{x\%}}$$ **Eq. 4.2**

APR_a is the average percentage rank of the number of actives recovered. All other values are the same as in the **EF** equation

- The Receiver Operator Characteristic (**ROC**): a measure of the accuracy of a docking program that can be plotted, producing a curve. The area under the **ROC** plot curve, or **AU-ROC**, indicates the probability of a random active molecule to appear in the earlier subsets of a database than a random decoy molecule. The equation for the this is:

$$AU - ROC = 1 - \frac{\sum_{i=1}^{n} r_i}{n(N-n)} + \frac{n+1}{2(N-n)}$$ **Eq. 4.3**

In this equation, **n** is the number of actives, **N** is the total number of compounds in the database and r_i is the rank of the **i**th active

- The Boltzmann-Enhanced Discrimination Receiver Operator Characteristic (**BEDROC**): uses an exponential decay function allowing the reduction of the influence of lower ranked compounds on the overall score. The equation for this is:

$$BEDROC = RIE \times \frac{\frac{1}{N}\sinh\left(\frac{\alpha}{2}\right)}{\cosh\left(\frac{\alpha}{2}\right) - \cosh\left(\frac{\alpha}{2} - \alpha\frac{n}{N}\right)} + \frac{1}{1 - e^{\alpha\left(\frac{N-n}{N}\right)}}$$ **Eq. 4.4**

Where **n** is the number of actives, **N** is the total number of compounds, the **α** parameter provides the definition of the early recognition problem. For example, if the value for the **α** parameter is 20, it would cause 80% of the final **BEDROC** score to be taken from the first 8% of the ranks in the data set.

4.3.9   Design of Pharmacophore Models

Ligand based pharmacophore modelling calculations were performed using Phase [v4.5] [111] The first models were generated from the 30 actives and 189 inactives from the active/decoy ligand set, and the second set of models was developed using a selection of 17 crystal structure from Doerksen et al [77]. Conformations for each of these ligands were either generated using ConfGen 2.8 with "thorough sampling" exploiting MacroModel 10.4 or else taken directly (unchanged) from crystallized protein complexes, as described in the results. Solvation effects were included using the generalized Born/surface area (GB/SA) model for water. A threshold value of 10 kcal/mol above the global minimum conformation was used for saving structures, with a RMSD value (heavy atoms) of ≤ 1.0 Å used to eliminate redundant conformations.

The Survival Score defines how well active compounds are mapped onto a pharmacophore and it also provides an overall ranking of the hypotheses. Contribution to the ranking of the hypotheses includes the quality of alignment, which comprises of three parameters: the site score, vector score and the volume score. Survival Scores were also generated for our inactive molecules which allowed us to generate a new score, by subtracting the inactive survival score from the active survival score.

4.4 Experimental details

4.4.1 *In Vitro* testing of GSK-3β activity

All chemicals were obtained from Sigma Aldrich (Poole, Dorset, UK) unless stated otherwise.

The compounds selected were then tested *in vitro* at the Centro de Investigaciones Biologicas (CIB) in Madrid. The CIB is a part of the Consejo Superior de Investigaciones Cientificas, the public research centre in Spain and the third largest research institute in Europe. Two different tests were performed, a kinase inhibition assay to ascertain which of the compounds were inhibitors, and then an IC50 assay to determine the potency of the kinase inhibitor.

4.4.2 Luminosity assay for percentage inhibition

The GSK-3β enzyme (Millipore, UK) was stored as 10µg in MilliQ water (100µg/mL) a concentration10x stronger than needed and the enzyme was then stored at 80°C. On the day of the experiment, the enzyme was thawed and kept on ice prior to use and diluted to a working concentration of (22.72ng/10µl). The GSK-3β activity was assayed in a buffer solution, the components of which are shown in Table 4.2 below.

Table 4.2: A table of the various components that make up the Kinase Buffer solution used in the kinetics assays. (A): DDT was initially added to the buffer, but was found not only to be none essential to the reaction, but to also block the effects of some inhibitors, and was therefore removed.

Compound	Stock (dilution)	Final Conc	Volumes for 20ml KB
HEPES	500mM (10x)	50mM	2ml
EGTA	50mM (50x)	1Mm	0.4ml
EDTA	500mM (500x)	1mM	0.04ml
Magnesium acetate	1M (67x)	15mM	0.3ml
BSA	2mg/ml^{-1}	0.1mg/ml^{-1}	1ml
DDT [(A)]	10mM (10x)	1mM	2ml
MiliQ water	-	-	14.26ml
Total	-	-	20ml

The substrate used in this assay was GS2 (phospho-glycogen synthase kinase peptide-2 (Millipore)) which has the amino acid sequence:

Y R R A A V P P S P S L S R H S S P H Q (pS) E D E E E.

This substrate was diluted to a working concentration of 100 μM. ATP (Sigma) was also used as a substrate. This was stored at -20°C, 2.21 mg/ml H_2O (4 mM). On the day of the experiment, the ATP was diluted, creating a concentration of 40 μM ATP. This was then diluted further to a 4 μM working solution. The ATP and GS2 were mixed in an Eppendorf to create a substrate solution of 50 μM GS2 and 2 μM ATP, making the final concentration in the well 25 μM of GS2 and 1μM ATP.

All inhibitor compounds tested were diluted to 5 mM, by adding a volume of DMSO based on their molecular weight. When the assay began, these were further diluted in the reaction mixture to a final concentration of 50 μM. The Luminescent Kinase Assay (Sigma)(Kinase-Glo), used to produce the luminescence measured was stored at -20°C, and always kept protected from light. When the aliquots were prepared, the solid luciferin powder was kept in an amber glass bottle to protect it from light.

The controls used in this experiment were:

- **The ATP control**: These wells had neither the enzyme nor an inhibitor, used to obtain the maximum fluorescence value, and therefore the minimum activity value for the enzyme.

- **The ENZ control**: These wells contain the substrate mixture and the enzyme, but no inhibitor. This gives the value for 100% activity of the enzyme.

Firstly, 10 µl of the inhibitor compounds (10 µM final concentration) were pipetted into each well, in duplicate. In the first 4 wells, the ATP and enzyme controls, DMSO was added as a vehicle control, with the same volume of kinase buffer. The enzyme and substrate solutions were then added to their respective wells. The plate was then placed in an incubator for 30 minutes at 30°C, for the reaction to take place. Once this incubation period was finished, the Kinase-Glo was added to each of the wells. The plate is then covered to protect the Kinase-Glo from light, and the reaction is left to progress for 10 minutes. The plate is then placed into the Varioskan equipment (Thermofisher, USA), which measures the luminosity produced by the luciferin reacting. Once the Varioskan is finished with the plate, a set of luminosity data is produced and inserted into a spreadsheet. Following the subtraction of the average maximum positive values produced by the enzyme control, data were expressed as a percentage of the ATP blank.

4.4.3 IC_{50}

The *in vitro* IC_{50} assays were all performed by a member of staff at the CSIC in Madrid using the standard luminosity IC_{50} methodology [61]. Three different concentrations were used to create the curve to derive the IC_{50} from.

4.5 Computational results

4.5.1 Active/Decoy Ligand Set Results

RMSD for Redocking Crystal Structure Ligands

Root-mean-square-deviation (RMSD) is commonly used to validate the accuracy of docking protocols by re-docking the native pose of a ligand taken from a selected crystallographic complex back into the complex. RMSD for comparing two poses (predicted and experimental) is calculated using the equation below: 1

$$RMSD = \sqrt{\frac{1}{N}\sum_{i=1}^{N}\delta_i^2} \qquad \textbf{Eq. 4.5}$$

where δ is the distance between the number of pairs (*N)* of equivalent atoms. The RMSD values were generated for each docking method and scoring function considered, by redocking the 2OW3 ligand back into its native site. As well as this, the poses of the other four actives present in the active/decoy ligand set that have solved crystal structures were also used in a cross-docking to the protein from 2OW3 to assess the similarity of their poses to that of their native crystal structures. The PDB codes for these ligands are: 3I4B, 1UV5, 4ACG and 1Q3D.The structures of all 5 of these ligands are shown in Figure 4.4, and the RMSD values for redocking are shown in Table 4.3.
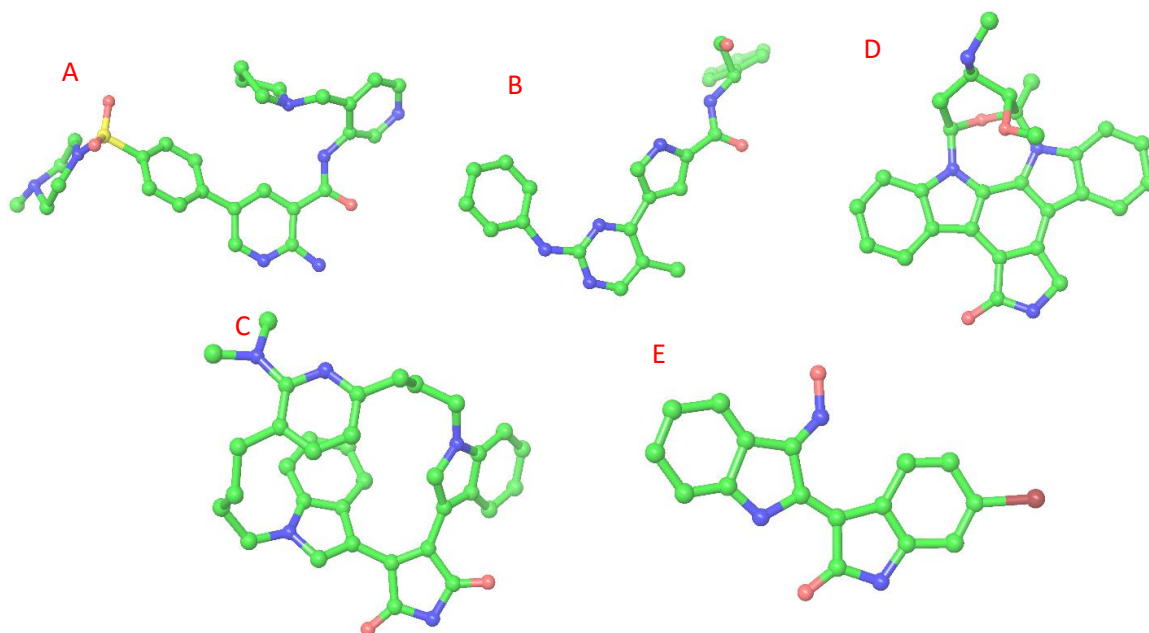
Figure 4.4: The structures of the 5 crystal complex ligands taken directly from their complex geometries in their bound conformations. **A**: 4ACG (CHEMBL2177173), **B**: 3I4B, **C**: 2OW3 (CHEMBL1087499), **D**: 1Q3D (CHEMBL388978), **E**: 1UV5 (CHEMBL3125370). Carbon atoms are displayed in green, oxygen in red, nitrogen in blue and sulphur in yellow.

An RMSD of <2.0 Å is generally considered a good value for docking poses compared to their crystallographic conformations. For 2OW3 (**C** Figure 4.4), the values for Glide-SP and Glide-XP, GOLD-ASP and GOLD-ChemPLP are all good RMSDs, less than 1Å. GOLD-ChemPLP, Glide-SP and Glide-XP are all Empirical Scoring functions, which could go some way to explain why their RMSD values are similar. The AutoDock scoring functions on the other hand, did not receive a score under 2 Å. The most plausible reason for this is the extremely large macrocyclic structure of the ligand, which may have caused the programs to penalize it based on its complexity. This could mean that these high RMSDs are not necessarily representative of what the RMSDs will be for all the other ligands in the database, which in general are a lot smaller.

Table 4.3: Redocking RMSD (Å) results (native and cross) for all of the scoring functions tested, Glide-SP and -XP, AutoDock 4, AutoDock Vina, GOLD-ASP and GOLD-ChemPLP. Scores below the generally accepted level of a good score (2.0 Å) are coloured green, scores just above this value are coloured amber, and scores more than 3.0 Å above this value are coloured red.

RMSD (Å)	Glide		AutoDock		GOLD	
PDB Code	SP	XP	AutoDock-4	Vina	ASP	ChemPLP
2OW3	0.711	0.732	3.772	3.383	0.781	0.717
3I4B	7.592	7.583	7.448	9.316	7.448	10.976
1UV5	1.275	2.291	1.305	5.407	6.265	2.410
4ACG	2.601	2.611	7.208	7.777	1.706	3.045
1Q3D	1.275	0.925	5.518	5.277	3.010	1.752

In contrast the ligand from PDB 3I4B (**B** Figure 4.4), another large ligand, received high RMSD values with all programs when cross-docked. While the crystal structure of 3I4B is positioned across the centre of the ATP binding site, the poses generated by the programs tended to bend around the cavity. This could be due to the shape of the 2OW3 cavity being larger, or due to the fact that this molecule is highly flexible, allowing the programs to drastically alter its shape while scoring it. Another ligand, 1UV5 (**E** Figure 4.4) received a very high RMSD of 5.407 Å with AutoDock Vina, which was much higher than the other programs, and a comparison between its pose and crystal structure can

be seen in Figure 4.5 below. The highest scoring pose has a high RMSD because it is flipped 180 degrees from the crystal structure pose. This, however, did not receive a docking score as bad as the RMSD would suggest. The reason for this could be that due to the shape of the molecule being similar on both sides, the score of the pose could have been improved greatly due to it being able to fit in the same space forming similar interactions. The cross-docking RMSDs are as expected not as good as those for the native redocking of the 2OW3 ligand. However, apart from the 3I4B ligand, RMSDs less than or close to 2 Å were obtained.
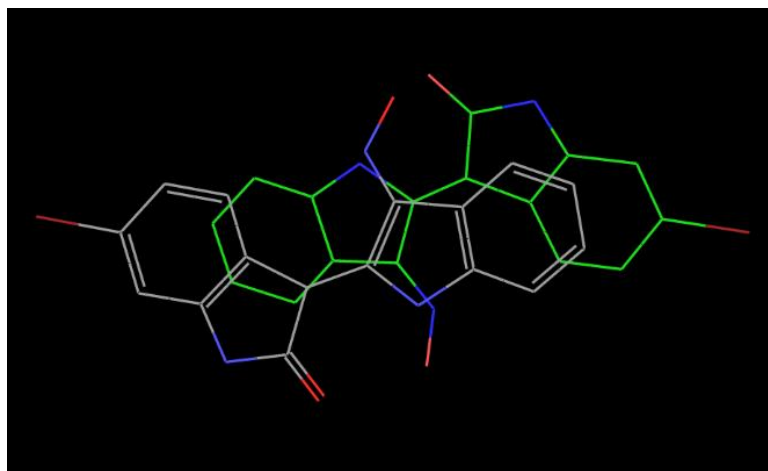
Figure 4.5: The crystal structure and the top AutoDock Vina pose for 1UV5 (Ligand E in Figure 4.4) superimposed on its crystal structure. The poses are flipped in relation to eachother, hence the RMSD of 5.407 Å.

Statistical Analysis of Docking Performance

The docking results produced by each of the programs used in the benchmarking screening (30 actives in a 2119 active/decoy set) were all assessed with Schrödinger's Enrichment calculator, the results of which are shown in Table 4.5 below. Performance was measured in terms of the ability of the methods to correctly identify and rank actives high in the database screened. A number of statistical metrics were considered for this purpose.

Table 4.5: Statistical analysis of benchmarking (active/decoy) screening results for the different scoring functions. The best score for each statistical metric produced by the individual docking programs are shown in *red italics*, while the best scores in each row for the tested consensus methods are in *blue italics*.

Statistical Parameters		Glide		AutoDock		GOLD		Consensus Method 1[a]		Consensus Method 2[b]		Consensus Method 3[c]	
		SP (GS)	XP (GS)	Vina	Auto-Dock4	ASP	Chem-PLP	SS [d]	ETW [e]	SS [d]	ETW [e]	SS [d]	ETW [e]
AU-ROC		*0.82*	0.79	0.75	0.68	0.79	0.71	0.87	0.88	0.87	0.86	0.89	*0.90*
BED-ROC	α=160.9	0.256	0.177	0.237	0.109	*0.262*	0.115	0.358	0.318	*0.375*	0.326	0.345	0.328
	α=20.0	0.382	0.319	0.299	0.156	*0.408*	0.201	*0.465*	0.456	0.434	0.421	0.455	0.472
	α=8.0	0.503	0.457	0.406	0.263	*0.521*	0.334	0.598	0.600	0.578	0.565	0.615	*0.630*
EF	1%	*20*	13	13	6.7	*20*	6.7	24	17	24	20	24	17
	5%	7.3	7.3	6	2.7	*8.7*	4	*11*	9.3	8.7	8	8.7	10
	10%	*5.3*	4	4	2.3	*5.3*	2.3	6.7	6.3	6.3	6	*7.3*	7
EF`	1%	*24*	14	22	8	21	7.3	36	25	*41*	31	33	29
	5%	13	10	10	4.2	*14*	5.8	*15*	*15*	14	14	14	*15*
	10%	8.5	6.8	6.5	3.3	*9.1*	4	*11*	10	9.8	9.4	*11*	*11*

[a] Glide XP and SP, GOLD ASP and ChemPLP, AutoDock Vina and AutoDock 4 [b] Glide-SP, Glide-XP, GOLD-ChemPLP and AutoDock Vina. [c] Glide-SP and -XP, GOLD-ASP, and AutoDock Vina [d] Simple Sum rank consensus method [e] Deprecated Sum rank (Exclude the worst). Docking programs were chosen based on the scores of the consensus methods, not their individual scores, which were used for comparison with those of the consensus methods.

In terms of individual programs and scoring functions, the two most accurate are shown to be Glide-SP and GOLD-ASP for the statistical parameters discussed in section 3.3.8. For AU-ROC, a value of 1 would indicate that a program returned all of the 30 actives as the top 30 ligands, where a value of 0.5 corresponds to random selection. The highest AU-ROC produced was Glide-SP with a value of 0.82, followed closely by GOLD-ASP (0.79) which was also equal to that of Glide XP. For the other methods, AutoDock Vina

(0.75), GOLD-ChemPLP (0.71) and AutoDock 4 (0.68), the values were all close to 0.7. To find the AU-ROC, a ROC plot is used. The ROC plots of Glide-SP, Glide-XP and GOLD-ASP, the three top performing programs in terms of AU-ROC are shown below in Figure 4.6.
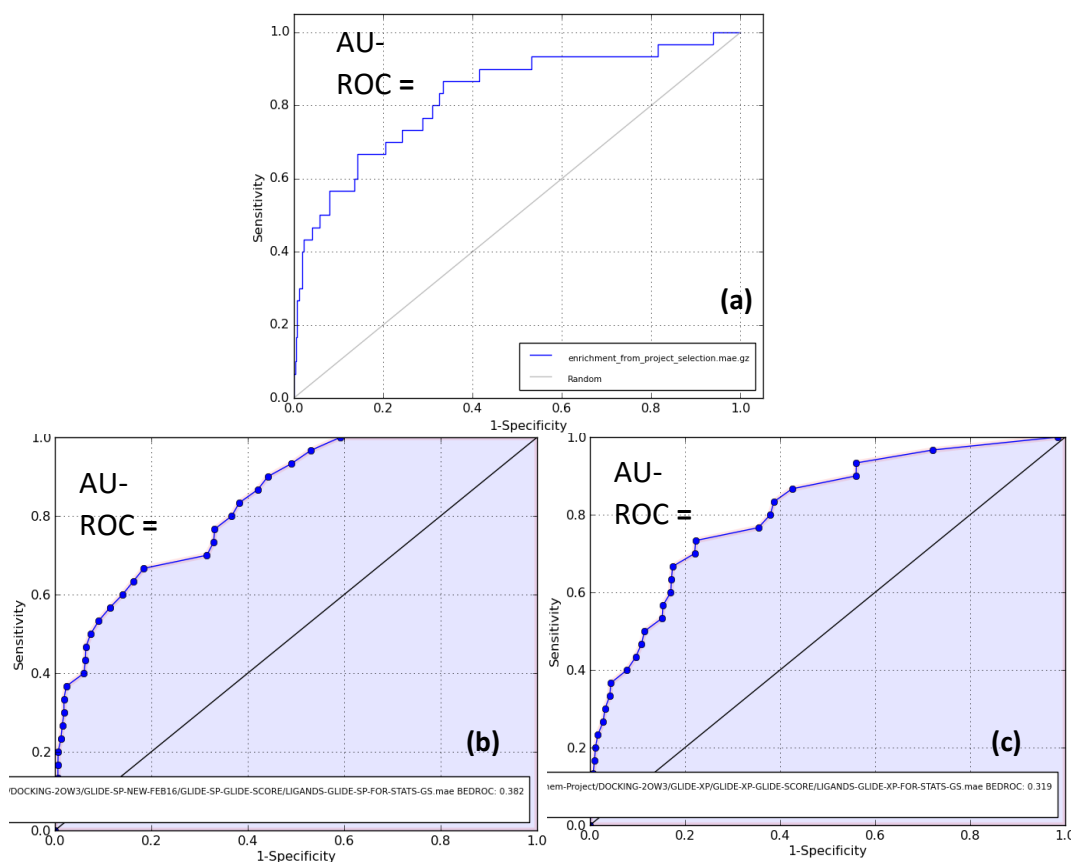
Figure 4.6: The ROC plots for the top 3 docking methods used and their AU-ROC values: (a) GOLD-ASP, (b) Glide-SP and (c) Glide-XP

While the AU-ROC values show that these programs were able to return the actives quite early, they are not good enough alone to assess the usefulness of a docking program for virtual screening. The next statistical parameter, the Enrichment Factor (EF) (Equation 4.1) can be calculated for certain percentages of the total number of ligands tested. In Table 4.2, the top 1%, 5% and 10% of the database have all been analysed, however, due to the fact that in large screenings only the top most part of the results is investigated, the 1% value will be taken to have more importance in terms of the accuracy of the method. In the case of the benchmarking database, the top 1% contains 21 compounds. For EF, a value of 1 would show that the programs ability to select actives from the database is equal to that of random selection. When the value is > 1, it multiplies the accuracy of the program at selecting an active from the database, for example a value of 4 would be four times better than random. Glide-SP and GOLD-ASP are the two highest scoring programs for EF, as they both received a value of 20 for the top 1%. This means that they are both 20 times better at returning actives in the top 1% compared to random selection. AutoDock Vina and Glide-XP are next, as they both produced a 1%

value of 13. This is then followed by GOLD-ChemPLP and AutoDock 4, which both produced a value of 6.7. In Figure 4.7 the EF values of Glide-SP and –XP, GOLD-ASP and AutoDock Vina are shown for the different percentages (1%, 5% and 10%) where we can clearly see higher and better values at 1% (The improved performance via consensus scoring will be discussed later).
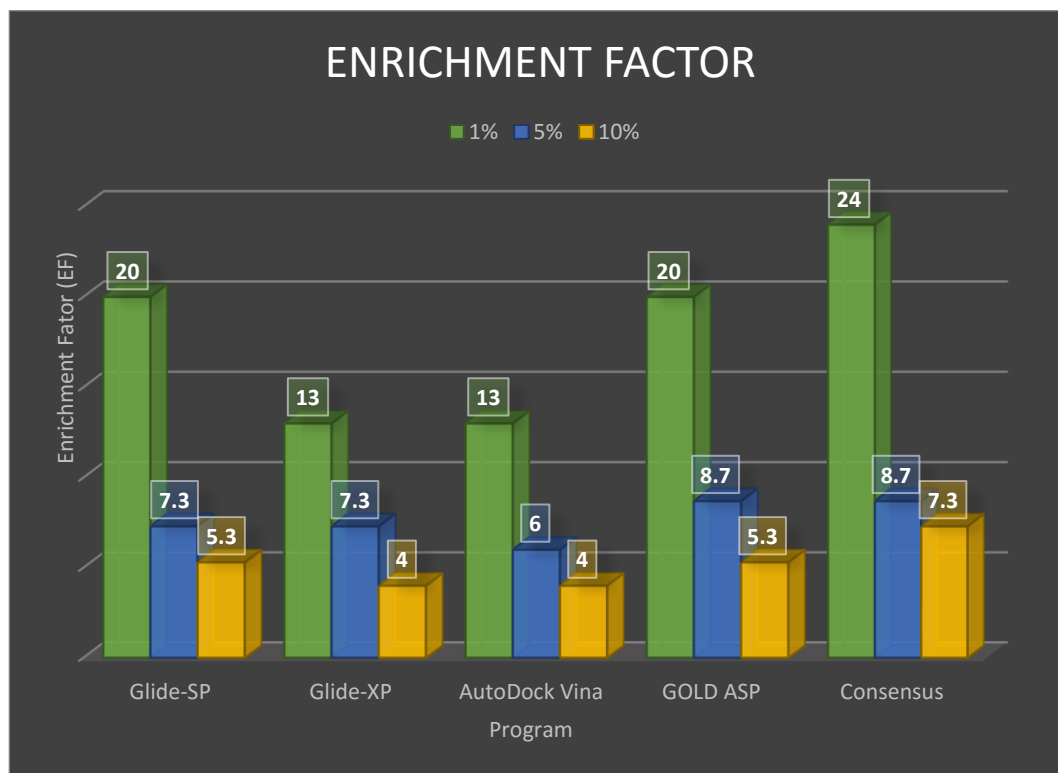
Figure 4.7: A comparison of the EF values obtained by the various programs and consensus method 3

Both AU-ROC and EF can be modified to account for the early recognition of compounds in the form of BEDROC (Equation 4.4) and EF' (Equation 4.2). As discussed above, in section 4.3.8, EF' is a version of EF that has been modified to take into account the early return of actives. BEDROC also focuses on early retrieval. The three BEDROC α values are similar to the three EF' percentages (1%, 5% and 10%). Similar to EF, we will focus on the 1% for EF' and the α value of 160.9 for BEDROC. The highest EF' value produced by any of the programs was a value of 24 for Glide-SP. Its BEDROC value was 0.256. GOLD-ASP on the other hand, which had the same value for EF, only received an EF' value of 21. While GOLD-ASP produced a BEDROC value similar to that of Glide-SP (0.262) its lower EF' value would indicate that Glide-SP was more accurate overall at selecting actives in the top 1%. While Glide-SP and GOLD-ASP returned the same number of actives in that section (1%), Glide-SP returned them earlier than GOLD-ASP. This means that EF' and BEDROC can be used to further differentiate between programs that produced the same EF values. Another example of this is AutoDock Vina and Glide-XP, which both produced the same EF value of 13. However, the 1% EF' value for

AutoDock Vina was 22, with a BEDROC value of 0.237, whereas Glide-XP produced lower values for both, with an EF' of 14, and a BEDROC of 0.177. AutoDock 4 and GOLD-ChemPLP had the lowest and similar EF' values of 8 and 7.3, respectively. The BEDROC were likewise similar at 0.109 and 0.115, respectively. Figure 4.8 below shows comparisons of the values for EF' and BEDROC of different docking programs. Again, the discussion of consensus method three can be found below.
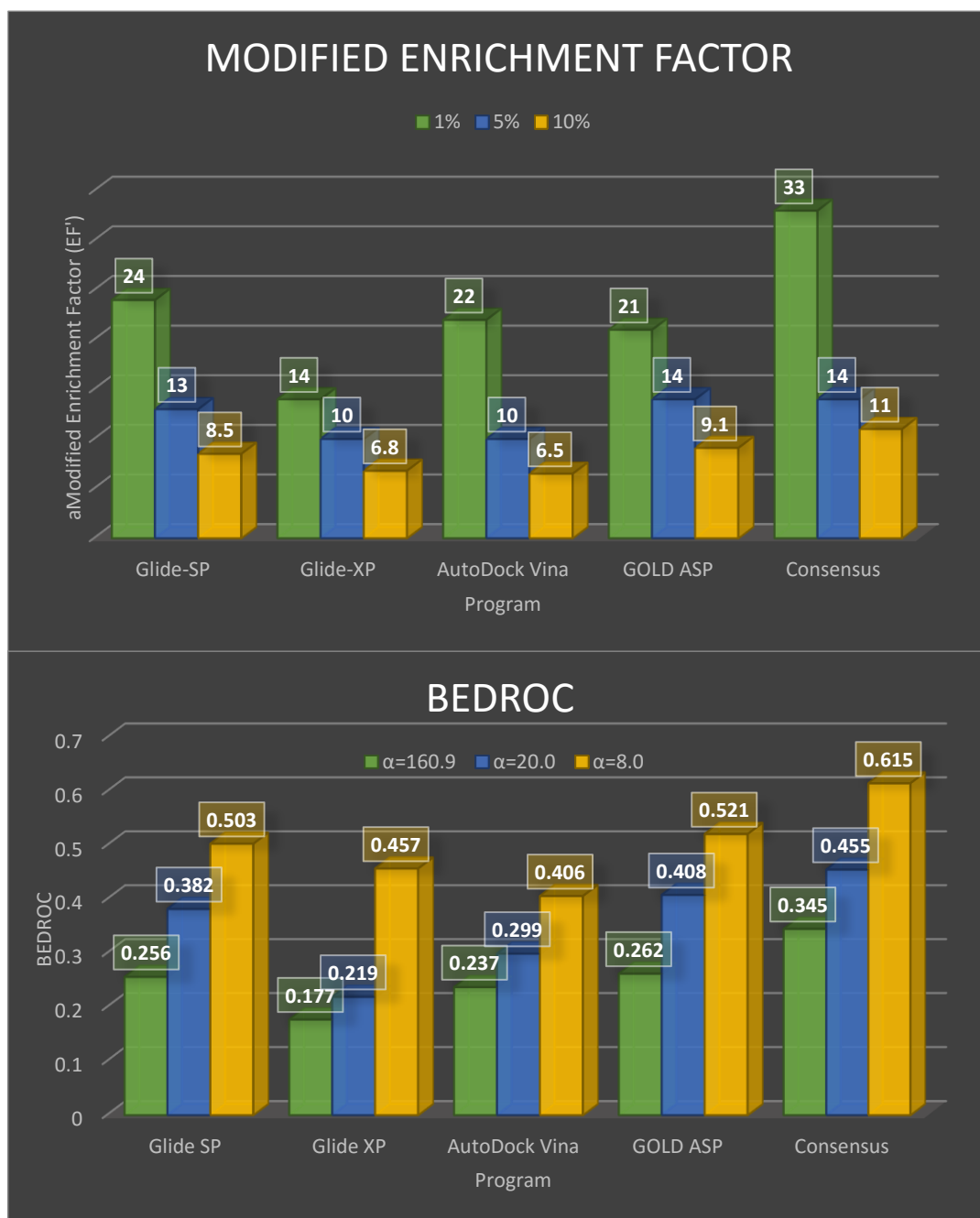
Figure 4.8: A comparison of the EF'(above) and BEDROC(below) values for each of the docking programs with those of the consensus method 3

Along with the statistical analysis, another good indicator of the comparative accuracy of each of the programs is to look at the ranks received by each of the 30 active compounds, shown below in Table 4.6. As can be seen, the native ligand for 2OW3,

CHEMBL1087499 (bis-(indole)malemide pyridinophane shown in Figure 4.2), was returned at an early rank by all six of the calculations. While this was an expected result, due to it being the native ligand, the fact that all of the programs recognised this ligand as a strong active is a good sign. The ligand was ranked first by both AutoDock programs, a stark contrast to the higher RMSD values these programs produced with the crystal structure, and the lowest rank it received was 28 (GOLD-ChemPLP), which was the only rank that placed it outside the top 1%. Actives that were ranked highly, were generally done so by a number of methods. Overall, most actives were ranked well by at least two programs.

Table 4.6: The ranks for the 30 known active compounds received from each of the docking programs used. The native ligand (2OW3) is shown in red.

Active	Vina	AutoDock	Glide-XP	Glide-SP	ASP	CHEMPLP
3I4B	758	296	240	206	595	217
CHEMBL1086735	573	1014	66	40	917	1741
CHEMBL1087499/2OW3	1	1	10	4	18	28
CHEMBL1092754	224	1033	383	48	50	268
CHEMBL1099297	865	1650	481	1266	285	355
CHEMBL1684800	33	858	1535	255	156	2
CHEMBL1940907	1576	1850	75	49	429	730
CHEMBL2048675	267	416	214	138	20	325
CHEMBL2071201	1494	849	816	823	515	938
CHEMBL215803	25	92	2085	790	1222	1640
CHEMBL2177173/4ACG	268	1719	486	170	14	122
CHEMBL2386093	2	17	25	11	38	452
CHEMBL2443026	34	543	1196	715	544	328
CHEMBL255735	1085	471	103	145	642	1024
CHEMBL270473	47	326	5	3	6	31
CHEMBL3085387	672	479	377	358	1577	1420

CHEMBL3091543	759	696	373	148	458	454
CHEMBL311228	1890	1856	1198	949	252	838
CHEMBL3125370/1UV5	574	74	42	20	1983	1729
CHEMBL317657	225	463	16	18	762	559
CHEMBL361708	1577	503	97	33	1933	2097
CHEMBL362155	5	195	763	709	7	64
CHEMBL380946	183	402	18	17	512	252
CHEMBL388978/1Q3D	48	626	30	60	89	288
CHEMBL402902	673	595	338	679	455	848
CHEMBL403405	269	681	914	311	59	411
CHEMBL412142	1086	1925	255	1053	129	595
CHEMBL472043	575	458	175	1137	30	79
CHEMBL562089	270	1444	833	405	3	20
CHEMBL65987	576	1203	333	904	9	387

Consensus Scoring Method

Various combinations of the docking programs in terms of consensus scoring methods were tested, to see which method was the most accurate at recognising the actives in the benchmarking library. This was done by applying either a simple sum rank (section 4.3.7) or depreciated sum rank (Exclude the worst), to the various combinations of programs. The statistics of the three main combinations are shown in Table 4.5, where they can be compared with the performances of the individual programs. As can be seen from Table 4.5, deprecated sum rank consensus scoring performed consistently worse than simple sum ranking and therefore will not be discussed further.

The first consensus method (**Consensus Method 1)** that was analysed with the benchmarking database was the combination as follows: Glide-SP, Glide-XP, AutoDock 4, AutoDock Vina, GOLD-ASP and GOLD-ChemPLP. The statistics produced by consensus scoring are shown in Table 4.5. Each statistical metric produced values superior to those of the individual programs e.g. EF'(1%) was 36 compared to the best value of 24 for an individual program (Glide-SP). However, during the full virtual screening, problems arose with the use of AutoDock 4, the program constantly struggled

with the size of the screening library. As well as taking over a month to finish the screening the program crashed constantly. It was therefore decided that a method would be designed that did not use AutoDock 4, as these problems were preventing the project from continuing.

Once AutoDock 4 had been removed from the various different combinations, there were two that gave similarly good results in terms of the statistics. **Consensus Method 2** contained: Glide-SP, Glide-XP, AutoDock Vina and GOLD-ChemPLP and **Consensus Method 3** contained: Glide-SP, Glide-XP, AutoDock Vina and GOLD-ASP

Both Consensus Method 2 and Consensus Method 3 contain 3 different search algorithms and 4 different scoring functions. They both outperformed the individual docking programs in all of the statistical metrics, for example their EF (1%) values of 24, compared to the highest single program which is Glide-SP with 20 as can be seen from Table 4.5. While their EF values are the same, Consensus Method 2 received the best 1% EF' (41) compared to that of Consensus Method 3 (33). For the actual screening, 157,238 ZINC compounds, both methods 2 and 3 were initially applied.

However, it was found that due to simple sum ranks being a total of their ranks across all of the programs, the totals for each ligand for method 2 were much higher than those of combination 3. Therefore method 3 produced a much closer consensus of the potential activity of the compounds in the screening library than method 2. As the aim of this screening is to use a selection of programs to obtain a largely unanimous consensus, this was deemed more beneficial to the results than having slightly better statistics in the benchmarking calculation. For example, despite method 3 having a lower value for the 1% of EF', this value only represents one or two actives performing better in the benchmarking database. On this basis Consensus Method 3 was applied, and the virtual screening was completed, taking around 4 to 5 weeks, with Glide-SP finishing the fastest.

Pharmacophore based analysis of virtual screening results

Once the virtual screening of the filtered database and ranking using Consensus Method 3 was completed, aided by the KNIME workflow shown in Figure 4.3, we selected the top ranked 200 compounds for further consideration. Another possible method that could help identify hits in our top 200 compounds was the design of a series of pharmacophore models that could identify compounds with groups conducive for favourable binding. The original attempt to design a pharmacophore model was based on all of the 30 active compounds in our active/decoy training set. However, the pharmacophore models produced were inaccurate in distinguishing the 30 actives from the 189 inactives, possibly due to the diversity within the active set; additionally confgen was used to generate the conformations. So, instead it was decided that a selection of X-ray

crystallographic poses of known active inhibitor compounds from a paper by Doerksen et al [72] would be used. 17 active inhibitor PDBs were selected from the paper, and the ligands were used in the poses in the PDBs, after the complexes had all been superimposed (PDBS: 2OW3, 1Q3D, 1Q3W, 1Q4L, 3I4B, 1UV5, 4ACG, 1Q5K, 1Q41, 2O5K, 3DU8, 3F7Z, 3F88, 3Q3B, 4ACC, 4ACD and 4ACH). Once the models had been designed, three were chosen, one 3-point, one 4-point and one 5-point pharmacophore. Table 4.7 below shows the statistics created for these and all pharmacophores (*c.f.* Section 4.3.9) by Phase [111] for all the Pharmacophores that were developed.

Table 4.7: The statistics for each of the pharmacophores generated by Phase [v4.5]. The models shown in bold were the three final models chosen (3-point, 4-point and 5-point pharmacophores)

No of Sites:	Hypothesis [a]	Survival score	Survival inactives	Active-Inactive	#MATCHES [b]
3	**ADR.6**	**6.269**	**5.303**	**0.966**	**15**
3	ADR.16	6.220	5.325	0.895	15
3	ADR.8	6.171	5.275	0.896	15
4	AADR.42	3.438	2.631	0.807	5
4	AARR.29	3.412	2.524	0.888	5
4	**ADRR.11**	**2.836**	**1.743**	**1.093**	**9**
5	**AAADR.3**	**3.024**	**2.078**	**0.946**	**5**
5	AAADR.2	2.742	1.724	1.018	5
5	AAADR.1	2.531	1.544	0.987	5

[a] A = H bond acceptor, D = H bond donor, R = Aromatic group [b] The number of actives out of the 17 inhibitors that matched the pharmacophore

The pharmacophores that were chosen were ADR.6 (3-point), ADRR.11 (4-point) and AAADR.3 (5-point) where A = H-bond acceptor, D= H-bond donor, R= Aromatic group. These were chosen based on mainly the Survival scores of the actives compared to those of the inactives (Active-Inactive)(Table 4.11) and represents the active survival score minus the inactive survival score. The higher the value, the greater the selectivity for actives over inactives. Another factor used in the design of these models was how many of the actual actives used in the design of the models fit the models: 15 for the 3-

point, 9 for the 4-point and 5 for the 5-point model. The 3D models of each of the three pharmacophores chosen are shown in Figure 4.9 below.
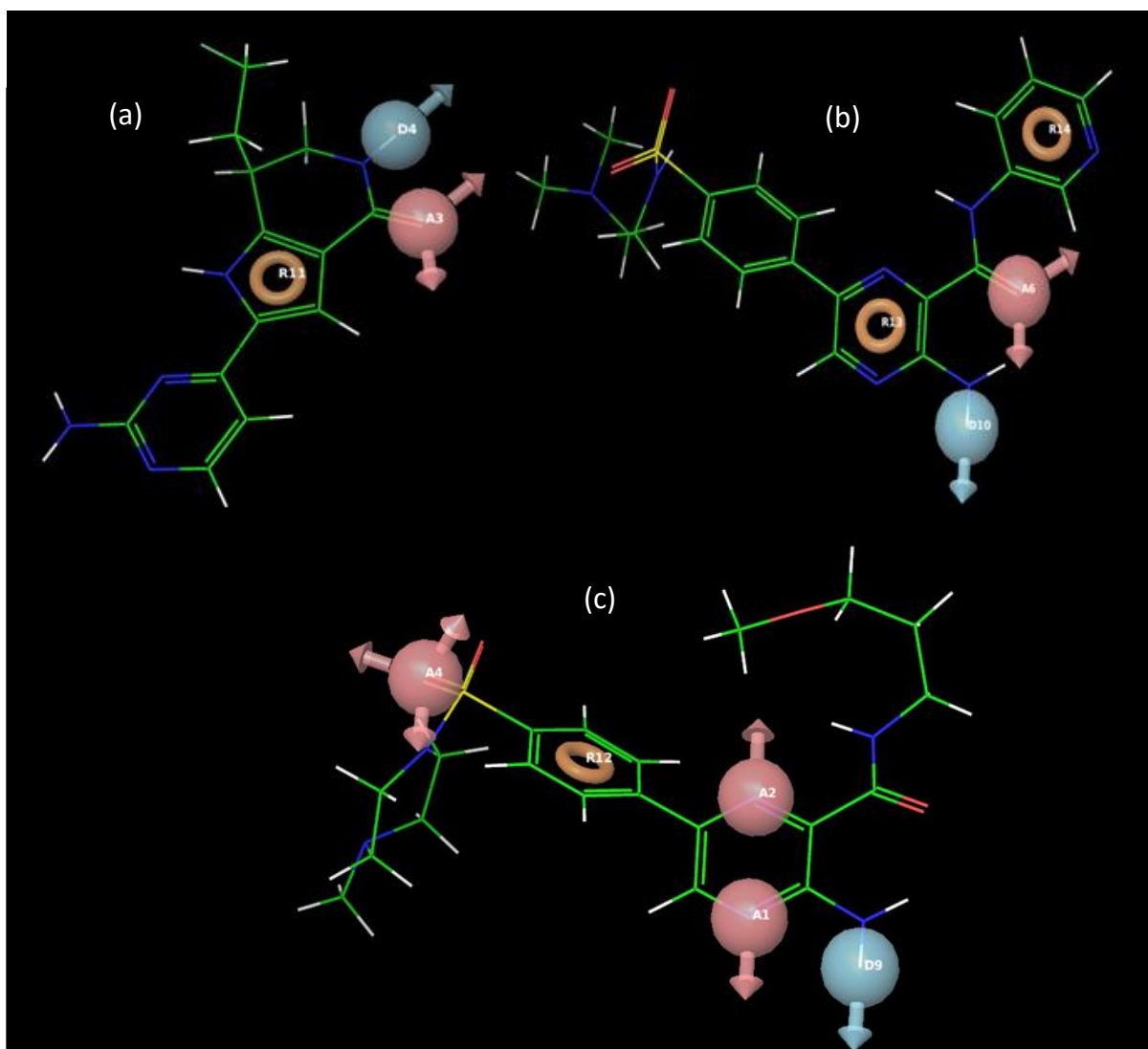
Figure 4.9: The 3D models of the three pharmacophores that were designed for use in this project. (a) ADR.6 the 3 point pharmacophore, (b) ADRR.11 is the 4 point pharmacophore and (c) AAADR.3 the 5 point pharmacophore. The red spheres indicate hydrogen bond   acceptors, the blue spheres indicate hydrogen bond donors, and the orange rings indicate aromatic groups.

These pharmacophores were then applied to our top 200 compounds. The number of compounds that fit the 3 point pharmacophore is 138, the 4 point pharmacophore fit 64 compounds, and the 5 point model fit 9. Data regarding which of the compounds fit the pharmacophore models produced after the virtual screening was added to the consensus method results using KNIME to be used as additional information for selecting the final compounds. These pharmacophore models were used at this stage after the virtual screening so that it did not reduce the number of compounds screened and particularly, the diversity. The full set of results (selection criteria) for the top 200 compounds are shown in the Appendix (Table S.1)

4.5.2 Selection of the compounds for purchasing

A total of 10 compounds (Figure 4.10) were selected for purchasing for the type I biological studies. Of these compounds, 6 were purchased from Enamine Ltd (ZINC000159432235, ZINC000273149682, ZINC000294625147, ZINC000355536096, ZINC000268128830 and ZINC000189195311) with purities of >95% in amounts of 3mg. The other 4 (ZINC000067820131, ZINC000072152229, ZINC000096131333 and ZINC000028406051) were purchased from Molport, with purities of above 90% in amounts of 1mg to 3mg. These compounds were selected by taking into account their consensus scoring rank, various ranks from the individual programs, as well as their binding interactions, and how well they fit the three pharmacophore models (Table 4.8). Another factor in the decision to select these compounds for further study was the diversity of their binding modes. While the hinge region has great importance in the binding of inhibitors to the ATP binding site, it has already been explored in great detail [30], and to avoid trying to "reinvent the wheel", we allowed for a much higher diversity in the selected compounds. On top of this, Bharatam et al. [90] outlined a selection of interactions that ligands can have with the enzyme that improved kinase selectivity. Key examples of this are residues Phe67, Arg141, Pro136 and Cys199. These interactions were also searched for with our selected ligands.
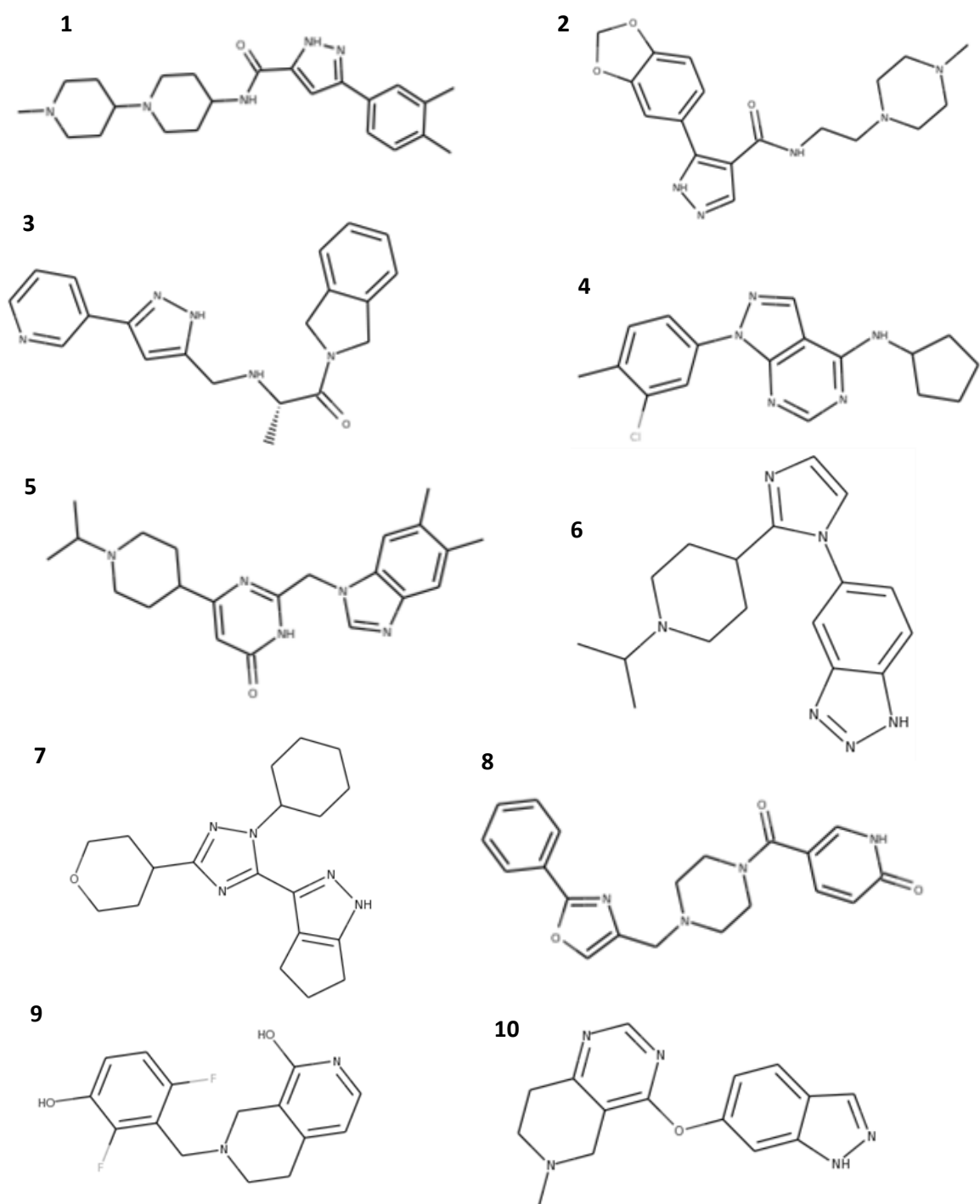
Figure 4.10: The structures of the 10 potential type I inhibitors selected for further testing from the completed *in-silico* study. They are in order: (**1**) Z189195311, (**2**) Z27314982, (**3**) Z355536096, all three of which are all Pyrazole derivatives, (**4**) Z28406051, a derivative of Pyrazolo Pyrimadine, (**5**) Z67820131, a Pyrimidinone, (**6**) Z72152229, an Imidazole, (**7**) Z96131333, a Triazole, (**8**) Z159432235, a Napthyridine, (**9**) Z294625147, a Pyperazine, and (**10**) Z268128830 an Indazole.

Table 4.8: The consensus ranks from method 3, individual program ranks and other information used to select the 10 compounds chosen for biological assessment.

Title	Consensus Rank	SP Rank	XP Rank	ASP Rank	Vina Rank	#rotor	CNS	Mw (Da)	3Pt	4Pt	5Pt
Z67820131	6	287	463	1714	252	3	1	379.504	1	1	0
Z355536096	7	1050	649	142	990	4	1	347.419	1	1	0
Z159432235	20	68	50	282	5542	3	1	364.403	0	0	0
Z72152229	24	94	1557	926	3992	1	1	310.401	1	0	0
Z96131333	50	5033	1777	1098	1172	0	1	341.455	1	0	0
Z273149682	89	4308	3641	2281	1757	4	1	357.411	1	0	0
Z28406051	92	80	173	7889	3918	2	1	327.816	1	1	0
Z189195311	98	758	2601	7866	1692	2	1	395.547	1	0	0
Z268128830	125	722	7717	4785	1258	2	1	281.316	1	0	0
Z294625147	152	5	640	5131	10314	3	1	292.285	1	1	0

As can be seen from Table 4.8, the compounds that were selected range in consensus rank between 6 and 152. Similar to the actives in the benchmarking study, all of these compounds were ranked well (possible ranks 1-157,238) by the individual programs used in the consensus method. Very few compounds received more than one rank over 5000 and generally at least 2 docking programs ranked each compound in the top 1% (<1572). The table also shows that the compounds selected have at most 4 rotatable bonds, with the average being 2.4. This shows that they are relatively rigid, an important quality for inhibitors and also values were consistent with blood brain barrier activity. The range of molecular weights for the 10 compounds is 280-396 Da which, when compared to bis-(indole)malemide pyridinophane ligand native to 2OW3 (541.665 Da) is much smaller but similar to that of other active ligands. On top of this, they all received a CNS value of 1, which indicates the ability to cross the blood brain barrier, further validation of this would involve an *in vitro* blood brain barrier model. The final set of information shown in Table 4.12 is the ability of each compound to match the 3 developed pharmacophore models. While all but one of the chosen compounds fit the 3-point model, only 4 fit the 4-point pharmacophore. The 5-point pharmacophore produced no matches with any of these compounds, however, this is unsurprising, as we selected molecules of a smaller size, meaning that the 5-point pharmacophore tended to be too large. It was

also found that the 5-point pharmacophore matched compounds that were highly flexible in the top 200 (Table S.1), due to its large size, and therefore the ability to fit the 5 point model was not weighted as much as the 3 and 4-point models.

4.6 Biological results

4.6.1 Type I Luminosity assay results

The 10 compounds chosen for *in vitro* studies are shown in Figure 4.10. The first assay, involves the use of the GSK-3β enzyme to phosphorylate the substrate GS2 using ATP, which is then converted to ADP. There is also a second reaction employed after the first in this assay. This reaction uses ATP to convert beetle luciferin to Oxyluciferin +(Figure 4.12), which produces luminescence.
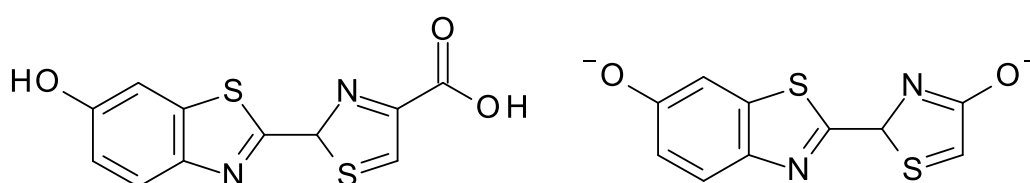
Figure 4.12: The structures of luciferin (left) and oxyluciferin (right)

Due to the fact that both consume ATP as part of the reaction, the second luminescence reaction can be used to quantify the activity of the enzyme during the first. This is because the stronger the luminescence produced, the more ATP is left over from the enzymatic process. Therefore if compounds that are able to inhibit the activity of GSK-3β are included in the first reaction then there will be more ATP available for the second, linking luminosity to % inhibition quantitatively. The results of this assay are recorded as a percentage of inhibition relative to the 100% ATP (average negative) and 0% enzyme (average positive) controls. This is calculated using the equation:

$$\%Inhibition = 100.0 \times \frac{(Raw\ data\ of\ compound - Average\ Positive)}{(Average\ Negative - Average\ Positive)} \qquad \textbf{Eq. 4.5}$$

No changes to the method were made during the assay, and the results that were obtained are shown below in Table 4.9.

Table 4.9: the experimental data produced for each of the 10 Type I compounds that were tested in the assay. The only compounds that produced an inhibition of over 50% (relative to the ATP control) at 50 mM is shown in bold.

Type 1 Compounds	Compound number (Zinc code)	Mw	Purity (%)	% Inhibition	IC$_{50}$ (µM)
71574548	Compound **5** (ZINC000067820131)	379.508	>90	21.04±2.55	-
43020696	**Compound 6 (ZINC000072152229)**	**310.405**	**>90**	**74.58±1.49**	**24.69 ±0.73**
13803800	Compound **7** (ZINC000096131333)	341.459	>90	20.11±2.17	-
STK889681	Compound **4** (ZINC000028406051)	327.82	>90	22.64±3.08	-
Z1505361204	Compound **8** (ZINC000159432235)	364.405	>95	1.61±3.81	-
Z1654883190	Compound **2** (ZINC000273149682)	357.414	>95	1.05±2.26	-
Z2226503926	Compound **9** (ZINC000294625147)	292.285	>95	4.33±1.60	-
Z3183855702	Compound **3** (ZINC000355536096)	347.422	>95	25.19±1.57	-
Z1408593245	Compound **10** (ZINC000268128830)	281.319	>95	1.22±1.22	-
Z1764937623	Compound **1** (ZINC000189195311)	395.551	>95	20.92±2.03	-

As can be seen from the table, we obtained a range of percentage inhibitions, with the highest being ZINC000072152229 (Compound **6**, Figure 4.10) with 74.58% and the

lowest being ZINC000273149682 (Compound **2**) with 1.05%. 6 compounds in total received an inhibition of over 20% and only one received an inhibition of over 50%. A noticeable trend in the results however, is that the compounds that were supplied by Enamine Ltd. mostly struggled to achieve an inhibition of over 5%. On the other hand, every compound that was ordered form Molport produced an inhibition of over 20%. The binding modes of the two compounds with the highest percentage inhibitions, Compound **6** and Compound **3** are shown in Figure 4.13.

As can be seen in Figure 4.13, both of the two best performing ligands formed multiple interactions with the hinge region (hydrogen bonding with Asp133 O and Val135 NH). This is unsurprising, as hinge region interactions greatly increase the potency of kinase inhibitors. The best performing ligand, Compound **6** (ZINC000072152229), as well as forming two interactions with the hinge region, hydrogen bonds with the Asn96 sidechain O towards the back of the site. These interactions keep the ligand, locked in its position. The positively charged nitrogen of the ligand is positioned near the acid group of Asp200, allowing a strong ionic interaction to take place (seen clearly in the 2D representation). In terms of selectivity, compound **6** only formed one of the interactions Bharatam et al. described as favourable, a π-cation bond between the positive nitrogen and the phenyl ring sidechain of Phe67. Compound **3** (ZINC000355536096) on the other hand forms 3 hydrogen bond interactions, all with the hinge region. The only other interaction it forms is the selective π- π stacking interaction with Phe 67. Its IC_{50} value 24.69±0.73 µM

The similarity in interactions between these two ligands cause them to have comparable binding modes. Neither ligand forms any strong selective interactions and the bulk of their binding happens at the hinge region. The biggest difference between the binding modes of these two compounds is the strong ionic interaction between compound **6** and the acid of Asp200. This interaction is therefore likely the cause of the large difference in potency. However, compound **3** was chiral, purchased as a racemic mixture, so here in relativity the R enantiomer that we screened is likely to have a greater inhibition value, as the other enantiomer in the racemic mixture has no potency.
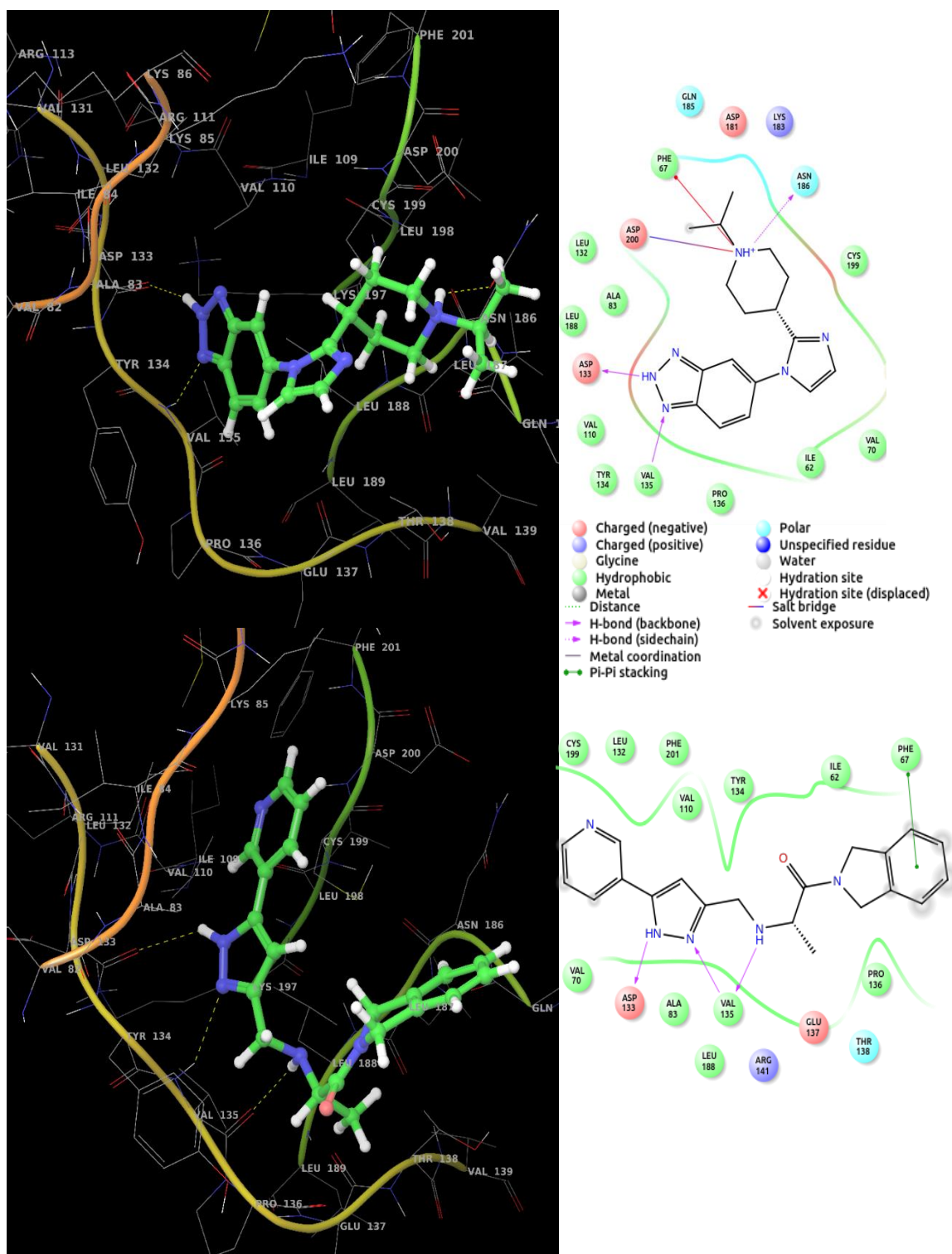
Figure 4.13: The binding modes, in 2D and 3D, of the two inhibitor compounds with the highest percentage inhibition values, A) Compound 6 (ZINC000072152229) (74.58%) and B) Compounds 3 (ZINC000355536096) (25.19%).

4.6.2 Type I IC$_{50}$ Assay Results

As it was the only compound of the 10 tested to receive an inhibition of over 50% at 50µM, ZINC000273149682 (compound **6**) was the only compound to have its *in vitro* IC$_{50}$ tested. The plotted graph of this is shown below, in Figure 4.14, and the IC$_{50}$ taken from this graph is 24.69 ± 0.73 µM.
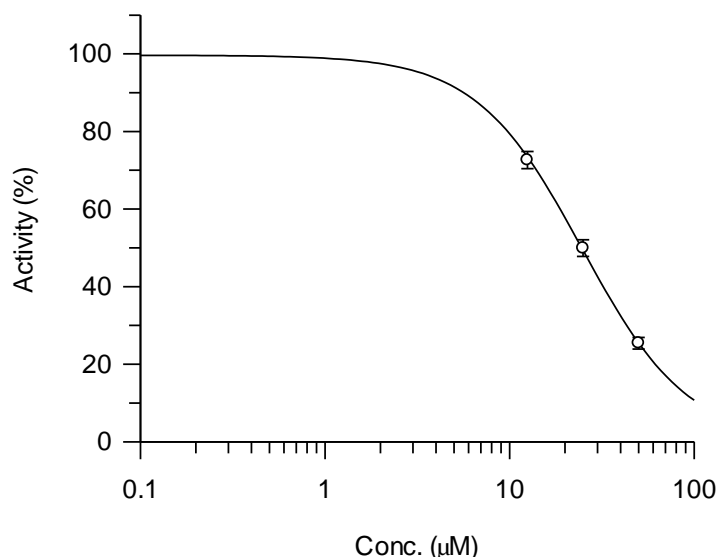
Figure 4.14: The % activity of GSK-3β plotted against concentration of the inhibitor ZINC000273149682.

While this value is relatively high when compared to the IC$_{50}$ of the native ligand of 2OW3 (3 nM), it shows the ligand has potential for modification to improve its binding affinity. The lower potency of compound **6** will also cause it to have reduced toxicity, as well as a reduction in the potential for side effects.

4.7 Conclusion

From the results of the benchmarking screening shown in this chapter it can be concluded that the consensus scoring was successful in terms of more accurately selecting active compounds from an active/decoy training set of ligands. The first evidence of this is the statistical values produced for EF (Figure 4.7), EF' and BEDROC (Figure 4.8) by the final consensus method. The values for each of the metrics are all significantly greater than those of the individual programs. This shows that the consensus method consistently outperformed the individual programs in the benchmarking study. On top of the consensus scoring method that was used, other methods of improving the accuracy of the results were also trialled. The pharmacophore models served to create an extra set of data with which the accuracy could be improved. As can be seen from the final 10 structures of the compounds selected, while they are diverse, they also share common features. We tried to select compounds with various other interactions as well as inhibitors that bind to the hinge region, which have been

explored in depth as we wanted to avoid "reinventing the wheel". The results of the luminosity assay showed 6 of our 10 compounds to have a percentage inhibition of over 20%, with compound **6** even receiving a value as high as ~75% at 50 µM , and an IC_{50} of 24.69 ± 0.73 µM. As compound **6** binds mainly via the hinge region, its activity was not a large surprise; however, it also forms an ionic interaction at the back of the binding site with Asp200. The ligand is not inherently selective, however, further modifications could be made to improve its selectivity at a later stage. Looking at these results, the best course of action is possibly picking ligands with a larger amount of hinge interactions, and to take more into account the ligands size and flexibility, as the better performing ligands were smaller and more rigid. Based on the data obtained in this project, and looking at the compounds that were successful and those that were not, these two are factors affecting potency. Ionic interactions similar to that of compound **6** should also be searched for, as this interaction caused a clear increase in activity compared to the similarly binding compound **3**.

Chapter 5: *In Silico* Screening and Experimental Validation of GSK-3β Type II Inhibitors

5.1 Introduction

Alzheimer's disease (AD) is a neurodegenerative disease, and the most common type of dementia present in the world today. As all the treatments that are currently available do little more than alleviate the symptoms of the disease, there is a real need for new effective treatments to be designed, as the number of patients rises. Hooper et al. [18] published 'The GSK-3 Hypothesis of Alzheimer's Disease' in 2007, a paper summarising the evidence of the involvement of a Ser/Thr kinase; Glycogen Synthase Kinase-3 beta (GSK-3β), in the formation of amyloid plaques and neurofibrillary tangles. Therefore, inhibition of the enzyme has the potential to block the formation pathways of these two pathological features, producing a sorely needed new treatment for AD. While the type I inhibition (ATP binding site) of this kinase has been well explored, it suffers from large selectivity issues, and as such, researchers are turning to other types of inhibition. Type II inhibition in kinases is much less common than type I, and has the potential to be much more selective [112]. It involves the binding of inhibitors to the DFG-out conformation of the binding site (Figure 5.1), in which the DFG activation loop flips, placing the sidechain of the phenylalanine outside of the loop. This causes the opening of a new allosteric pocket that can be occupied by an inhibitor, preventing the loop from returning to its original position.
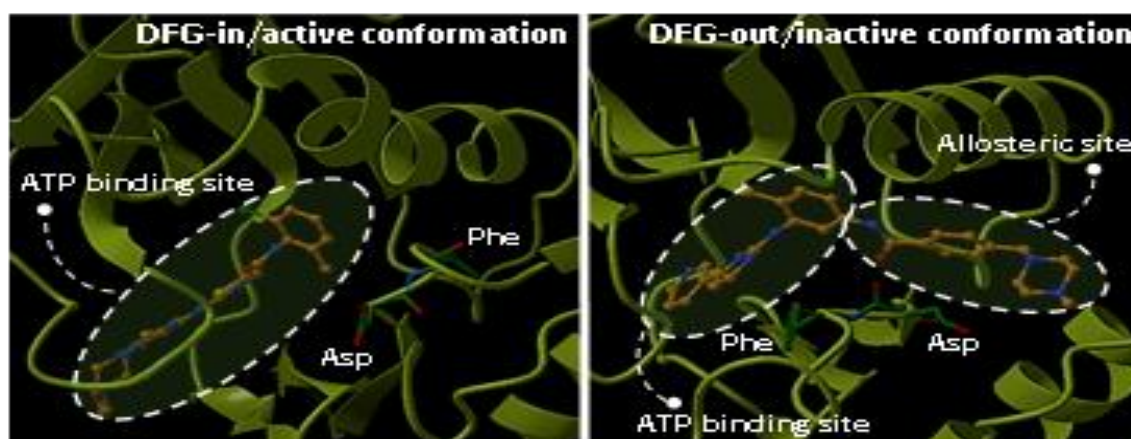
Figure 5.1: The difference between the DFG-in (left) and DFG-out (right) conformations of the activation loop in ABL kinase, co-crystallised with imatinib. The respective PDBs are 2GOG and 1IEP.

The opening of this loop also positions the backbone of the aspartic acid of the DFG-in such a way that allows formation of the "classical" interactions of a type II inhibitor, (a) one hydrogen bond with the DFG loop Asp, (b) one or two with the Glu from the αC helix and (c) an interaction with the hinge region. Type II inhibition is a much newer field than type I, and as such has not been fully proven to work with GSK-3β, as it is not possible

with all kinases. There are a number of factors that could prevent type II inhibition, the key factors being intermolecular interactions preventing the DFG loop flip, as well as the gatekeeper residue, which occupies the space near the opening of the allosteric pocket. If this gatekeeper is too large it can block the binding of inhibitors even if the loop is flipped out. Recently, Grütter et al [56] published evidence of the *Ustilago Maydis* form of GSK-3β undergoing type II inhibition. While doing this they also showed the same type II inhibitors interacting and inhibiting (although less strong) the human form of the enzyme, potentially indicating that the type II inhibition of human GSK-3β is possible. If true, this would provide a selective new option of the inhibition of the enzyme as a possible pathway towards ne AD treatments. In this chapter, we present the *in silico* design of two different DFG-out models, created using two different methods. The first will be created using DOLPHIN (Deletion Of Loop PHe-gly-IN) docking, which is a method of creating a Type II screenable structure without forming a DFG-out conformation. Proposed in a paper by Kufareva et al [34], DOLPHIN involves the deletion of the phenylalanine from the DFG loop, along with the next 4 residues. The deletion of this section does not affect any of the important interactions that are formed in Type II complexes in this area of the site, for example the hydrogen bonds with the glutamine of the C-Helix, and the hydrogen bond with the aspartate of the DFG loop. The conservation of these interactions means that even though a section of the loop has been deleted, the binding mode of type II inhibitors can still be accurately explored. The second will be made using a combination of Prime loop prediction to flip the DFG loop out, induced fit docking to further refine the site around a known type II inhibitor (sorafenib) and then molecular dynamics for a final structural refinement. These models were then used to screen a database of compounds taken from the Biogenics subset of the ZINC database [33]. The results of these screenings were combined into a consensus score, and this was used to select 20 potential type II inhibitors. Following this, these compounds were taken to the Consejo Superior De Investigaciones Cientificas (CSIC), for *in vitro* validation binding assays of enzyme inhibition.

5.2 Aim

To design two accurate DFG-out models of GSK-3β for use in the *in silico* screening of a database for the selection of a group of potential type II inhibitors. The *in vitro* testing of the selected candidates with human GSK-3β will then follow this.

5.2.1 Specific Objectives

- To design two DFG-out models of GSK-3β, using two different techniques; DOLPHIN docking and Prime/Molecular Dynamics predictions

- To validate these models using known inhibition data of sorafenib and BIRB analogues from Grütter's paper

- To use these two designed models for GSK-3β type II inhibition to screen a subset of the ZINC database for potential lead compounds

- To choose a selection of compounds from the *in silico* screening for biological validation, with the human GSK-3β

5.3 Computational Methods

5.3.1 Creation of the Type II Validation Ligand Set

A set of ligands were first used for validating the designed type II models. For this, 8 ligands of the two type II inhibitor scaffolds, sorafenib (3 analogues) and BIRB (5 analogues) previously studied for human GSK-3β inhibition (as well as fungal *Ustilago Maydis* GSK-3β inhibition) were chosen. Their structures, together with their inhibition data is shown below in Figure 5.2. These ligands were built using Maestro and prepared for docking using LigPrep, at a pH of 6-8 with the chiralities determined from the 3D structure. After Ligprep [v3.6] the total amount of ligands was still 8, and this ligand set was ready for the validation screenings.
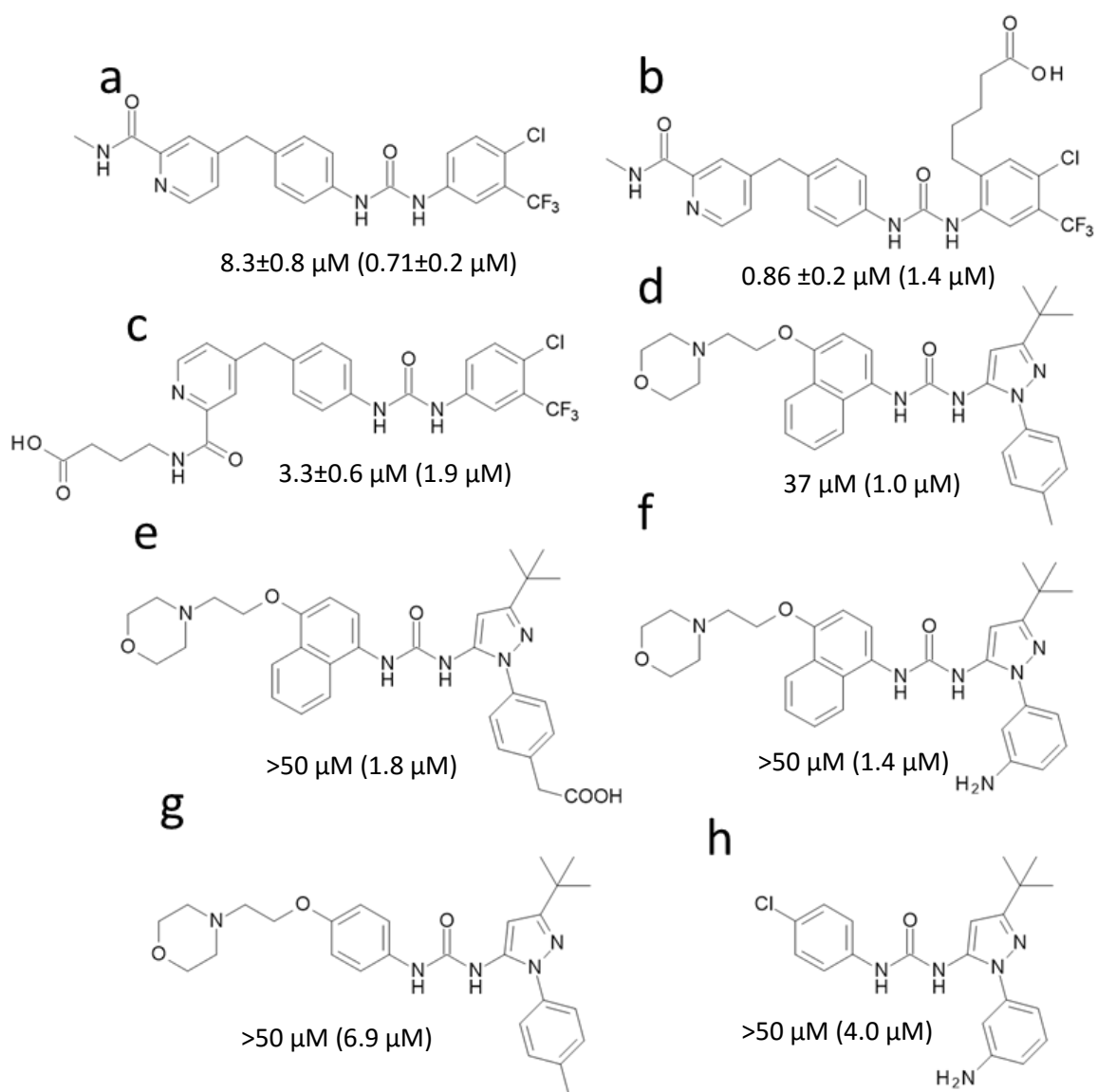
Figure 5.2: The analogues of sorafenib and BIRB used to create the validation ligand set together with their inhibition data against human GSK-3β. IC_{50} against fungal Ustilago Maydis GSK-3β are given in parenthesis. (a) sorafenib, (b) sorafenib 16, (c) sorafenib 17, (d) BIRB, (e) BIRB 12, (f) BIRB 13, (g) BIRB 14 and (h) BIRB 15

5.3.2 Acquisition of the Biogenics Subset Database from ZINC15

The Biogenics subset from the ZINC15 database was used for the actual virtual screening. The Biogenics subset is a database containing 135,000 compounds, 61,000 of those being purchasable. The purchasable filter was applied to the Biogenics subset and the compounds were downloaded. When the purchasable compounds were downloaded, only 47,000 natural products and their derivatives and chemically modified versions were openable in Maestro. Once the subset was fully downloaded, the structures were minimised with Macromodel, using OPLS3 as the force field, TCNG (Truncated Newton Conjugate Gradient) was selected as the minimisation method, and the maximum iterations used was 300. The rest of the settings were left as their defaults.

Qikprop [v4.6] was then used to predict values with which to filter the compounds, all settings for this were left as default. It was filtered using the filter rules shown in section 4.3.2 (MW ≥ 200 and ≤ 650, logP O/W between and including 0 and 5, amount of Hydrogen Bond Acceptors (HBAs) on the molecule ≥ 0 and ≤ 10, amount of Hydrogen Bond Donors (HBDs) on the molecule ≥ 0 and ≤ 5, number of rotatable bonds less than or equal to 8 and a predicted CNS of 0 or above) to increase the potential of the compounds to cross the blood brain barrier, which left 27286 compounds. This filtered screening database was prepared using the same LigPrep protocol as the validation ligand set. Once the database was prepared, the total ligand amount came to 45092 with tautomers and ionisation states.

5.3.3 DOLPHIN Model

Model Creation

The PDB that was used to create this DOLPHIN model was 2OW3. The preparation of the protein was carried out with Schrödinger`s Protein Preparation Wizard[113]. Water molecules more than 5 Å from heterogenic groups were removed, bond orders were assigned and all missing hydrogen atoms were added. The OPLS3 forcefield was used for a restrained minimisation to refine the system, with heavy atom convergence set to an RMSD of 0.3 Å to remove steric cla

shes. The rest of the water molecules were then removed to prepare the enzyme for a subsequent docking. Using Schrodinger's Maestro, the phenylalanine of the DFG loop (Phe201) was selected and deleted, along with the next 4 residues (202-205). A Glide grid-generation was then attempted, however, it failed due to incomplete valences. In the original DOLPHIN paper they had left these sections uncapped, however, as this was not possible in Maestro, the use of a hydrogen atom to cap the backbone sections that had incomplete valences was investigated. Upon contact with the author, the possibility of using these caps was discussed, it was decided that it would not affect the overall accuracy of the models structure. Once these sections had been capped, the Glide grid generation was then continued. Furthermore, the use of a similar approach in the original paper yielded consistent results with the electrostatic/DOLPHIN approach.

DOLPHIN Docking Details

To create an initial Glide grid for positioning a ligand into the site, the centre of a selection of residues was chosen to be the centre of the grid (dimensions; x = 30 Å y = 30 Å z = 30 Å). These residues were: the hinge region (Asp133-Val135) and the DFG loop Asp200. Then to obtain a second and more accurate grid for the validation of the model and the subsequent screening, sorafenib was docked to the newly created site with Glide-SP, the most accurate individual docking program from the type I study (Table 4.5).

In terms of settings, OPLS3 was used as the forcefield, the van der Waals radii factor was set to 0.80 and the partial charge cut off was set to 0.15. Flexible ligand sampling, nitrogen inversion sampling and the sampling of ring conformations including input ring conformations were selected also. For results output after the calculation, post docking minimization was selected, along with strain correction terms. Once this docking had been completed, one of the poses for sorafenib that clearly showed a type II style binding mode was selected as the centre of the second Grid, that would be used in all future screenings and dockings with this DOLPHIN structure (dimensions; x = 29.513 Å y = 29.513 Å z = 29.513 Å). Essentially, using this new grid, the analogies of sorafenib and BIRB (Figure 5.2) were screened to validate the model. Once the model had been validated, the same settings as the previous docking were used in a virtual screening with the full Biogenics subset database.

5.3.4 Prime/Molecular Dynamics Model

Loop Refinement

The second method that was used to design a type II structure of GSK-3β for the virtual screening Prime [114] loop prediction. The protein prepared in section 5.3.2 prior to the deletion of the 5 residues was used for the calculations. Prime uses a selection of rotomer libraries, as well as the OPLS3 force-field [110] to explore new conformations of a selected loop of a protein. It was therefore decided that this sampling technique could potentially be used to produce a DFG-out structure, for us to refine further. To initially test this method, we first ran a loop prediction on the *Ustilago Maydis* form of GSK-3β (prepared using the same method as section 5.3.2 with no residues deleted) that was shown to undergo Type II inhibition in Grütter's paper. Therefore, because it is known to form a DFG-out experimentally, Prime should also be able to do so.

In terms of settings, the solvation model used was VSGB; the forcefield used was OPLS3 and the loop selected for refinement was residues 199-204. Pleasingly, the loop prediction did produce a DFG-out conformation, with an energy of -13441.3 kcal/mol, which was ranked 27 (shown below in Figure 5.3) compared to the top ranked DFG-in conformation (-13445.8 kcal/mol).
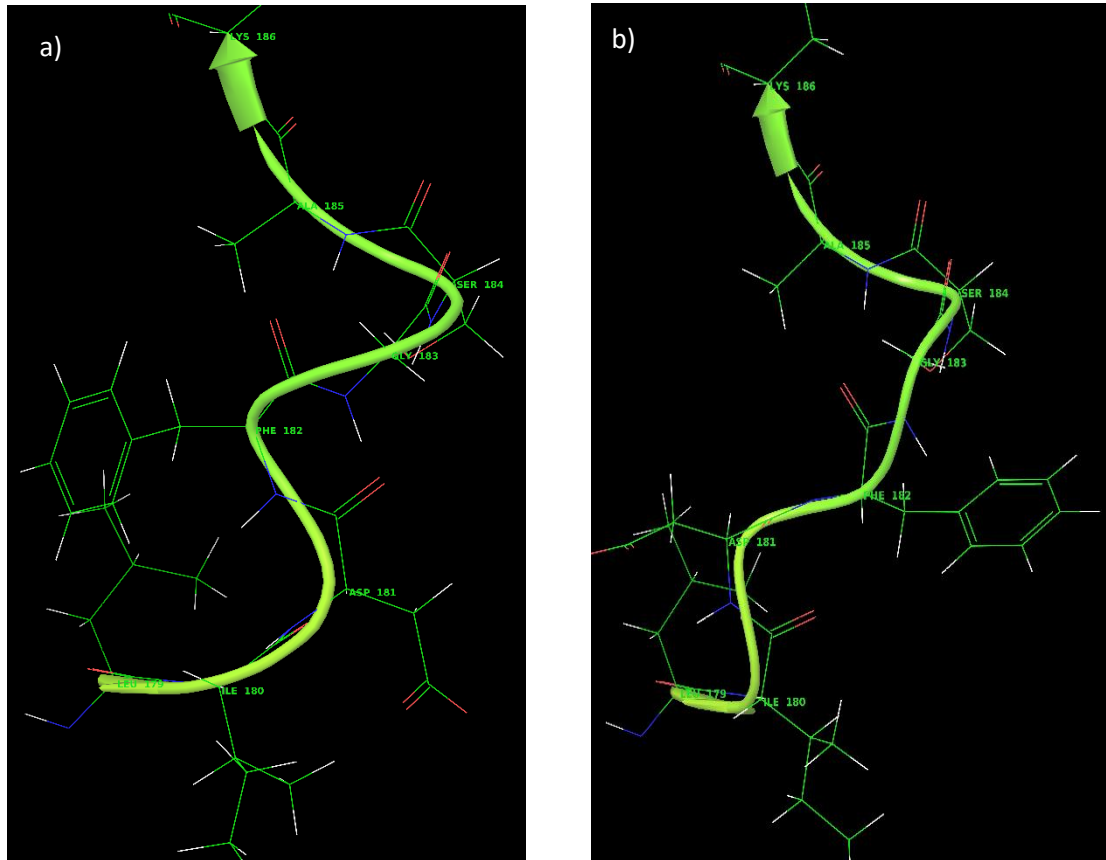
Figure 5.3: The DFG-in conformation (a) of *Ustilago Maydis* GSK-3β obtained using Prime loop prediction, compared to the DFG-out (b)

Based on this, we used the same settings for simulating the human form DFG-out loop conformations. However, this did not produce a DFG-out conformation. When investigated further, in Grütter's paper, it suggests that the salt bridge residues of Lys103, Gln206 and Phe175 could be the cause of this (Figure 5.4), as it is not present in the fungal form. The Prime loop prediction was tried again, but this time the Lys103 residue was mutated to an isoleucine (Ile), which is the same as the residue from the fungal form, and this produced the DFG-out conformation as described in the results section. The mutated residues (not part of the DFG loop) were restored based on their positions in the original structure (via superposition). A further prime refinement was then performed using the same settings as before.
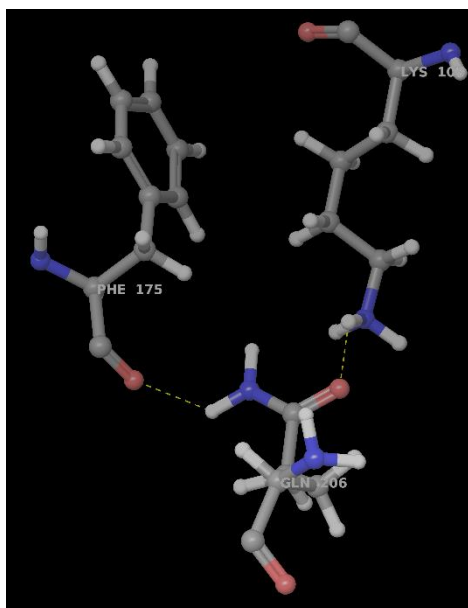
Figure 5.4: The salt bridge between residues Lys103, Gln206 and Phe175 that prevented the initial formation of the DFG-out conformation.

Induced Fit Docking

The next step was to use IFD to further refine the new DFG-out conformation from the loop prediction around a type II inhibitor pose. The ligand pose used for the centre of the grid was the sorafenib pose from the final DOLPHIN grid, superimposed into the site. As for the IFD settings, the forcefield used was OPLS3, and the standard protocol that generates up to 20 poses was applied, and residues within 7 Å of the ligand set as flexible. Two residues were selected for mutation to Ala during the initial docking, Met101 and Asp200, as this would increase the size of the pocket opening initially. The ligand used for the IFD was sorafenib.

MD refinement

The final step for this approach to generating a DFG-out conformation of GSK3- β is to use molecular dynamics to assess the stability of the structure over time using Schrodinger's Desmond [115]. The top scoring IFD pose of sorafenib (sorafenib, Figure 5.2) was taken and the protein ligand complex prepared for dynamics using the Desmond system builder. For the system the TIP3P solvation model was used, and the simulation box shape was set to orthorhombic. The box volume after minimisation was 530034 Å^3, and contained 15064 water molecules. 6 Cl$^-$ ions were then added to balance the charge. Standard equibrilation was used, the length of the simulation was set to 20 ns, the NPT ensemble (P=1atm, T=298.15K) was selected, the recording interval was set to 5.0 ps and the trajectory was also set to 5.0 ps. Once the simulations had finished, the trajectory was visually inspected and analysed to see if the structure of the site varied to a large degree. Further analysis was performed using the SID (Simulation Interactions Diagrams) tool in Maestro, to see how long the structures took to equilibrate. Once the

point of equibrilation had been found, the simulation was cut using a python script (manipulate_tr.py, activated using the command shown in Section S1 in the appendix) supplied by Schrodinger. The remaining frames (4000) were then clustered into ten clusters using the Desmond Trajectory Clustering script available in Maestro, and a representative was taken from the most populated cluster to be used as the final DFG-out structure.

Docking Details

Similarly to the DOLPHIN structure, the Prime DFG-out structure was validated using the type II sorafenib and BIRB analogues and Glide docking. For the centre of the docking grid, the sorafenib molecule was selected. Once the model was validated (*c.f.* results section), it was then used to screen the Biogenics subset database. The settings for both dockings were the same as those in section 5.3.2.

5.3.5 Type II Consensus Scoring

Once the screening had been completed using the DOLPHIN and Prime/molecular dynamics models, the ranks from each of the two complexes were combined in a Simple Sum Rank consensus method. This was done using the KNIME workflow shown below in Figure 5.5, which had been derived from the original type I inhibitor design workflow (Chapter 4).
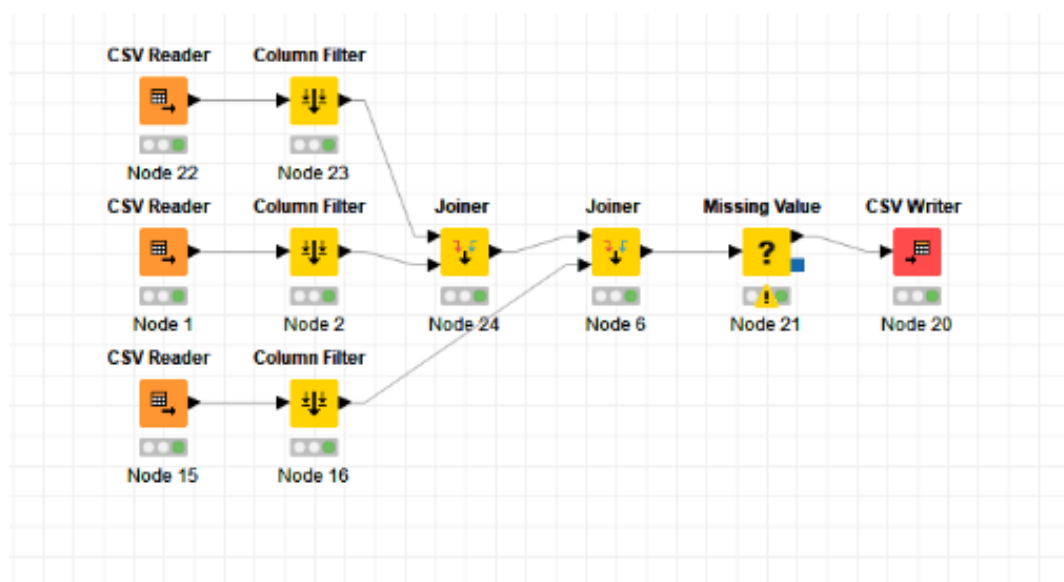
Figure 5.5: The KNIME workflow used to combine the .csv files containing the results of the screenings

5.4 Experimental Details

5.4.1 Type II Luminosity Assays

The experimental methods used in the luminosity assays for *in vitro* validation of the the results of the *in silico* screenings were the same as those from the previous chapter (Section 4.4.2)

5.4.2 Type II IC$_{50}$ Assays

Once again, the in vitro IC$_{50}$ calculations for any compounds that achieved over 50% inhibition at 50 μM concentration were carried out by a colleague at the CSIC, using the same standard method as that used in the type I assay.

5.5 Computational Results

5.5.1 DOLPHIN Model Validation

The Design of the DOLPHIN Model

The resultant DOLPHIN structure from the successful protocol outlined in the computational details is shown in Figure 5.6 below.
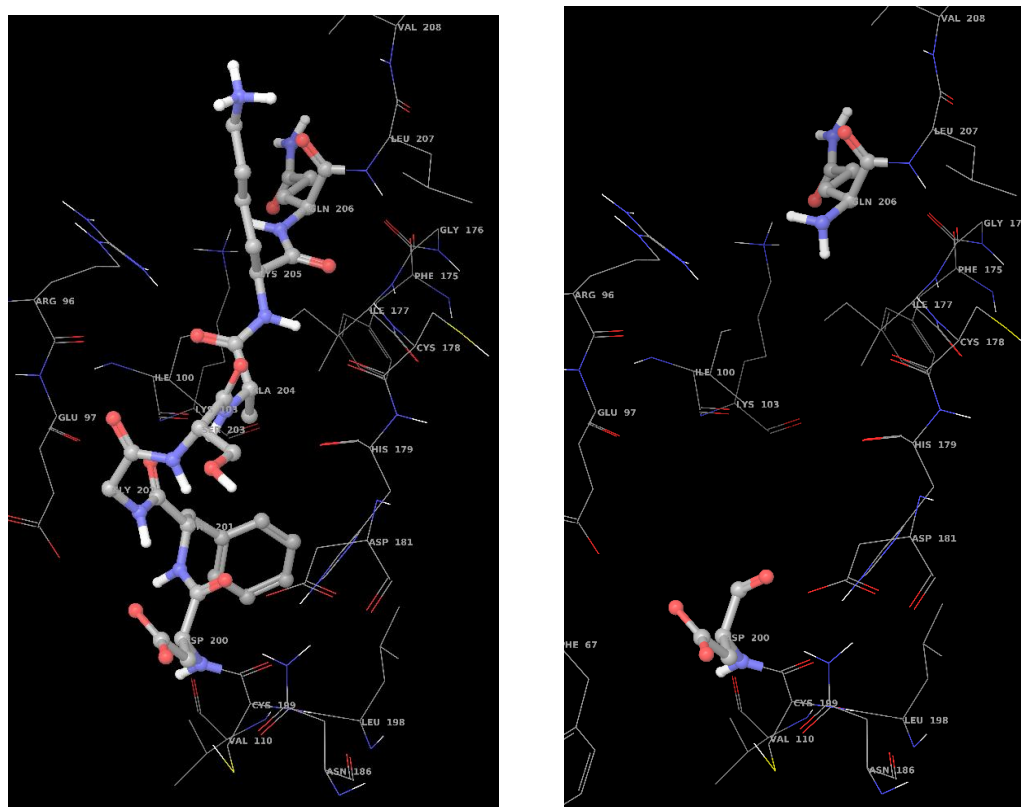
Figure 5.6: The allosteric pocket and binding site of the DOLPHIN structure, once the residues have been removed (right) compared to the regular structure (left).

As can be seen from Figure 5.6, the deletion of the 5 residues opens up the space at the entrance to the allosteric site behind the DFG loop. This opening provides plenty of space for a type II ligand to occupy both the hinge region and the allosteric site. As can also be

seen from the structure, none of the classical type II interactions will be affected by the deletion of these residues, with Asp200, Glu97 and Val135 all still available for hydrogen bond interactions. One other noteworthy feature of this structure is the increased overall size of the binding site. The deletion of the loop opens up an extra section of the side of the cavity (allosteric site), creating a larger space past the DFG loop. This allows potential for ligands normally too large for this site (in DFG-in) to be docked into it.

Results of the DOLPHIN Validation Screening

Once the initial validation screening was completed for the ligands shown in Figure 5.2, the results were compared to those of the experimental inhibition values [56]. These results are shown below in Table 5.1.

Table 5.1: The ranks and Glide scores for the analogues of the known type II inhibitors (Figure 5.2) used in the validation screening obtained using the DOLPHIN model, compared to the experimental activity taken from the literature [56].

Analogue	*In silico* rank	Glide score	Experimental rank [a]	Experimental IC_{50} (µM)
Sorafenib 16	1	-10.26	1	0.86 ± 0.18
Sorafenib 17	2	-9.70	2	3.3 ± 0.6
Sorafenib	3	-9.25	3	8.3 ± 0.8
BIRB 13	4	-7.90	5	>50
BIRB 14	5	-7.82	5	>50
BIRB 12	6	-5.93	5	>50
BIRB	7	-4.84	4	37
BIRB 15	8	-4.72	5	>50

[a] The ranks of the analogues when ordered by experimental activity

As can be seen from Table 5.1, the order that the analogues were returned in is highly similar to that of the experimental values, with Sorafenib out preforming BIRB. This similarity therefore suggests that our model has a high accuracy. The top scoring pose of the best performing ligand, sorafenib 16, can be seen below in Figure 5.7.

As can be seen from Figure 5.7, the ligand forms three of the four classical interactions expected of a type II inhibitor, two hydrogen bonds with Glu97 from the α-C helix, and a hydrogen bond with Val135 in the hinge region. It does not form the interaction with Asp200, however, this is purely because the angle of the bond between them is too large (bond distance is 2.34 Å) for Maestro to recognise it as an interaction. It also forms two interesting hydrogen bond interactions with the sidechain NH_2s (overall +1 charged) of two different Arginine's (Arg96 And Arg180) at the top of the allosteric pocket, which could explain its high Glide score. As the ligand carboxylate is also charged, there will be some strong ionic interactions present as well. It can also be seen that the model in no way hinders its ability of the ligand to form these interactions, suggesting that this model has potential as an alternative to an actual DFG-out structure for virtual screening. On top of this, none of the validation analogues docked mainly inside the larger DOLPHIN allosteric site, as opposed to the ATP binding site exploiting some extra space in the accessible allosteric site (we should note that this was a problem for some of the ZINC15 database screened). The agreement between the results from the validation screening and the experimental data, along with the demonstration of the ligands ability to form all of the classical interactions, led us to decide that the DOLPHIN model would be suitable for the final Type II virtual screening.
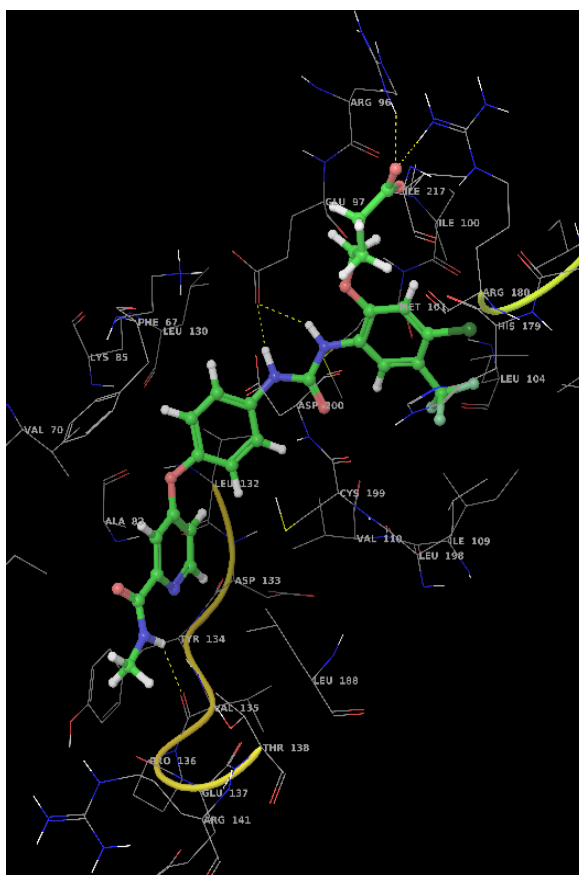
Figure 5.7: The top scoring pose for the best performing type II compound in the validation screening: Sorafenib 16.

5.5.2 Prime/Molecular Dynamics Model Validation

The Prime Loop refinement DFG-Out Structure

Once the mutation (Lys103 to Ile) had been made, the Prime loop prediction protocol was able to produce a DFG-out structure with 2OW3 with energy -13482.7 kcal/mol at rank 71, compared to the energy of the top ranking DFG-in pose -13497.4 kcal/mol. This indicates that the salt bridge hydrogen bond between Lys103 and Gln206 was the reason that the loop prediction was not initially forming a DFG-out structure in this case. This could also possibly explain the lower activity of the Type II inhibitors in Grütter's paper against the human form, as if type II inhibition of the enzyme is dependent on the salt bridge being broken, it would occur at a much lower frequency than in the fungal form. The salt bridge residue was then restored, and prime was repeated, producing the DFG-out structure shown below in figure 5.8.
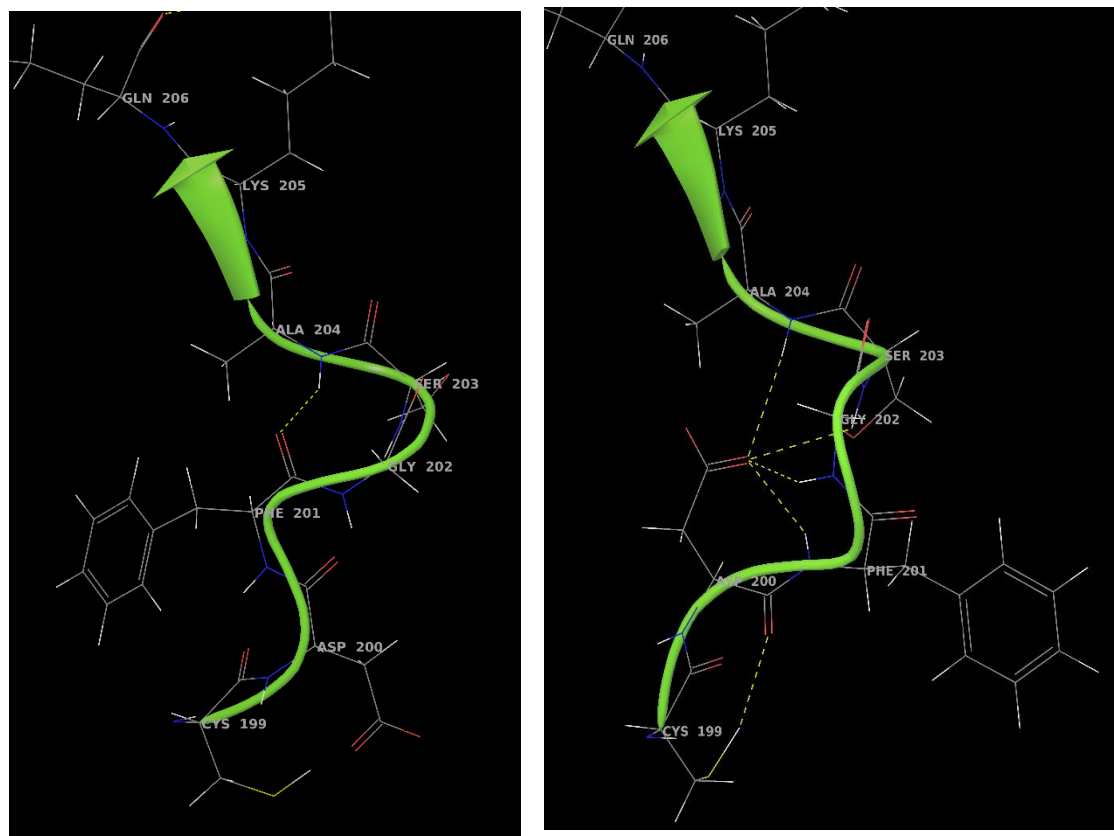
Figure 5.8: The DFG-out structure produced by prime loop prediction of the wild-type restored structure (right) (-13514.4 kcal/mol rank 70) compared to the top scoring DFG-in structure from the same calculation. (left) (-13527.7 kcal/mol)

In figure 5.8, it can be seen that the side chain of Asp200 has been tucked away into the new shape of the now flipped out DFG loop, as it is forming a multitude of hydrogen bonds with the backbone of the loop (residues 201-204). These interactions, coupled with the new shape of the loop, have considerably opened up the entrance to the allosteric site, which has created a space for the insertion of type II ligands into the site. Also, all of the residues needed for the formation of the classical type II interactions, can

be seen to be positioned correctly in this model. Based on this, this structure was approved for the next step, which was induced fit docking.

Induced Fit Docking Refinement Results

The superimposed DOLPHIN ligand was merged with the DFG-out structure and IFD was initiated. The top pose for sorafenib was chosen be used for the molecular dynamics simulation is shown below in Figure 5.9.
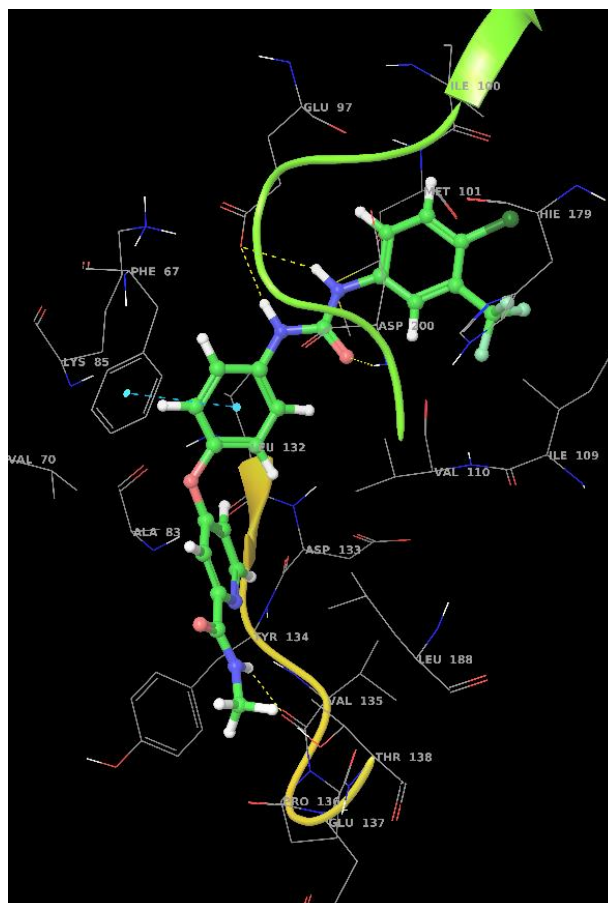
Figure 5.9: The top scoring pose for sorafenib 4 (Figure 5.2) produced by induced fit docking. Hydrogen bonds with (Residues) are formed, IFD score= -696.940 Glidescore = -10.79

As can be seen from Figure 5.9, the sorafenib inhibitor properly forms all of the classical interactions that type II ligands are expected to form, and the residues that line the entrance to the allosteric site have rearranged to better accommodate the ligand.

Molecular Dynamics Simulation Results

The 20 ns simulation on the top ranked pose from the IFD calculations took approximately 5 days on a 3.4 GHz hexacore workstation. Once the molecular dynamics simulation was finished, the first step was to find the point of the simulation where the system reaches equilibrium, as before this time the simulation is unusable due to the structural effects of the equibrilation. This was done using the chart shown below in

Figure 5.10. From the chart, the RMSD over time for the backbone and sidechains can be seen to stabilise at around 5 ns. Therefore, we cut this section from the simulation and began the full analysis on the frames from 5 ns-20 ns. The new trajectory file was then analysed again using SID. This produced a variety of charts which are shown below in Figure 5.11.
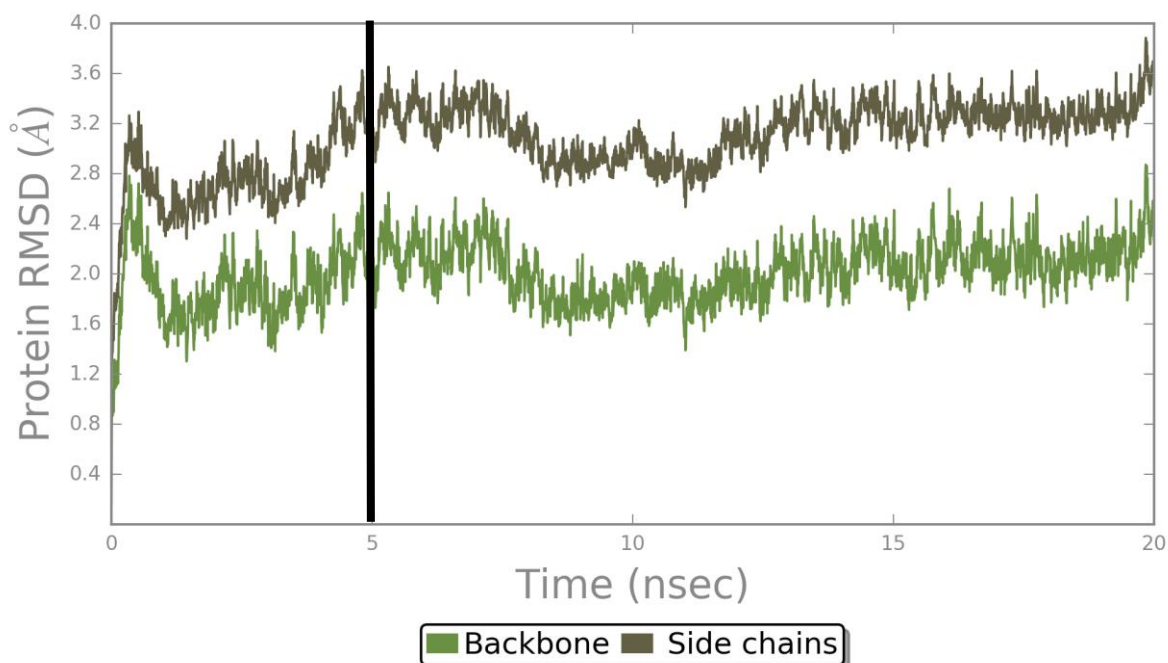
Figure 5.10: The RMSD over time of the backbone and sidechains of 2OW3 during the full 20 ns simulation. The black line indicates the time (5-20 ns) used for analysis following equibrilation.

As can be seen in Figure 5.11, the classical interactions that are expected to occur in type II inhibition and that were present in our DOLPHIN model were also shown to be present between 90-95% of the duration of the simulation. This strongly indicates that this binding mode is stable. As well as this, the flipped DFG loop did not at any point during the simulation begin to flip back into the cavity, even with the salt bridge being reconstructed during the Prime loop prediction step. There two things combined show that the DFG-out conformation that has been created in this model is favourable and can interact with ligand molecules in the desired type II manner. Another noteworthy is the interaction with the gatekeeper residue, Leu132. As can be seen from the lower percentage (just over 50%), this residue does not interact with the ligand strongly enough to in anyway interfere with its binding mode in relation to the classical interactions, meaning that it would not prevent type II inhibition taking place.
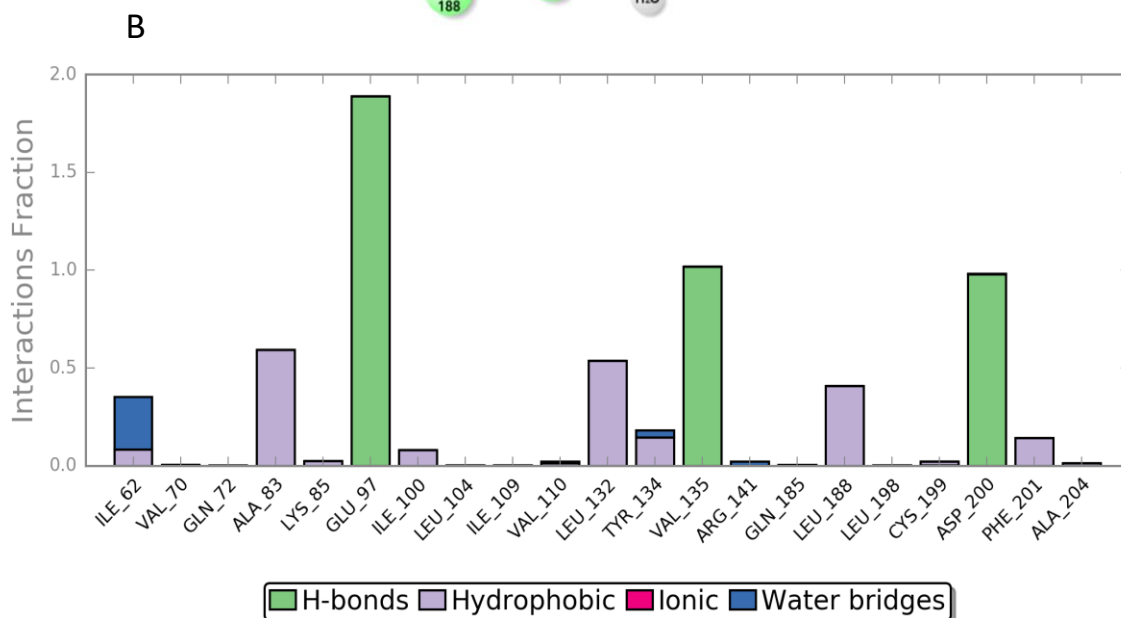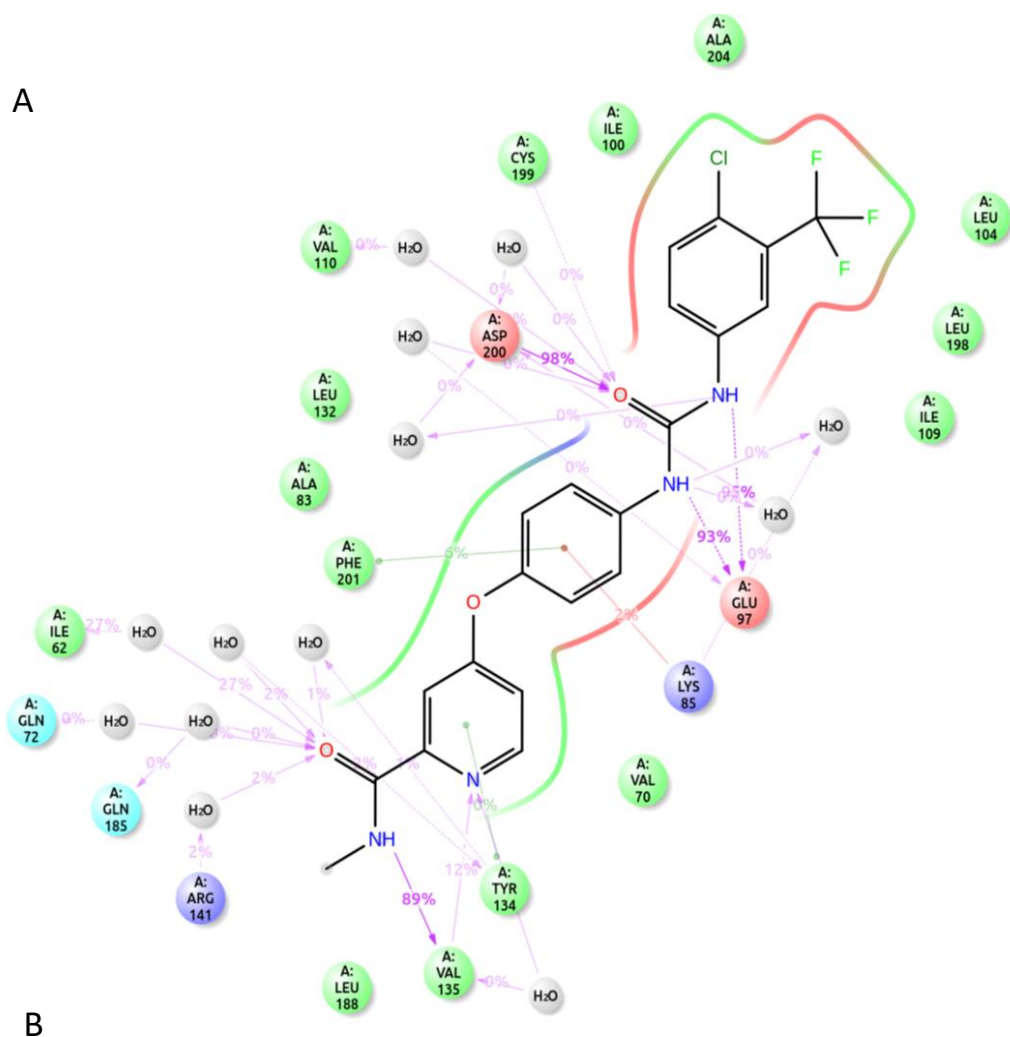
Figure 5.11: The Simulation Interactions Diagrams created for the final 15 nanoseconds of the molecular dynamics simulation. (A) displays the prevalence of the interactions that the ligand forms during the simulation, and (B) shows these interactions relative to the 2D structure of the ligand and binding site.

The frames were then clustered, and the most populated cluster contained 2011 structures. The representative taken from this cluster is shown below in Figure 5.12.
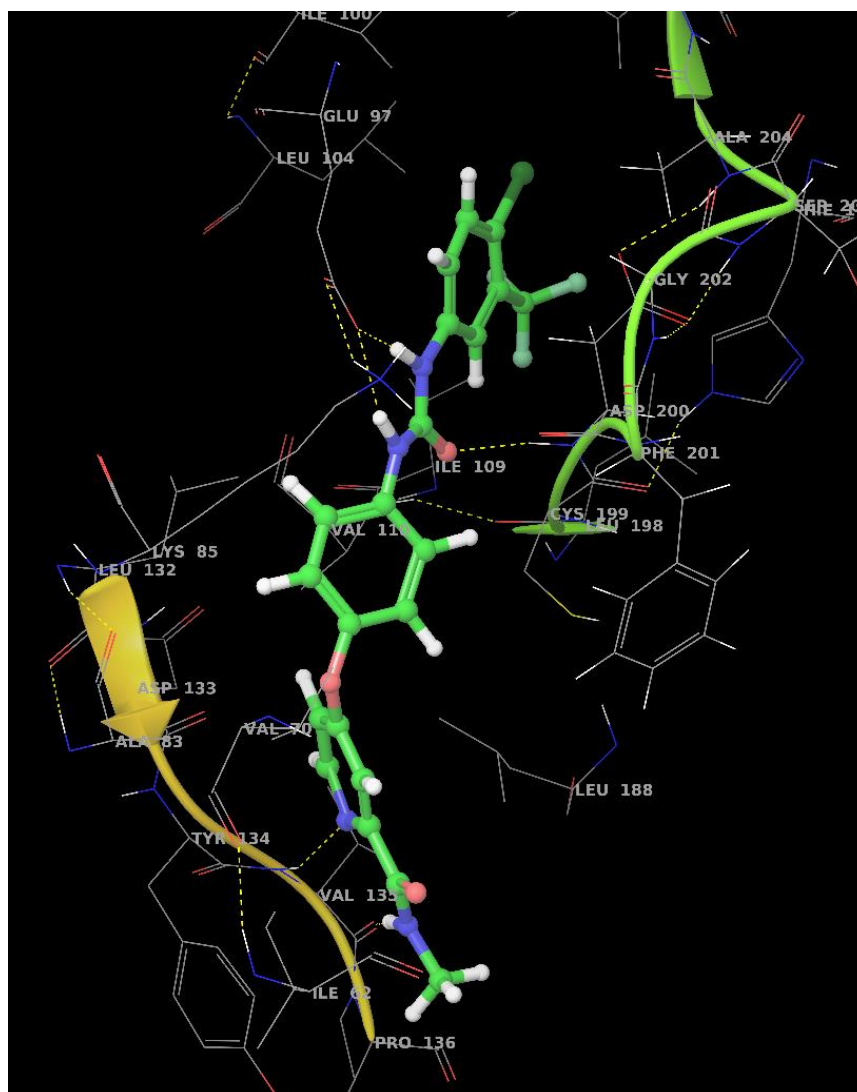
Figure 5.12: The representative structure from the most populated molecular dynamics frame cluster.

As can be seen from Figure 5.12, the residues around the ATP binding site and the allosteric pocket entrance have adjusted further than they did in the IFD, with the DFG-out loop also moving to a better binding position. The opening to the allosteric site has remained large enough to accommodate the sorafenib molecule, and potentially bind larger type II inhibitors also.

Validation of Prime/Molecular Dynamics Model

As with the DOLPHIN model, the resultant model of the Prime/Molecular Dynamics was validated using the set of sorafenib and BIRB analogues. The results of the docking are shown below in Table 5.2.

Table 5.2: The ranks and Glide scores for the analogues of the type II inhibitors (Figure 5.2) used in the validation screening with the MD model, compared to the experimental activity.

Analogue	*In silico* rank	Glide score	Experimental rank [a]	IC$_{50}$
Sorafenib 17	1	-12.95	2	3.3 ± 0.6
Sorafenib 4	2	-11.78	3	8.3 ± 0.8
Sorafenib 16	3	-11.50	1	0.86 ± 0.18
BIRB 13	4	-10.76	5	>50
BIRB 3	5	-10.38	4	37
BIRB 14	6	-9.69	5	>50
BIRB 12	7	-9.48	5	>50
BIRB 15	8	-6.22	5	>50

[a] The ranks of the analogues when ordered by experimental activity

As can be seen from the results, the predicted activity of the analogues puts them in a similar order to the experimental values, with one or two exceptions. For example, sorafenib 16, the best performing ligand experimentally, is ranked 3rd. This result, similarly to the DOPLHIN results, serves to suggest that the designed model will be accurate for screening for type II activity. In the screening with sorafenib and BIRB the binding mode for these complexes was mainly type II, with the ligands having enough space to extend into the allosteric site. All 4 classical interactions, the hydrogen bond with Asp200, the two hydrogen bonds with Glu97 and a hydrogen bond with Val135 of the hinge region were formed by the top scoring ligands.

5.5.3 DOLPHIN and Prime comparison

When compared to the DOLPHIN pose, the final binding position of the sorafenib ligand obtained from Prime/Molecular Dynamics model is positioned closer to the centre of the allosteric site, whereas the DOLPHIN pose is closer to the DFG Asp200. The most plausible reason for this is the increased size of the allosteric pocket near the DFG loop in the DOLPHIN model, which allows the section of the ligand inside the site to position closer to that side than is possible if the loop was still there. The main interactions that appear in the DOLPHIN model, the hydrogen bonds with Glu97, Asp200 and Val135 are also present in the new Prime complex too. As can be seen from the chart in Figure 5.11,

during the molecular dynamics simulation these interactions were the most prevalent, appearing for around 89-95% of the total reaction time. The biggest difference between the two models, is that the deletion of the loop in the DOLPHIN model creates a larger cavity than the Prime loop prediction. As mentioned above, this has the potential for larger sections of the ligand molecules to be docked inside the DOLPHIN allosteric pocket.

5.5.4 DOLPHIN and Prime Virtual Screening Results and Consensus scoring

Both docking calculations of the filtered ZINC15 biogenic database (27,286 ligands) using both DFG-out models of GSK-3β finished unhindered, and the results were combined using the Simple Sum Rank consensus scoring method (KNIME workflow in Figure 5.5). From the top 200, 65 compounds had Glide scores similar to the sorafenib analogues (≤ -10 for Prime/Molecular Dynamics model and ≤ -9 for DOLPHIN model) were chosen for further consideration. This score cut-off was chosen as the sorafenib compounds received low micromolar IC_{50} values, and therefore compounds with similar *in silico* scores have the potential for similar *in vitro* scores as well.

5.5.5 Type II Compound Selection

20 compounds from the top 65 were purchased, as well as sorafenib itself. Sorafenib allowed comparison to the experimental IC_{50} from in Grütter's paper and was therefore used as a benchmark. Of these compounds, 20 were purchased from Analyticon (ZINC000008299930, ZINC000004259649, ZINC000008297322, ZINC000008623925, ZINC000004200864, ZINC000004235515, ZINC000096112349, ZINC000096112343, ZINC000096112276, ZINC000096112042, ZINC000096112517, ZINC000004200873, ZINC000004200863, ZINC000096112052, ZINC000096112247, ZINC000096112049, ZINC000096112048, ZINC000096112254, ZINC000008635710 and ZINC000096112199), and sorafenib was purchased from Stratech. The structures of these compounds (**1-21**) are all shown in Figure 5.13.
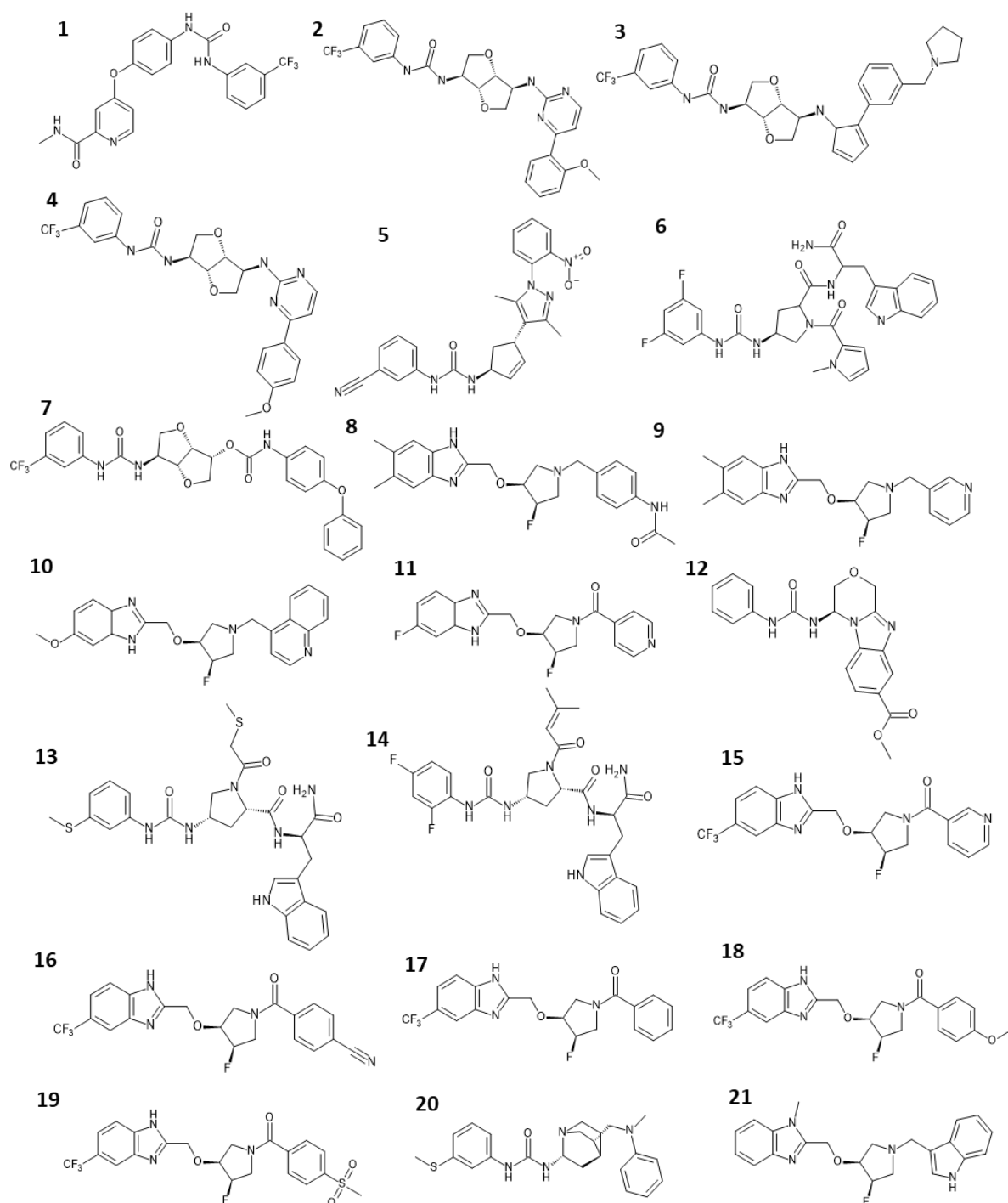
Figure 5.13: The structures of all of the type II compounds chosen for biological testing.
1) Sorafenib **2**) ZINC000008299930, **3**) ZINC000004259649, **4**) ZINC000008297322, **5**)
ZINC000008623925, **6**) ZINC000004200864, **7**) ZINC000004235515, **8**)
ZINC000096112349, **9**) ZINC000096112343, **10**) ZINC000096112276, **11**)
ZINC000096112042, **12**) ZINC000096112517, **13**) ZINC000004200873, **14**)
ZINC000004200863, **15**) ZINC000096112052, **16**) ZINC000096112247, **17**)
ZINC000096112049, **18**) ZINC000096112048, **19**) ZINC000096112254, **20**)
ZINC000008635710 and **21**) ZINC000096112199

These compounds were chosen based on their ranks and scores, as well as their various
interactions, with an emphasis on the previously discussed classical type II interactions

first. This was followed by an investigation of any extra interesting interactions that the ligands form, for example an extra hinge region interaction or a π-π stacking interaction with the phenyl group of the Phe201 from the DFG loop, which could serve to stabilise the DFG-out composition. Table 5.3 below shows the consensus ranks of the 20 compounds, as well as their ranks and scores with each model.

Table 5.3: The consensus ranks and predicted data of the 21 compounds chosen

Title [a]	DOLPHIN Rank	DOLPHIN Gscore	MD Structure Rank	MD Structure Gscore	Simple Sum Rank
ZINC000008299930 Compound **2**	17	-9.174	19	-10.487	7
ZINC000004259649 Compound **3**	37	-8.906	20	-10.486	11
ZINC000008297322 Compound **4**	181	-8.331	13	-10.605	30
ZINC000008623925 Compound **5**	158	-8.398	16	-10.578	29
ZINC000004200864 Compound **6**	4	-9.623	457	-9.223	55
ZINC000004235515 Compound **7**	370	-8.002	71	-10.112	54
ZINC000096112349 Compound **8**	21	-9.125	14	-10.599	6
ZINC000096112343 Compound **9**	12	-9.314	34	-10.319	9
ZINC000096112276 Compound **10**	64	-8.781	24	-10.444	14
ZINC000096112042 Compound **11**	29	-8.971	50	-10.224	13
ZINC000096112517 Compound **12**	183	-8.323	96	-10.003	44

ZINC000004200873 Compound **13**	2	-9.838	4	-11.017	2
ZINC000004200863 Compound **14**	195	-8.296	40	-10.271	35
ZINC000096112052 Compound **15**	39	-8.888	1	-11.244	8
ZINC000096112247 Compound **16**	56	-8.808	15	-10.598	12
ZINC000096112049 Compound **17**	27	-9.007	3	-11.023	5
ZINC000096112048 Compound **18**	13	-9.313	7	-10.794	4
ZINC000096112254 Compound **19**	6	-9.588	10	-10.703	3
ZINC000008635710 Compound **20**	439	-7.912	42	-10.269	56
ZINC000096112199 Compound **21**	24	-9.081	25	-10.435	10

a *c.f.* Figure 5.13

5.6 Biological Results

5.6.1 Type II Luminosity Binding Assay Results

The results of the type II luminosity assay can be seen below in Table 5.4.

Table 5.4: The results of the in vitro luminosity assay for the selected type II inhibitors, along with their purities, molecular weights and any calculated IC_{50} values.

Type 2 Inhibitors	Zinc code and Compound Number	Mw (Da)	Purity		% Inhibition	IC50 µM
Sorafenib	-	**464.831**	**95%**		**64.54±1.59**	**32.64 ± 0.76 µM**
NAT6-321961	ZINC000008299930 Compound **2**	**515.492**	**100.000**	**99.012**	**74.45±2,37**	**26.96 ± 1.77 µM**
NAT6-297729	ZINC000004259649 Compound **3**	543.55	96.086	86.454	7.17±2,27	-
NAT6-321324	ZINC000008297322 Compound **4**	**515.429**	**99.389**	**93.636**	**89.87±2,72**	**9.75 ± 2.2 µM**
NAT16-353088	ZINC000008623925 Compound **5**	442.479	100.000	92.034	25.54±1,06	-
NAT3-155416	ZINC000004200864 Compound **6**	577.592	99.574	87.958	5.64±3,17	-
NAT6-270085	ZINC000004235515 Compound **7**	543.498	100.000	100.000	41.78±1,83	-
NAT37-534362	ZINC000096112349 Compound **8**	410.493	100.000	97.712	2.40±2,71	-
NAT37-534352	ZINC000096112343 Compound **9**	354.429	100.000	98.840	4.69±1,97	-
NAT37-534198	ZINC000096112276 Compound **10**	406.461	100.000	91.753	12.71±1,69	-

NAT37-532879	ZINC000096112042 Compound **11**	358.348	97.249	86.062	2.01±0,93	-
NAT41-514998	ZINC000096112517 Compound **12**	380.404	100.000	92.403	0.65±2,88	-
NAT3-155435	ZINC000004200873 Compound **13**	568.725	97.665	92.216	5.30±1,71	-
NAT3-155413	ZINC000004200863 Compound **14**	552.582	100.000	100.000	4.80±0,90	-
NAT37-532925	ZINC000096112052 Compound **15**	408.355	100.000	94.923	13.97±1,26	-
NAT37-534097	ZINC000096112247 Compound **16**	418.394	100.000	98.341	7.20±1,78	-
NAT37-532911	ZINC000096112049 Compound **17**	407.367	100.000	92.125	19.18±1,03	-
NAT37-532910	ZINC000096112048 Compound **18**	437.393	100.000	96.465	18.96±1,62	-
NAT37-534136	ZINC000096112254 Compound **19**	471.476	98.607	92.786	32.60±1,62	-
NAT13-339804	ZINC000008635710 Compound **20**	424.614	100.000	90.187	0.80±0,63	-
NAT37-534009	ZINC000096112199 Compound **21**	378.451	99.717	95.230	13.76±3,42	-

As can be seen from Table 5.4, there were three type II compounds from the 21 including sorafenib (64.54%), ZINC000008299930 (compound **2**) (74.45%) and ZINC000008297322 (compound **4**) (89.87%) that received percentage inhibition values of over 50%. The rest of the compounds ranged from less than 1% inhibition to 41%. The binding modes of these three molecules are shown below in Figure 5.15.
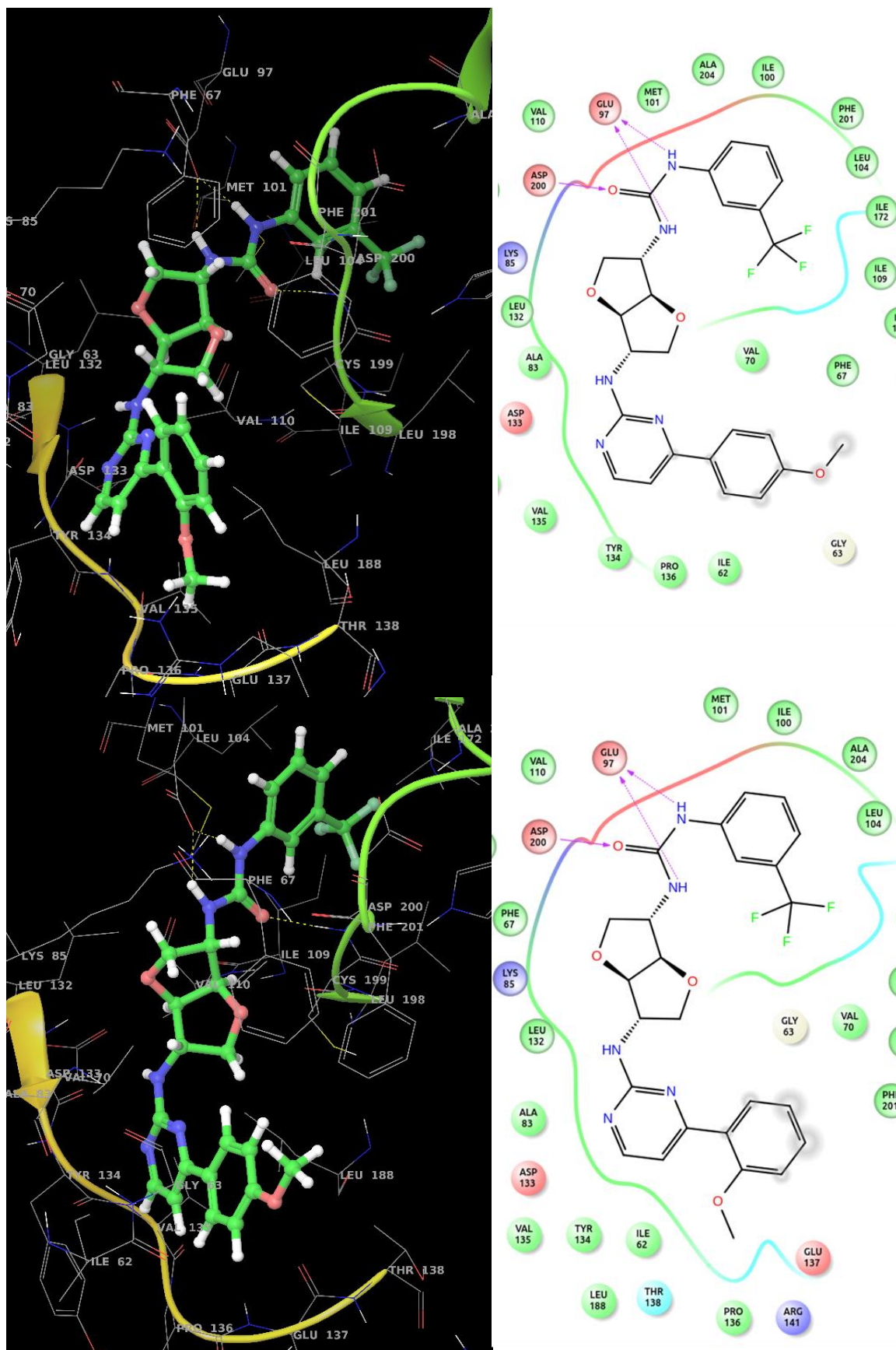
Figure 5.14: The binding modes, both in 2D and 3D of ZINC000008299930 (A) and ZINC000008297322 (B).

As can be seen in Figure 5.14, both of these inhibitor molecules form the classical interactions for type II compounds, a hydrogen bond with the backbone NH of Asp200, 2 hydrogen bonds with the sidechain COO^- of Glu97 on the α-C helix. They also form the hydrogen bond with the backbone C=O Val135 in the hinge region, but this is not displayed by Maestro once again because of the angle. Both of these inhibitors also form an additional with the hinge region, a hydrogen bond with the backbone of Asp133. Compound **2** and compound **4** share multiple common structural features, for example they both contain an interesting fused hexahydrofuro-furan ring structure. The compounds high similarity means that the large difference in their activity can be potentially attributed to the positioning of the OMe group on the hinge region end aromatic ring of the ligand molecule. In compound **2**, the OMe is ortho substituted whereas in compound **4** it is para substituted. This is the only major difference between these two structures, and therefore this positioning is potentially very important for potency.

5.6.2 Type II IC_{50} Results

As the only compounds with percentage inhibition values of over 50% sorafenib, compound **2** and compound **4** were all tested for their experimental IC_{50} values.

Sorafenib obtained an IC_{50} value of 32.64 ± 0.76 µM, which was derived from the graph below in Figure 5.15.
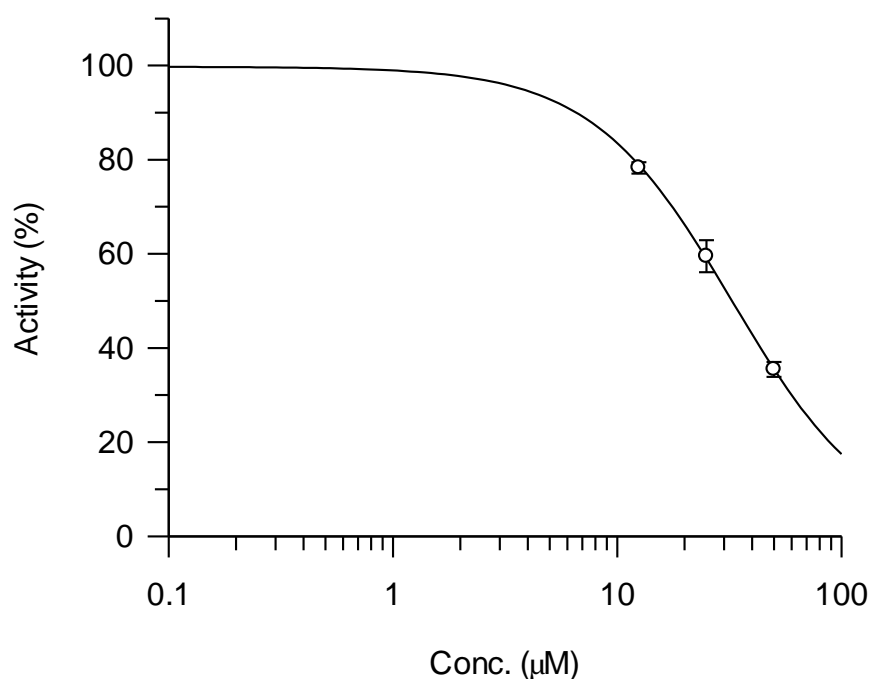
Figure 5.15: The graph used to calculate the *in vitro* IC_{50} of Sorafenib, with % activity plotted against concentration.

While the IC_{50} is much higher than the value obtained in Grütter's publication, provided all other ligands are assayed in identical conditions to this it can provide a solid benchmark potency with which to compare the other values.

The second ligand, compound **2** obtained an IC_{50} value of 26.96 ± 1.77 µM, derived from the graph below in Figure 5.16.
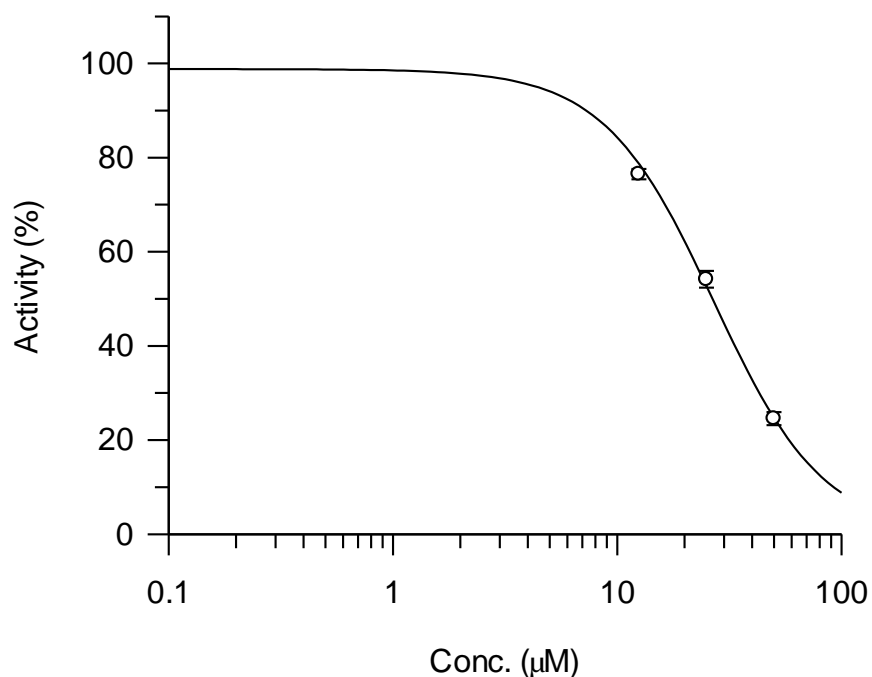
Figure 5.16: The graph used to calculate the *in vitro* IC_{50} of compound **2** by plotting % activity against concentration.

The IC_{50} of this compound is higher than that of sorafenib. This is possible due to its increased amount of hinge region interactions, which could explain the higher potency of this ligand over that of Sorafenib.

The final inhibitor, compound **4** produced an IC_{50} value of 9.75 ± 2.2 µM, which was obtained using the graph below in Figure 5.17.
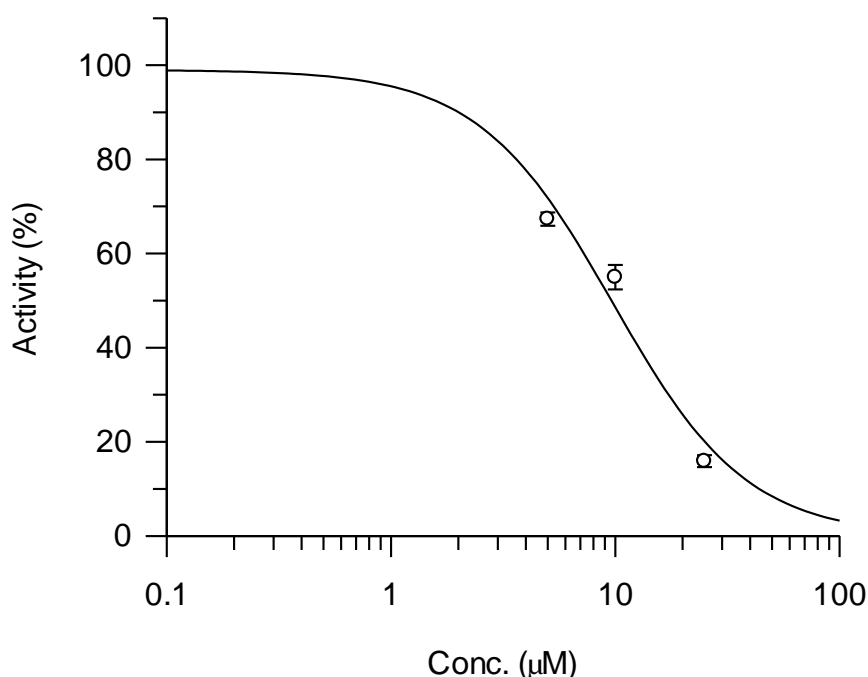
Figure 5.17: The graph with % activity of GSK-3β plotted against concentration of compound **4**, used to calculate the *in vitro* IC_{50}.

This ligand also received an IC_{50} lower than that of sorafenib, receiving the lowest IC_{50} out of the three inhibitors. It also forms an extra hinge region interaction compared to sorafenib, further confirming that this causes the increase in potency.

Overall, all three inhibitors received relatively good IC_{50} values. Both of the ligands selected in the *in silico* screening, compound **2** and compound **4**, achieved potencies higher than that of sorafenib. As the structures of these two ligands are very similar, the only real difference being the position of the OMe group on the aromatic ring at the hinge region end of the molecule, it can be deduced that this difference is the main reason for the large disparity between their activities. For compound **2**, the OMe group is ortho substituted whereas in compound **4** the OMe group is para. These IC_{50} results also suggest that the binding mode of these inhibitor compounds is indeed type II. This is due to the fact that due to their larger size and flexibility, these compounds would be unable to achieve type I IC_{50} values lower than that of type I compound **6** (section 4.5). Therefore, it is reasonable to conclude that the binding modes of these compounds is indeed type II. Also, due to the fact that the IC_{50} of sorafenib is a lot higher than the experimental value Grütter obtained, it is possible that the values for the other two inhibitors are potentially equally high, and could be a lot more potent than is shown in this study.

5.7 Conclusion

In this project, we developed two different type II DFG-out models, both of which were shown to be accurate at predicting the binding modes of type II ligands by the validation screenings of the sorafenib and BIRB analogues. The DOLPHIN model produced had a larger allosteric cavity than normal, due to the deletion of the 5 residues, and this caused type II ligands to bind closer to the DFG Asp200 residue. However, the model was still able to form all of the classical interactions, and the validation results it produced were quite similar to the experimental results. The Prime/Molecular Dynamics structure on the other hand, has a smaller allosteric site, due to the fact that the loop was still present. Once the mutation of the salt bridge was applied, the loop flipped to the DFG-out position without hindrance, and produced a model that could be refined into a type II structure. The IFD docking successfully refined this structure, repositioning the residues near the opening of the allosteric site around the superimposed ligand, increasing the size of the opening of the pocket and further stabilising the position of the ligand. Through the molecular dynamics, this structure was shown to be stable, and the classical interactions were present for over 90% of the simulation. This model also performed well during the validation screenings, returning values that were very close to the experimental results from the paper by Grütter et al, with the exception of sorafenib 16, which ranked 3rd instead of 1st. The next step, the screening of the ZINC15 Biogenic subset database was completed without any problems, and the results were found to combine well into a simple sum rank consensus score. The top compounds of the consensus scored database almost all formed the four classical interactions, with some of the compound missing one of the hydrogen bonds with Glu97 or the hydrogen bond with Val135. The final selected 20 compounds were all extremely similar in general structure and shape to sorafenib, which shows that this geometry is preferential for type II inhibitors. The type II ligands gave a very wide variety of percentage inhibitions, ranging from as low as 0.6% to upwards of 80% at 50 μM. The three best performing ligands in this assay were: sorafenib (64.54%), compound **2** (74.45%) and compound **4** (89.87%). The IC_{50} value for sorafenib was 32.64 ± 0.76 μM, compared to the 8.3 μM value from Grütter. While the value we obtained is much higher, as long as the other type II inhibitors are assayed in identical conditions, this value can provide a solid benchmark potency that can be used to assess the potency of the other two inhibitors. It also presents the possibility that, as this value is so much higher than that of Grütter, the IC_{50} values for the other compounds could also be higher than normal, and therefore our type II inhibitors are potentially even more potent that their values would suggest. In effect, compound **2** (26.96 ± 1.77 μM) and compound **4** (9.75 ± 2.2 μM) were both shown to be more potent than sorafenib. As their structures have the same core scaffold, this result suggests that the groups that they have, the hexahydrofuro-furan fused ring structure, the pyrimidine

ring near the hinge and the terminal OMe group are all potentially conducive to the potency of the inhibitors. The only difference in structure is the position of the OMe group, for compound **2** (26.96 ± 1.77 µM) the group is ortho substituted and for compound **4** (9.75 ± 2.2 µM) the OMe is para substituted. This, therefore, indicates the difference between the ortho and para substitution caused the 17 µM difference in their IC_{50} values. Their IC_{50} values also serve to indicate that their binding mode is indeed type II, as these ligands are too large and flexible, with too few hinge region interactions to compensate, to achieve such a high type I potency. Based on the results of this project, the next step could be to search the top part of the consensus ranked database for various compounds with structures similar to those of the two potent inhibitors, to see if any other groups could potentially be used to increase their potency. It would also be beneficial to further explore the reason why the para substituted OMe performed so much better than the ortho OMe, as this could give new insight into the optimisation of binding ligands to this area of the ATP binding site, regardless of the type of inhibition. In conclusion, two designed DFG-out GSK-3β type II structures were used to screen a database of natural product molecules and successfully identified two novel potential type II inhibitors for further study. Additionally, other ligands from the screening can be selected for further *in vitro* validations.

Chapter 6: Conclusion

There were four overall aims for this project outlined in section 1.5. In this conclusion I will address these four objectives, and how they were met.

1) To investigate and design novel type I (ATP binding site) and type II (activation loop out) inhibitors of GSK-3β.

Upon the completion of this project, we have successfully designed inhibitors of GSK-3β of both types, with IC50 values in the micromolar range. These inhibitors were designed using a variety of other techniques, as set out in the subsequent objectives, and active inhibitor compounds were selected and biologically validated for each type.

2) To apply a consensus scoring method involving a virtual screening with 4 different programs, GOLD, Glide-SP, Glide-XP and AutoDock to a large database taken from the ZINC docking database website (www.ZINC15.org) [33].

For the development of potential type I ATP binding site inhibitors, an *in silico* virtual screening docking method based on consensus scoring was devised. This was done using a benchmarking screening to assess various different combinations of docking programs, by screening an active/decoy ligand set containing 30 known active compounds, 189 real inactive compounds, and 1800 decoy inactives generated using DUDE[98]. A series of statistical metrics were employed to assess the accuracy of these different combinations, including the enrichment factor (EF), modified enrichment factor (EF') and BEDROC. The final consensus method that was chosen was a combination of Glide-SP and –XP, AutoDock Vina and GOLD ASP, with a simple sum ranking method as the statistical values produced are significantly higher compared to those of the individual programs. Pharmacophore models were applied to create an extra set of data with to improve the overall accuracy of the results. Once the virtual screening had finished, all of the information generated during the preparation of the database and the creation of the method was used to select 10 final compounds, which are diverse but also share common features conducive to binding.

3) To design two novel type II structures of GSK-3β, using different computational methods, molecular dynamics and DOLPHIN docking[34], and to use them to screen a database *in silico*. The results for these two models are to be combined using a consensus scoring method.

For the investigation of type II inhibition of GSK-3β, two different type II DFG-out models were developed. The first model was created using DOLPHIN docking, which involved the deletion of 5 residues (201-205). This model was found to have a larger allosteric site due to the deletion, and this caused type II ligands to bind closer to the DFG Asp200

residue. This difference in the size of the site however did not affect the models ability to form the classical type II interactions. The second model was designed using a combination of Prime loop refinement, induced fit docking and molecular dynamics. This produced a structure with a DFG loop in the out position, with a smaller allosteric pocket, due to the fact that the loop was still present. Both models were then validated using a selection of type II ligands and their corresponding experimental data. Once both models were validated, they were the used to screen the Biogenic subset database (27,286 Compounds) taken from ZINC15[33]. The two resultant ranks for each of the compounds were combined into a simple sum consensus score rank. It was noted that most of the compounds at the top consensus scored database formed the four classical type II interactions. Also many of the compounds at the top of the database were similar in general structure and shape to sorafenib, showing that this type of geometry is preferential for type II inhibitors. From this consensus ranked database, 20 compounds were selected for biological validation.

4) To select the top compounds from both the type I and type II screenings for transportation to the CSIC in Madrid on an Erasmus+ placement where they will have their IC_{50} values tested *in vitro*

The first assay involved the use of a luminescence reaction involving ATP to calculate the percentage inhibition of the inhibitors. Overall, 6 of the 10 type I inhibitors produced a percentage inhibition of over 20% at 50 μM, with one of the compounds, type I compound **6** (ZINC000072152229) even receiving a value as high as 74.58%. The type II compounds produced a large range of percentage inhibitions in the first assay, with one value as low as 0.6% at 50 μM and another being upwards of 80%. The three ligands that performed the best in this assay were: sorafenib (64.54%), compound **2** (ZINC000008299930) (74.45%) and compound **4** (ZINC000008297322) (89.87%). In the second assay, the IC_{50} of type I compound 6 was investigated, as it was the only inhibitor with a percentage inhibition over 50%. The IC_{50} of this compound was found to be 24.69 ± 0.73 μM. Due to compound 6 mainly binding via the hinge region, it was expected to have a relatively high potency; however, it was noticed that it also forms an ionic interaction with Asp200 at the back of the ATP binding site, which is likely to greatly increase its potency. The ligand also only formed one of the various selective interactions with Phe67. The IC_{50} values of the type II compounds, Sorafenib, compound **2** and compound **4** were; 32.64 ± 0.76 μM, 26.96 ± 1.77 μM and 9.75 ± 2.2 μM respectively. As the structures of compound **2** and compound **4** are considerably similar. The only difference in their structures is the position of the OMe group, this difference between the ortho and para substitution is implicated heavily in the 17 μM difference in their IC_{50} values.

References:

[1]- *Béatrice Duthey,* Update on 2004 Background Paper, BP 6.11 Alzheimer Disease, Priority Medicines for Europe and the World "A Public Health Approach to Innovation", World Health Organisation, 2013

[2]- *Jennifer L. Shaffer, Jeffrey R. Petrella, Forrest C. Sheldon, Kingshuk Roy Choudhury, Vince D. Calhoun, R. Edward Coleman, P. Murali Doraiswamy,*Predicting, Cognitive Decline in Subjects at Risk for Alzheimer Disease by Using Combined Cerebrospinal Fluid, MR Imaging, and PET Biomarkers and For the Alzheimer's Disease Neuroimaging Initiative, Radiology 2013, 266, 583-591

[3]- *National Institute of Aging* Alzheimer's Disease Fact Sheet, US Department Of Health And Human Services, https://www.nia.nih.gov/health/alzheimers-disease-fact-sheet, last visited 28/09/2018

[4]- *Rainulf A. Stelzma, H. Norman Schnitzlein, F. Reed Murtagh*, An English Translation of Alzheimer's 1907 Paper, "Uber eine eigenartige Erkankung der Hirnrinde", Clinical Anatomy, 1995, 8, 429-431

[5]- ApexBio, Amyloid beta-peptide, http://www.apexbt.com/amyloid-peptide-25-35-human.html, last visited 28/09/2018

[6]- *David Bradley,* Lead and IQ: Toxic effects and tau protein, 2012, SpectroscopyNow, http://www.spectroscopynow.com/details/ezine/3613801/Lead_and_IQ_Toxic_effects_and_tau_protein.html?tzcheck=1, last visited 28/09/2018

[7]-*Paulina V. Arriagada, John H. Growdon, E. Tessa Hedley-Whyte and Bradley T. Hyman*, Neurofibrillary tangles but not senile plaques parallel duration and severity of Alzheimer's disease, Neurology 1992, 42, 631

[8] -*Ana Paula Barbosa, Jeronimo Hartmann, Sérgio Monteiro de Almeida, José Antonio Livramento, Ricardo Nitrini, Daniel Takahashi, Paulo Caramell*, Arq. Neuro-Psiquiatr, 2004, 62, 751-755

[9]- *Bayles, K. A., Kaszniak, A. W., & Tomoeda, C. K.* Communication and cognition in normal aging and dementia. Boston, MA, US: College-Hill Press/Little, Brown & Co., 1987

[10]- *Linn RT, Wolf PA, Bachman DL, et al*, The 'Preclinical Phase' of Probable Alzheimer's Disease: A 13-Year Prospective Study of the Framingham Cohort. Arch Neurol., 1995, 52(5), 485–490

[11]- *La Rue, Asenath, Jennifer Watson, and Daniel A. Plotkin.* "First symptoms of dementia: A study of relatives' reports." International journal of geriatric psychiatry, 1993, 8(3), 239-245

[12]- *Sperling R. A., Aisen P. S., Beckett L. A., Bennett D. A., Craft S., Fagan A. M., Park D. C.* Toward defining the preclinical stages of Alzheimer's disease: Recommendations from the National Institute on Aging-Alzheimer's Association workgroups on diagnostic guidelines for Alzheimer's disease. Alzheimer's & dementia, 2011, 7(3), 280-292

[13]- *McKhann G., Drachman D., Folstein M., Katzman R., Price D., & Stadlan E. M.* Clinical diagnosis of Alzheimer's disease Report of the NINCDS-ADRDA Work Group* under the auspices of Department of Health and Human Services Task Force on Alzheimer's Disease. Neurology, 1984, 34(7), 939-939

[14]- *Paraskevaidi M., Morais C., Freitas D. L. D., Gomes de Lima K. M., Mann D. M. A., Allsop D., Martin F. L.* (2018). Blood-based near-infrared spectroscopy for the rapid low-cost detection of Alzheimer's disease. The Analyst

[15]- *World Health Organisation*, Dementia, http://www.who.int/news-room/fact-sheets/detail/dementia, last visited 28/09/2018

[16]- *Qiu C, Kivipelto M, von Strauss E.* Epidemiology of Alzheimer's disease: occurrence, determinants, and strategies toward intervention. *Dialogues in Clinical Neuroscience*. 2009;11(2):111-128.

[17]- *Rupert McShane, Delia Bishara, Roy Jones and Jill Mann*, Drug treatments for Alzheimer's disease, The Alzheimer's Society, 2014, Factsheet 407LP, alzheimers.org.uk

[18]- *Claudie Hooper, Richard Killick and Simon Lovestone*, The GSK-3 hypothesis of Alzheimer's disease, Neurochemistry, 2008, 104, 1433-1439

[19]- *Nathan Herrmann, Sarah A. Chau, Ida Kircanski and Krista L. Lancto*, Current and Emerging Drug Treatment Options for Alzheimer's disease A Systematic Review, Drugs 2011, 71, 2031-2065

[20]- *Danysz W., & Parsons C. G.* The NMDA receptor antagonist memantine as a symptomatological and neuroprotective treatment for Alzheimer's disease: preclinical evidence. International journal of geriatric psychiatry, 2003, 18(S1), S23-S32.

[21]- *Michael E Hasselmo*, The role of acetylcholine in learning and memory, Current Opinion in Neurobiology, 2006, 16(6), 710-715

[22]- *Rogers S. L., Doody R. S., Mohs R. C., Friedhoff L. T*. Donepezil improves cognition and global function in Alzheimer disease: a 15-week, double-blind, placebo-controlled study. Archives of Internal Medicine, 1998, 158(9), 1021-1031.

[23]- *Rosler M., Anand R., Cicin-Sain A., Gauthier S., & Agid Y. Dal Bianco P, Stähelin HB, Hartman R, Gharabawi M, on behalf of the B303 Exelon Study Group.*: Efficacy and safety of rivastigmine in patients with Alzheimer's disease: international randomised controlled trial, BMJ, 1999 318, 633-638

[24]- *Raskind M. A., Peskind E. R., Wessel T., Yuan W.*, Galantamine USA-Study Group.. Galantamine in AD A 6-month randomized, placebo-controlled trial with a 6-month extension. Neurology, 2000, 54(12), 2261-2268.

[25]- *E. Rockenstein, M. Mallory, M. Mante, M. Alford, M. Windisch, H. Moessler, E. Masliah*, Effects of Cerebrolysin on amyloid-beta deposition in a transgenic model of Alzheimer's disease, Neural Transmission Supplements, 2002, 62, 327-336

[26]- *I. Veinbergs, M. Mante, M. Mallory, E. Masliah,* Neurotrophic effects of Cerebrolysin in animal models of excitotoxicity, Advances in Dementia Research, 2000, 273-280

[27]- *Edward Rockenstein, Magdalena Torrance, Michael Mante, Anthony Adame, Amy Paulino, John B. Rose, Leslie Crews, Herbert Moessler and Eliezer Masliah*, Cerebrolysin decreases amyloid-beta production by regulating amyloid protein precursor maturation in a transgenic model of Alzheimer's disease, Neuroscience Research, 2006, 83, 1252-1261

[28]- *Kiren Ubhi, Edward Rockenstein, Edith Doppler, Michael Mante, Anthony Adame, Christina Patrick, Margarita Trejo, Leslie Crews, Amy Paulino, Herbert Moessler, Eliezer Masliah*, Acta Neuropatholica, Neurofibrillary and neurodegenerative pathology in APP-transgenic mice injected with AAV2-mutant TAU: neuroprotective effects of Cerebrolysin, 2009, 117, 699-712

[29]- *Xiong H, Wojtowicz JM, Baskys A*, Brain tissue hydrolysate acts on presynaptic adenosine receptors in the rat hippocampus, Can J Physiology and Pharmacology, 1995, 73, 1194-1197

[30]- *Ana Martinez, and Daniel I. Perez*, GSK-3 Inhibitors: A Ray of Hope for the Treatment of Alzheimer's Disease?, Journal of Alzheimer's Disease, 2008, 15, 181–191

[31]- *D. Terwel, D. Muyllaert, I. Dewachter, P. Borghgraef, S. Croes, H. Devijver and F. Van Leuven*, Amyloid Activates GSK-3β to Aggravate Neuronal Tauopathy in Bigenic Mice, The American Journal of Pathology, 2008, 172(3), 786–798

[32]- *Shweta Mandrekar and Gary E. Landreth*, Microglia and Inflammation in Alzheimer's disease, CNS & neurological disorders drug targets, 2010, 9, 156-167

[33] *Sterling and Irwin*, ZINC 15 – Ligand Discovery for Everyone, j. Chem. Inf. Model, 2015, 55(11), 2324-2337

[34] - Kufareva, I., & Abagyan, R. (2008). Type-II kinase inhibitor docking, screening, and profiling using modified structures of active kinase states. Journal of medicinal chemistry, 51(24), 7921-7932.

[35]- *Lefker, M.A. Brodney, S.M. Sakya, B.A. Hay, M.D. Wessel and E.L. Conn*, Pyrimidone compounds as GSK-3 inhibitors, *B.A.* World Intellectual Property Organization, 2008

[36]- *C.W. Lee, K.F. Lau and C.C. Miller*, Glycogen synthase kinase-3 beta mediated tau phosphorylation in cultured cell lines, Neuroreport 2003, 14, 257–260

[37]- *C.J. Phiel, C.A. Wilson, V.M. Lee and P.S. Klein*, GSK-3α regulates production of Alzheimer's disease amyloid-β peptides, Nature, 2003, 423, 435–439

[38]- *T. Terao, H. Nakano, Y. Inoue, T. Okamoto, J. Nakamura and N. Iwata*, Lithium and dementia: a preliminary study, Progress in Neuro-psychopharmacology and Biological Psychiatry 2006, 30, 1125–1128

[39]- *Chemdiv*, GSK3β-Targeted Library, http://www.chemdiv.com/wp-content/uploads/2014/02/GSK3b-Targeted-Library.pdf, last visited 28/09/2018

[40]- *Rana Dajani, Elizabeth Fraser, S.Mark Roe, Neville Young, Valerie Good, Trevor C. Dale, Laurence H. Pearl*, Crystal Structure of Glycogen Synthase Kinase 3β: Structural Basis for Phosphate-Primed Substrate Specificity and Autoinhibition, Cell, 2001, 105, 721–732

[41]- *Wang, Z., Harkins, P.C., Cobb, M.H., and Goldsmith, E.J.*, The structure of the mitogen-activated protein kinase p38 at 2.1 A° resolution, Proc. Natl. Acad. Sci. USA, 1997, 94, 2327–2332.

[42]- *L. Meijer, A. L. Skaltsounis, P. Magiatis et al.*, GSK-3-selective inhibitors derived from Tyrian purple indirubins, Chemistry and Biology, 2003, 10, 1255–1266

[43]- *Ernst ter Haar, Joyce T. Coll, Douglas A. Austen, Hsun-Mei Hsiao, Lora Swenson and Jugnu Jain,* Structure of GSK3β reveals a primed phosphorylation mechanism, Nature Structural Biology, 2001, 8, 593 – 596

[44]- *Rana Dajani1, Elizabeth Fraser, S.Mark Roe1, Maggie Yeo, Valerie M.Good1, Vivienne Thompson, Trevor C.Dale2 and Laurence H.Pearl*, Structural basis for recruitment of glycogen synthase kinase 3b to the axin-APC scaffold complex, The EMBO Journal, 2003, 22, 494-501

[45]- *J. A. Bertrand, S. Thieffine, A. Vulpetti, C. Cristiani, B. Valsasina, S. Knapp, H. M. Kalisz and M. Flocco,* Structural Characterization of the GSK-3b Active Site Using Selective and Non-selective ATP-mimetic Inhibitors, J. Mol. Biol., 2003, 333, 393–407

[46]- *Mukesh K. Pandey, Timothy R. DeGrado*, Glycogen Synthase Kinase-3 (GSK-3)-Targeted Therapy and Imaging, heranostics, 2016, 6, 571-593

[47]- *Thomas Kramer, Boris Schmidt, and Fabio Lo Monte*, Small-Molecule Inhibitors of GSK-3: Structural Insights and Their Application to Alzheimer's Disease Models International Journal of Alzheimer's Disease, 2012, Article ID 381029, 32,

[48*]- Roskoski Jr, R.*. Classification of small molecule protein kinase inhibitors based upon the structures of their drug-enzyme complexes. Pharmacological research, 2016, 103, 26-48.

[49]- *Minhajul Arfeen and Prasad V. Bharatam*, Design of Glycogen Synthase Kinase-3 Inhibitors: An Overview on Recent Advancements, Current Pharmaceutical Design, 2013, 19, 4755-4775

[50]- *Omura S, Iwai Y, Hirano A, Nakagawa A, Awaya J, Tsuchya H, Takahashi Y, Masuma R*, A new alkaloid AM-2282 OF Streptomyces origin. Taxonomy, fermentation, isolation and preliminary characterization, The Journal of Antibiotics 1977, 30(4), 275-282

[51]- *S. Leclerc, M. Garnier, R. Hoessel et al*, Indirubins inhibit glycogen synthase kinase-β and CDK5/P25, two protein kinases involved in abnormal tau phosphorylation in Alzheimer's disease. A property common to most cyclin-dependent kinase inhibitors?, The Journal of Biological Chemistry, 2001, 276, 1, pp. 251–260

[52]- *Leost M, Schultz C, Link A, Wu Y Z, Biernat J, Mandelkow E M, Bibb J A, Snyder G L, Greengard P, Zaharevitz D W, Gussio R, Senderowicz A M, Sausville E A, Kunick C and Meijer L*, Paullones are potent inhibitors of glycogen synthase kinase-3β and cyclin-dependent kinase 5/p25. European Journal of Biochemistry, 2000, 267, 5983–5994.

[53]- *M. Leost, C. Schultz, A. Link et al.*, Paullones are potent inhibitors of glycogen synthase kinase-β and cyclin-dependent kinase 5/p25, European Journal of Biochemistry, 2000, 267, 5983–5994

[54]- *M. Saitoh, J. Kunitomo, E. Kimura et al.*, "Design, synthesis and structure-activity relationships of 1,3,4-oxadiazole derivatives as novel inhibitors of glycogen synthase kinase-β," Bioorganic and Medicinal Chemistry, 2009, 17(5), 2017–2029,

[55]- *R. Roskoski Jr.,* A historical overview of protein kinases and their targetedsmall molecule inhibitors, Pharmacol. Res. 100 (2015) 1–23.

[56]- *Grütter, Christian, et al.* "Targeting GSK3 from Ustilago maydis: type-II kinase inhibitors as potential antifungals." *ACS chemical biology* 7.7 (2012): 1257-1267.

[57]- *World Health Organisation*, Safety Study of a Glycogen Synthase Kinase 3 (GSK3) Inhibitor in Patients With Alzheimer´s Disease, http://apps.who.int/trialsearch/Trial2.aspx?TrialID=NCT00948259, last visited 28/09/2018

[58]- *ClinicalTrials.gov,* Safety Study of a Glycogen Synthase Kinase 3 (GSK3) Inhibitor in Patients With Alzheimer´s Disease, https://clinicaltrials.gov/ct2/show/record/NCT00948259, last visited 28/09/2018

[59]- *Georgievska Biljana, Sandin Johan, Doherty James, Mörtberg Anette, Neelissen Jan, Andersson Anita, Gruber Susanne, Nilsson Yvonne, Schött Pär, Arvidsson Per I., Hellberg Sven, Osswald Gunilla, Berg Stefan, Fälting Johanna, Bhat Ratan V.*, AZD1080, a novel GSK3 inhibitor, rescues synaptic plasticity deficits in rodent brain and exhibits peripheral target engagement in humans, J. Neurochem., 2013, 125, 446–456

[60]- *Adis Insight*, Discontinued - Phase-I for Alzheimer's disease in United Kingdom, URL- http://adisinsight.springer.com/drugs/800021264, last visited 28/09/2018

[61]- *A. Martinez, M. Alonso, A. Castro, C. Perez and F.J. Moreno*, First non-ATP competitive glycogen synthase-3 (GSK-3β) inhibitors: thiadiazolidinones (TDZD) as potential drugs for the treatment of Alzheimer disease, J Medicinal Chemistry, 2002, 45, 1292–1299

[62] - *del Ser T, Steinwachs KC, Gertz HJ, Andrés MV, Gómez-Carrillo B, Medina M, Vericat JA, Redondo P, Fleet D, León, T* Treatment of Alzheimer's disease with the GSK-3 inhibitor tideglusib: a pilot study, J Alzheimers Dis, 2013, 33, 205-215

[63]- *Sigma-Aldrich*, TDZD-8, http://www.sigmaaldrich.com/catalog/product/sigma/t8325?lang=en&region=GB, last visited 09/28/2018

[64]- *Medchem Express*, Tidesglub, https://www.medchemexpress.com/tideglusib.html, Last Visited 28/09/2018

[65]- *MPBio*, Lithium Carbonate, URL- http://www.mpbio.com/product.php?pid=02152537&country=, last visited 28/09/2018

[66]- *Medchem Express*, AZD1080, URL- https://www.medchemexpress.com/AZD1080.html, last visited 28/09/2018

[67]- *ClinicalTrials.gov*, Evaluation of Lithium as a Glycogen-Synthase-Kinase-3 (GSK-3) Inhibitor in Mild Cognitive Impairment, URL- https://clinicaltrials.gov/ct2/show/record/NCT02601859, last visited 28/09/2018

[68]- *Chemdiv*, GSK3β-Targeted Library, URL- http://www.chemdiv.com/portfolio/gsk3%CE%B2-targeted-library/, last visited 28/09/2018

[69]- *Lovestone S, Boada M, Dubois B, Hüll M, Rinne JO, Huppertz HJ, Calero M, Andrés MV, Gómez-Carrillo B, León T, del Ser T; ARGO investigators*, A phase II trial of tideglusib in Alzheimer's disease, J Alzheimers Dis., 2015, 45, 75-88

[70]- *Akansha Saxena, Diana Wong, Karthikeyan Diraviyam*, and David Sept, The Basic Concepts of Molecular Modeling, Methods in Enzymology, 2009, 467, 307-334

[71]- *Gramatica, P*, Principles of QSAR models validation: internal and external, QSAR Comb. Sci., 2007, 26, 694–701

[72]- *Doerksen et al*, Pharmacophore Modeling, Ensemble Docking, Virtual Screening, and Biological Evaluation on Glycogen Synthase Kinase-3β., Molecular Informatics, 2014, 33(9), 610-626.

[73]- *RSCB Protein Data Bank*, http://www.rcsb.org/pdb/home/home.do, last visited 28/09/2018

[74]- *M.J.L Schoonman, R.M.A Knegtel, P.D.J Grootenhuis,* Practical evaluation of comparative modelling and threading methods, Computers & Chemistry, 1998, 22(5), 369–375

[75]- *A. Filipponi, A. Di Cicco, T.A. Tyson, R. Natoli*, "Ab-initio" modelling of x-ray absorption spectra, Solid State Communications, 1991, 78(4), 265-268

[76]- *OF Guner*, Pharmacophore perception, development, and use in drug design, International University Line, La Jolla, CA, 2000

[77]- *Gramatica, P*, Principles of QSAR models validation: internal and external, QSAR Comb. Sci., 2007, 26, 694–701

[78]- *Hansch C*, Structure Activity Relationship of mutagenic Aromatic and Heteroaromatic Nitro-Compounds – Correlation with Molecular-Orbital Energies and Hydrophobicity, Journal Of Medicinal Chemistry, 1991, 34(2), 786-797, DOI: 10.1021/jm00106a046

[79]- *Andrew R. Leach, Brian K. Shoichet, Catherine E. Peishoff,* Prediction of Protein−Ligand Interactions. Docking and Scoring: Successes and Gaps, Journal of Medicinal Chemistry 2006 49 (20), 5851-5855 DOI: 10.1021/jm060999m

[80]- *Berry, Michael, Burtram Fielding, and Junaid Gamieldien*, Practical considerations in virtual screening and molecular docking, Emerging Trends in Computational Biology, Bioinformatics, and Systems Biology; Tran, QN, Hamid, AR, Eds, 2015, 487-502.

[81]- *Tewari, P.C., Khanduja, R. & Gupta*, M., Performance enhancement for crystallization unit of a sugar plant using genetic algorithm technique, J Ind Eng Int, 2012, 8(1)

[82]- *G. Jones, P. Willett, R. C. Glen, A. R. Leach and R. Taylor*, Development and Validation of a Genetic Algorithm for Flexible Docking, J. Mol. Biol., 267, 727-748, 1997

[83]- **Schrödinger Release 2017-1:** Glide, Schrödinger, LLC, New York, NY, 2017.

[84]- **Schrödinger Release 2017-1**: Maestro, Schrödinger, LLC, New York, NY, 2017

[85]- *Friesner, R. A.; Banks, J. L.; Murphy, R. B.; Halgren, T. A.; Klicic, J. J.; Mainz, D. T.; Repasky, M. P.; Knoll, E. H.; Shaw, D. E.; Shelley, M.; Perry, J. K.; Francis, P.; Shenkin, P. S.,* Glide: A New Approach for Rapid, Accurate Docking and Scoring. 1. Method and Assessment of Docking Accuracy, J. Med. Chem., 2004, 47, 1739–1749

[86]- *Joseph-McCarthy, Diane, et al,* Lead optimization via high-throughput molecular docking, Current opinion in drug discovery & development, 2007, 10(3), 264-274.

[87]- *Böhm, Hans-Joachim,* The development of a simple empirical scoring function to estimate the binding constant for a protein-ligand complex of known three-dimensional structure, Journal of computer-aided molecular design, 1994, 8(3), 243-256

[88]- *M.P.Allen and DJ Tildesly*, Computer Simulation of Liquids, Clarendon press, Oxford, 1987

[89]- *Van Gunsteren WF, Berendsen HJ*. A leap-frog algorithm for stochastic dynamics. Molecular Simulation, 1988, 1(3):173-85.

[90]- *Arfeen, M., Patel, R., Khan, T., & Bharatam, P. V.*, Molecular dynamics simulation studies of GSK-3β ATP competitive inhibitors: understanding the factors contributing to selectivity. Journal of Biomolecular Structure and Dynamics, 2015, 33(12), 2578-2593

[91]- *G. Jones, P. Willett, R. C. Glen, A. R. Leach and R. Taylor,* Development and Validation of a Genetic Algorithm for Flexible Docking, J. Mol. Biol., 267, 727-748, 199

[92]- *O. Trott, A. J. Olson*, AutoDock Vina: improving the speed and accuracy of docking with a new scoring function, efficient optimization and multithreading, Journal of Computational Chemistry 31 (2010) 455-461

[93]- *Bento A.P et.al*. The ChEMBL bioactivity database: An update. *Nucleic Acids Research*. 2014;42:1083-1090.

[94]- *Raees Ahmed*, Final Year Project, Submitted to the University of Central Lancashire

[95]- **Schrödinger Release 2017-1**: LigPrep, Schrödinger, LLC, New York, NY, 2017

[96]- *Schrödinger*. What is the OPLS3 force field?.
https://www.schrodinger.com/kb/1929, last visited 28/09/18

[97]- *Duan J, Dixon S.L, Lowrie J.F & Sherman W*. Analysis and comparison of 2D fingerprints: Insights into database screening performance using eight fingerprint methods. *Journal of Molecular Graphics and Modelling*. 2010;29(2):157-170.

[98]- *Mysinger M.M, Carchia M, Irwin J.J & Shoichet B.K*. Directory of useful decoys, enhanced (DUD-E): Better ligands and decoys for better benchmarking.. Journal of Medicinal Chemistry. 2012;55(14):6582-6594.

[99]- *Graves A.P, Brenk R & Shoichet B.K*. Decoys for docking. Journal of Medicinal Chemistry. 2005;48(11):3714-3728.

[100]- *Matthew Davies*, Final Year Project, Submitted to the University of Central Lancashire

[101]- **Schrödinger Release 2017-1**: Canvas, Schrödinger, LLC, New York, NY, 2017

[102]- **Schrödinger Release 2017-1**: MacroModel, Schrödinger, LLC, New York, NY, 2017

[103]- **Schrödinger Release 2017-1**: QikProp, Schrödinger, LLC, New York, NY, 2017

[104]- *Lipinski CA*, Drug-like properties and the causes of poor solubility and poor permeability, J Pharmacol Toxicol Methods, 2000, 44(1), 235-49

[105]- *Ghose, Arup K., et al*, Knowledge-based, central nervous system (CNS) lead selection and lead optimization for CNS drug discovery." ACS chemical neuroscience 3.1 (2011): 50-68.

[106]- *Veber DF, Johnson SR, Cheng HY, Smith BR, Ward KW, Kopple KD*, Molecular properties that influence the oral bioavailability of drug candidates, J Med Chem, 2002, 45(12), 2615-23

[107]- *Kitchen, D.B., Decornez, H., Furr, J.R. and Bajorath, J.*, Docking and scoring in virtual screening for drug discovery: methods and applications. Nature reviews Drug discovery, 2004, 3(11), 935-949.

[108]- *Houston, Douglas R., and Malcolm D. Walkinshaw.*, Consensus docking: improving the reliability of docking in a virtual screening context, Journal of chemical information and modeling, 53.2, 2013, 384-390

[109]- *Truchon, Jean-François, and Christopher I. Bayly*, Evaluating virtual screening methods: good and bad metrics for the "early recognition" problem, Journal of chemical information and modelling, 2007, 47(2), 488-508.

[110*]- Harder E, Damm, W. Maple, J. Wu, C. Reboul, M. Xiang, J.Y. Wang, L.; Lupyan, D.; Dahlgren, M.K.; Knight, J.L.; Kaus, J.W.; Cerutti, D.S.; Krilov, G.; Jorgensen, W.L.; Abel, R.; Friesner, R.A.*, "OPLS3: A Force Field Providing Broad Coverage of Drug-like Small Molecules and Proteins," J. Chem. Theory Comput., 2015, DOI: 10.1021/acs.jctc.5b00864

[111]- **Schrödinger Release 2018-3**: Phase, Schrödinger, LLC, New York, NY, 2018

[112]- *Liu Y., Gray N. S.*. Rational design of inhibitors that bind to inactive kinase conformations. *Nat Chem Biol,* 2006 2, 358-364

[113]- **Schrödinger Release 2018-3**: Schrödinger Suite 2018-3 Protein Preparation Wizard; Epik, Schrödinger, LLC, New York, NY, 2016; Impact, Schrödinger, LLC, New York, NY, 2016; Prime, Schrödinger, LLC, New York, NY, 2018.

[114]- **Schrödinger Release 2018-3**: Prime, Schrödinger, LLC, New York, NY, 2018

[115]- **Schrödinger Release 2018-3**: Desmond Molecular Dynamics System, D. E. Shaw Research, New York, NY, 2018. Maestro-Desmond Interoperability Tools, Schrödinger, New York, NY, 2018

Appendix

S1: List of Commands used

Ubuntu terminal commands in this project:

-Removal of the additional sections Goldmine adds to the names of the actives

:%s/(phrase)/(newphrase)/g

-Running of ZINC tranche download files

Chmod u+x (filename)

-Then to run the executable:

./(filename)

-Moving all of the SMILES patterns downloaded from ZINC into one file:

cat input>output

-Removing unwanted lines from the SMILES pattern files before random selection:

find . –type f –print0 |xargs -0 sed –I /zinc-id/d

-Selecting 500,000 random lines from the newly combined file:

shuf –n 500,000 input>output

-Trimming the length of the Molecular dynamics trajectory:

$SCHRODINGER/run –FROM desmond manipulate_trj.py (original trajectory .cms file) (new filename) "output- directory-name"

Excel formulae used in this project:

Simple sum:

=A2+B2+C2+D2

The exclusion of the worst rank:

=MAX(range,cell)

The calculation of the Deprecated sum rank:

=E2-F2

S2: Data produced by the consensus scouring process for the type I and type II studies

Table S.1: The Consensus ranks and other values generated for the top 200 compounds from the type I virtual screening

Title	Consensus Rank	SP Rank	XP Rank	ASP Rank	Vina Rank	MW	3Pt	4Pt	5Pt
ZINC000450524273	198	1095	308	15094	1442	321.424	1	0	0
ZINC000071967954	94	574	4766	6278	628	340.381	1	0	0
ZINC000096131333	50	5033	1777	1098	1172	341.455	1	0	0
ZINC000289288811	31	656	2180	2238	2449	369.398	0	0	0
ZINC000020892148	197	2375	12221	2732	598	387.858	1	1	0
ZINC000072152229	24	94	1557	926	3992	310.401	1	0	0
ZINC000262476404	122	37	397	8220	5804	314.389	1	0	0
ZINC000288905010	77	40	292	604	10249	325.293	1	0	0
ZINC000294563530	180	161	6062	8455	2471	328.385	0	1	0
ZINC000278292143	40	31	1042	5593	1767	343.403	0	0	0
ZINC000452372528	171	2197	608	9017	5052	305.275	0	0	0
ZINC000057813806	74	483	3697	2922	3959	320.393	1	0	0
ZINC000125990757	108	4538	1254	5639	2207	321.378	0	0	0
ZINC000281451553	156	2524	8990	2267	2409	327.281	1	0	0
ZINC000272945127	195	615	14990	514	1756	331.324	0	0	0
ZINC000123763813	83	3145	440	7835	182	332.404	0	0	0
ZINC000065164461	200	11976	3054	2316	827	339.344	0	1	0
ZINC000339309810	76	1484	9217	449	14	340.329	0	0	0
ZINC000370567443	105	447	4242	6906	1924	341.308	1	1	0
ZINC000262042192	181	10481	2209	3593	921	347.419	0	0	0
ZINC000186647315	127	275	819	3811	9713	359.445	1	0	0
ZINC000030030588	177	887	1839	13895	441	360.458	1	1	0
ZINC000268128830	125	722	7717	4785	1258	281.316	1	0	0
ZINC000199720928	66	63	592	8695	911	307.247	0	1	0
ZINC000127453735	75	905	1022	5068	4113	310.373	1	1	0
ZINC000373427455	175	262	3206	11557	1934	312.368	0	0	0
ZINC000185165653	79	69	1244	9942	186	324.382	0	0	0
ZINC000028406051	92	80	173	7889	3918	327.816	1	1	0
ZINC000171617571	147	4676	5844	4959	263	330.388	0	0	0
ZINC000155200372	16	270	925	3248	1196	336.436	1	1	0
ZINC000459356124	22	1794	2617	1024	745	338.384	0	0	0
ZINC000337570093	85	555	2141	2899	6184	340.424	1	0	0
ZINC000093642388	54	482	4458	1365	2968	356.424	1	0	0
ZINC000020540831	1	2	24	38	159	375.396	1	0	0
ZINC000189195311	98	758	2601	7866	1692	395.547	1	0	0
ZINC000292555245	118	3945	1826	3664	4561	296.295	1	0	0
ZINC000333894224	196	1970	7882	1913	6158	309.413	1	0	0
ZINC000330030716	113	1513	405	10866	962	312.414	1	0	0
ZINC000369213404	49	1295	1472	1292	4880	313.297	0	0	0
ZINC000059228950	97	2279	6673	2158	1565	314.343	0	0	0
ZINC000284431465	158	1946	6758	5071	2424	324.425	0	0	0

ZINC000459377677	51	1731	417	4247	2728	325.41	1	0	0
ZINC000338569359	26	560	2656	1612	1851	335.38	0	0	0
ZINC000423021568	131	1387	1157	10484	1962	336.433	0	0	0
ZINC000328691701	111	243	3327	4001	6113	337.427	1	1	0
ZINC000095965527	130	2425	3017	2338	7087	341.35	0	0	0
ZINC000340416229	179	8478	728	4411	3463	344.36	1	0	0
ZINC000368168772	95	2674	7932	1555	286	344.415	0	0	0
ZINC000183269073	73	1207	218	8642	899	345.416	1	0	0
ZINC000023126377	172	4728	5670	5887	605	346.446	0	0	0
ZINC000330176611	104	3074	2311	3474	4625	347.324	0	0	0
ZINC000248069775	164	2611	844	11352	1717	349.388	1	1	0
ZINC000331884986	14	103	1078	2418	1833	364.394	1	0	0
ZINC000008249063	18	3899	1112	782	51	406.501	1	1	0
ZINC000294625147	152	5	640	5131	10314	292.285	1	1	0
ZINC000285351235	65	433	3374	3818	2432	309.41	1	0	0
ZINC000372806516	21	87	34	3241	2633	324.382	1	1	0
ZINC000580212021	58	215	44	4191	5151	325.413	1	0	0
ZINC000332282303	47	2519	2584	1271	2500	334.368	1	1	0
ZINC000125697807	144	104	147	11113	4108	344.431	0	0	0
ZINC000067679223	2	138	794	31	624	356.429	0	0	0
ZINC000159432235	20	68	50	282	5542	364.403	0	0	0
ZINC000263619162	80	7016	1538	2978	46	366.849	1	1	0
ZINC000067820131	6	287	463	1714	252	379.504	1	1	0
ZINC000364094692	112	4054	1551	1745	6376	296.295	0	0	0
ZINC000288214615	12	418	651	1538	2446	324.425	0	0	0
ZINC000279014268	93	4622	464	3880	3279	324.425	1	1	0
ZINC000261732557	185	3056	2097	7936	4335	326.397	1	0	0
ZINC000362869142	199	471	3492	12661	1372	328.37	1	0	0
ZINC000286076105	37	1154	1365	1162	4520	328.413	0	0	0
ZINC000343735908	101	408	772	1508	10617	329.33	1	1	0
ZINC000092013697	110	2806	410	3373	7067	333.362	1	0	0
ZINC000052856983	141	876	1158	9373	3946	335.405	0	0	0
ZINC000301167184	148	3332	4318	4734	3381	337.467	0	0	0
ZINC000370730930	71	250	512	1333	8494	339.371	1	1	0
ZINC000368382090	38	665	1971	813	4871	339.399	1	0	1
ZINC000072322171	35	2332	322	2196	2934	339.436	0	0	0
ZINC000264929496	170	10501	1400	564	4358	344.723	1	0	0
ZINC000372407284	25	48	192	5988	398	348.447	0	1	0
ZINC000020024316	23	178	1212	2181	2841	350.367	0	0	0
ZINC000009461191	78	1221	1922	5487	2800	351.346	1	1	0
ZINC000179744911	17	1169	64	306	4203	351.407	0	0	0
ZINC000071753872	129	492	7297	1509	5354	352.356	1	1	0
ZINC000271290060	114	44	615	3126	10004	355.457	0	0	0
ZINC000290893683	86	295	2460	3029	6035	355.826	1	1	0
ZINC000377434377	159	151	800	12677	2652	358.439	1	0	0
ZINC000270370414	90	5057	629	3131	3219	358.87	0	0	0
ZINC000377586544	166	1829	6018	5125	3647	368.435	1	1	0

ZINC000292820293	70	2710	1020	798	6054	371.402	0	0	0
ZINC000091894386	9	127	25	146	2963	371.413	1	0	0
ZINC000046053995	67	1419	210	7120	1557	375.485	1	0	0
ZINC000019497338	162	4918	1055	8873	1526	382.505	1	0	0
ZINC000263617294	3	1138	427	21	95	388.803	1	1	0
ZINC000019574126	167	8906	1636	848	5248	400.541	0	1	0
ZINC000072393713	4	493	446	748	88	406.502	0	0	0
ZINC000002738092	143	6271	8975	32	147	463.474	1	1	0
ZINC000071315326	184	584	3715	1390	11647	301.434	0	0	0
ZINC000257265440	39	22	4893	251	3188	334.423	1	1	0
ZINC000355536096	7	1050	649	142	990	347.419	1	1	0
ZINC000097505396	42	2068	1620	2705	2179	356.424	1	1	1
ZINC000273149682	89	4308	3641	2281	1757	357.411	1	0	0
ZINC000048367002	102	4880	1353	4962	2115	307.394	1	1	0
ZINC000237440882	53	628	3353	1009	4281	308.385	1	1	0
ZINC000272590346	87	927	5376	2342	3237	312.414	0	0	0
ZINC000255369784	57	932	1671	3755	3185	322.406	1	0	0
ZINC000122196365	163	2463	46	2109	11860	323.397	1	0	0
ZINC000559958970	136	1350	376	6699	6749	328.337	1	0	0
ZINC000422946798	124	516	364	2429	11171	330.404	1	1	0
ZINC000343859200	192	6353	4855	4703	1871	331.364	1	0	0
ZINC000451290903	139	382	5633	4249	5048	331.389	1	0	0
ZINC000436385819	45	3806	3066	789	1034	332.447	1	0	0
ZINC000026875067	88	1074	5035	542	5281	337.383	0	0	0
ZINC000527996390	194	5782	388	6592	5109	338.405	1	1	0
ZINC000487549914	64	779	3576	605	5084	339.36	1	0	0
ZINC000122153639	30	2278	1003	1092	3014	343.4	1	0	0
ZINC000332477740	193	3397	5453	5553	3411	344.416	1	0	0
ZINC000420187294	160	414	2185	12332	1417	346.379	1	0	0
ZINC000216621950	82	783	4169	4338	2301	346.431	0	0	0
ZINC000337214634	120	314	611	120	13297	347.419	1	1	0
ZINC000354749349	63	1511	2634	4462	1361	348.831	1	0	0
ZINC000281583613	140	3815	4449	6876	192	350.34	1	0	0
ZINC000275642118	48	2039	950	2670	3258	350.422	1	1	0
ZINC000091165972	174	1321	92	10150	5392	350.823	1	1	0
ZINC000270976355	72	2022	190	2827	5847	357.408	1	0	0
ZINC000064758501	84	565	4001	237	6973	364.449	1	0	0
ZINC000270482066	8	234	76	1463	1263	367.493	0	0	0
ZINC000261665889	96	1360	638	6169	4333	371.478	0	0	0
ZINC000020292321	69	1200	1293	1185	6882	375.445	0	0	0
ZINC000095378901	149	2097	13456	88	181	378.47	1	0	0
ZINC000095500815	10	264	600	1699	853	385.465	0	0	0
ZINC000020115971	56	2888	3091	630	2842	399.507	1	1	0
ZINC000072359421	128	10313	3062	113	1144	413.924	1	1	0
ZINC000358060689	61	206	1427	3326	4804	330.386	1	0	1
ZINC000072469924	44	1239	1823	1573	4005	379.504	0	0	0
ZINC000067714443	123	12487	1387	141	453	381.409	1	1	0

ZINC000344434637	46	2060	1831	1350	3481	326.37	1	1	0
ZINC000370688320	132	285	2108	1685	10961	327.816	1	1	0
ZINC000238074825	168	4791	4102	4612	3171	334.42	1	0	0
ZINC000188429278	146	3144	5938	873	5679	340.424	1	1	0
ZINC000292435054	119	1220	2024	2962	7948	341.409	1	0	0
ZINC000275492132	191	233	434	1119	15994	343.403	1	1	0
ZINC000036753814	126	960	387	10342	2881	343.425	1	0	0
ZINC000423993887	169	5965	5651	3138	1967	347.847	0	0	0
ZINC000492277385	100	7260	1723	545	3772	348.407	1	0	0
ZINC000179629498	34	195	150	4278	3093	348.447	0	0	0
ZINC000191806771	68	4859	3014	1931	662	348.447	0	0	0
ZINC000040118557	176	246	2257	2942	11585	355.479	0	0	0
ZINC000095372670	109	735	433	5395	7079	356.467	1	1	0
ZINC000361218831	91	1549	855	7056	2583	360.498	1	0	0
ZINC000275119766	117	1816	6641	1112	4417	370.328	1	0	0
ZINC000103449421	161	6160	2511	3621	4059	370.45	1	0	0
ZINC000068202913	52	996	1228	3061	3983	374.482	0	0	0
ZINC000065531780	121	4745	8796	48	830	391.429	1	0	1
ZINC000055254089	99	4748	3979	252	3952	395.442	0	0	0
ZINC000072372430	116	2328	9133	917	1585	397.559	1	0	0
ZINC000095356616	15	562	234	2556	2167	398.504	1	0	0
ZINC000013692664	41	4863	3484	128	36	400.433	0	0	0
ZINC000020519057	29	2153	2107	230	2847	411.503	1	0	1
ZINC000023844492	133	11854	749	401	2083	432.521	1	0	0
ZINC000023560369	103	2291	9900	663	606	452.527	1	0	0
ZINC000041585043	28	5476	938	598	59	461.492	1	1	0
ZINC000013626739	36	5955	1653	172	107	464.492	1	0	1
ZINC000024767799	81	9171	1602	471	334	471.353	1	0	0
ZINC000340524328	13	1037	538	378	3464	330.336	1	0	1
ZINC000187804366	11	2018	175	717	901	370.407	1	1	0
ZINC000431476232	155	936	4773	1739	8736	310.37	1	1	0
ZINC000275640860	107	591	114	7028	5894	321.421	1	1	0
ZINC000289852136	187	1606	8959	2352	4545	322.409	1	0	0
ZINC000123797419	190	2215	2036	1611	11866	330.404	1	1	0
ZINC000414381194	178	2790	1175	1998	11101	339.415	1	0	0
ZINC000134272869	60	642	347	4628	4124	340.467	1	1	0
ZINC000013998761	165	626	273	4134	11514	342.824	1	1	0
ZINC000190622496	106	3536	3861	1921	4245	343.4	1	0	0
ZINC000421188100	134	2575	10300	816	1421	343.4	1	1	0
ZINC000152216644	154	2220	14	4481	9461	344.431	1	0	0
ZINC000364190188	151	8464	2650	72	4836	346.434	1	0	0
ZINC000023989544	55	2460	1683	3657	1539	363.458	1	1	0
ZINC000246977920	43	3015	790	521	4305	372.466	1	1	0
ZINC000013596742	5	836	698	419	315	373.497	0	0	0
ZINC000044443334	145	5912	5126	578	3936	380.464	1	0	0
ZINC000020235952	182	7601	9600	29	81	389.496	1	0	0
ZINC000027365919	189	3606	13475	14	608	391.518	0	0	0

ZINC000072371357	137	7839	275	71	7010	410.438	1	1	0
ZINC000015734989	33	686	3727	1654	1523	448.572	1	0	0
ZINC000016393552	115	7283	398	1043	5236	461.021	0	0	0
ZINC000032903749	153	9853	6038	123	119	462.547	1	1	1
ZINC000189024853	59	1713	52	6967	904	322.406	1	1	0
ZINC000279814647	32	237	933	3132	3283	349.475	1	0	0
ZINC000014971305	157	325	669	3687	11516	339.393	1	0	0
ZINC000097568925	62	43	30	436	9311	353.463	0	0	0
ZINC000363085131	188	2849	55	3730	10853	372.509	1	0	0
ZINC000012718228	186	9367	1877	997	5218	382.505	1	0	1
ZINC000011911811	173	10307	4557	51	2032	441.959	0	0	0
ZINC000019793351	19	2820	2526	411	116	453.583	0	1	0
ZINC000034681715	150	3717	9283	85	2876	466.966	1	1	0
ZINC000014532622	183	13359	3622	121	228	467.61	1	0	0
ZINC000134487938	135	366	212	2627	11922	336.433	1	1	0
ZINC000019848477	27	2523	776	3421	236	376.497	1	0	0
ZINC000055171898	142	8197	2970	244	3951	377.442	1	1	0
ZINC000012685012	138	11632	3351	49	226	498.58	1	1	0

Table S.2: The top 200 type II compounds, their ranks and scores for each of the two models, and their consensus ranks

Title	DOLPHIN Rank	DOLPHIN gscore	MD Rank	MD gscore	Simple Sum Rank
ZINC000096112051	1	-10.28	2	-11.098	1
ZINC000004200873	2	-9.838	4	-11.017	2
ZINC000096112254	6	-9.588	10	-10.703	3
ZINC000096112048	13	-9.313	7	-10.794	4
ZINC000096112049	27	-9.007	3	-11.023	5
ZINC000096112349	21	-9.125	14	-10.599	6
ZINC000008299930	17	-9.174	19	-10.487	7
ZINC000096112052	39	-8.888	1	-11.244	8
ZINC000096112343	12	-9.314	34	-10.319	9
ZINC000096112199	24	-9.081	25	-10.435	10
ZINC000004259649	37	-8.906	20	-10.486	11
ZINC000096112247	56	-8.808	15	-10.598	12
ZINC000096112042	29	-8.971	50	-10.224	13
ZINC000096112276	64	-8.781	24	-10.444	14
ZINC000096112378	9	-9.483	80	-10.064	15
ZINC000096112245	11	-9.347	84	-10.053	16
ZINC000096112255	48	-8.838	51	-10.215	17
ZINC000004899492	57	-8.807	46	-10.244	18
ZINC000004147673	84	-8.679	27	-10.409	19
ZINC000004259418	108	-8.558	9	-10.741	20
ZINC000004259703	80	-8.691	53	-10.204	21
ZINC000004259576	72	-8.736	67	-10.127	22
ZINC000096112324	96	-8.617	49	-10.224	23
ZINC000096112392	26	-9.052	124	-9.908	24
ZINC000096112354	91	-8.646	61	-10.152	25
ZINC000096112383	116	-8.537	48	-10.225	26
ZINC000096112075	90	-8.646	76	-10.072	27
ZINC000096112040	92	-8.644	75	-10.076	28
ZINC000008623925	158	-8.398	16	-10.578	29
ZINC000008297322	181	-8.331	13	-10.605	30
ZINC000096112290	169	-8.365	30	-10.337	31
ZINC000096112074	15	-9.243	197	-9.677	32
ZINC000096112358	135	-8.451	83	-10.053	33
ZINC000003841754	141	-8.436	88	-10.033	34
ZINC000004200863	195	-8.296	40	-10.271	35
ZINC000005415248	234	-8.225	5	-10.958	36
ZINC000096112357	19	-9.165	223	-9.613	37
ZINC000008297285	189	-8.314	55	-10.196	38
ZINC000096112259	236	-8.224	12	-10.649	39
ZINC000004235417	231	-8.226	26	-10.428	40
ZINC000096112291	229	-8.234	31	-10.332	41
ZINC000004222877	205	-8.271	57	-10.174	42
ZINC000096112257	240	-8.214	38	-10.279	43
ZINC000096112517	183	-8.323	96	-10.003	44

ZINC000008254491	283	-8.144	8	-10.763	45
ZINC000096112258	316	-8.08	21	-10.472	46
ZINC000005398917	263	-8.179	77	-10.071	47
ZINC000008623923	254	-8.201	92	-10.017	48
ZINC000020464047	274	-8.158	73	-10.097	49
ZINC000012602805	282	-8.144	89	-10.03	50
ZINC000008635898	288	-8.138	87	-10.048	51
ZINC000096112252	360	-8.013	43	-10.266	52
ZINC000004571260	5	-9.615	413	-9.287	53
ZINC000004235515	370	-8.002	71	-10.112	54
ZINC000004200864	4	-9.623	457	-9.223	55
ZINC000008635710	439	-7.912	42	-10.269	56
ZINC000008623263	418	-7.935	74	-10.079	57
ZINC000008297827	467	-7.865	45	-10.246	58
ZINC000008299947	494	-7.838	18	-10.515	59
ZINC000003842094	481	-7.852	56	-10.182	60
ZINC000004200876	10	-9.377	580	-9.092	61
ZINC000049169096	614	-7.745	11	-10.674	62
ZINC000096112057	642	-7.715	62	-10.15	63
ZINC000096112353	658	-7.701	52	-10.214	64
ZINC000008623031	696	-7.667	58	-10.171	65
ZINC000096112311	689	-7.672	81	-10.064	66
ZINC000096112395	25	-9.074	859	-8.867	67
ZINC000012489972	810	-7.597	79	-10.066	68
ZINC000096112256	30	-8.957	132	-9.869	69
ZINC000096112242	50	-8.824	128	-9.885	70
ZINC000096112038	63	-8.794	118	-9.935	71
ZINC000005396040	76	-8.718	107	-9.972	72
ZINC000096112066	86	-8.655	104	-9.98	73
ZINC000096112047	73	-8.734	126	-9.892	74
ZINC000096112108	55	-8.809	145	-9.803	75
ZINC000096112312	79	-8.699	122	-9.916	76
ZINC000096112109	35	-8.918	169	-9.737	77
ZINC000084711477	61	-8.797	160	-9.757	78
ZINC000096112328	53	-8.815	209	-9.642	79
ZINC000004270569	137	-8.446	134	-9.858	80
ZINC000096112036	89	-8.646	189	-9.687	81
ZINC000096112063	104	-8.584	178	-9.718	82
ZINC000008635535	153	-8.407	141	-9.812	83
ZINC000096112083	174	-8.35	137	-9.844	84
ZINC000020464030	160	-8.397	153	-9.779	85
ZINC000096112237	54	-8.812	260	-9.54	86
ZINC000004147676	33	-8.926	294	-9.479	87
ZINC000096112062	51	-8.822	276	-9.514	88
ZINC000004235603	196	-8.293	138	-9.844	89
ZINC000096112246	93	-8.635	242	-9.564	90
ZINC000096112249	126	-8.499	224	-9.61	91
ZINC000004259578	58	-8.806	299	-9.47	92

ZINC000005434050	245	-8.209	114	-9.952	93
ZINC000030879565	74	-8.728	297	-9.474	94
ZINC000096112028	165	-8.374	218	-9.624	95
ZINC000012529846	185	-8.322	200	-9.656	96
ZINC000008300469	204	-8.274	185	-9.697	97
ZINC000096112283	175	-8.35	216	-9.629	98
ZINC000096112250	246	-8.208	147	-9.792	99
ZINC000096112372	275	-8.156	130	-9.882	100
ZINC000030879845	40	-8.883	371	-9.349	101
ZINC000096112078	237	-8.222	181	-9.708	102
ZINC000096112235	154	-8.407	270	-9.523	103
ZINC000004259582	161	-8.393	265	-9.529	104
ZINC000096112270	151	-8.411	278	-9.511	105
ZINC000096112054	34	-8.925	401	-9.31	106
ZINC000096112070	82	-8.683	355	-9.372	107
ZINC000096112337	217	-8.258	228	-9.607	108
ZINC000096112273	321	-8.075	125	-9.905	109
ZINC000096112295	281	-8.145	167	-9.745	110
ZINC000096112064	81	-8.691	382	-9.339	111
ZINC000004222811	348	-8.031	116	-9.937	112
ZINC000096112177	356	-8.016	112	-9.957	113
ZINC000004259272	99	-8.609	373	-9.347	114
ZINC000096112213	168	-8.366	309	-9.455	115
ZINC000004259381	371	-8.002	109	-9.968	116
ZINC000015673884	324	-8.07	157	-9.763	117
ZINC000014779351	111	-8.55	372	-9.348	118
ZINC000096112216	45	-8.852	441	-9.247	119
ZINC000030879550	69	-8.757	419	-9.277	120
ZINC000096112387	382	-7.986	111	-9.961	121
ZINC000096269383	59	-8.802	438	-9.25	122
ZINC000096112065	46	-8.848	455	-9.224	123
ZINC000096112297	159	-8.398	343	-9.391	124
ZINC000096112390	105	-8.583	405	-9.306	125
ZINC000014610053	103	-8.592	416	-9.284	126
ZINC000096112035	87	-8.65	435	-9.256	127
ZINC000004259111	372	-8	152	-9.781	128
ZINC000225407026	390	-7.968	148	-9.789	129
ZINC000096112381	252	-8.204	311	-9.449	130
ZINC000005433653	420	-7.931	150	-9.785	131
ZINC000005399735	314	-8.092	263	-9.535	132
ZINC000096112356	415	-7.937	164	-9.755	133
ZINC000004259117	331	-8.06	258	-9.545	134
ZINC000096112236	261	-8.183	331	-9.408	135
ZINC000096112110	52	-8.82	547	-9.134	136
ZINC000096112072	67	-8.761	535	-9.14	137
ZINC000008300038	289	-8.138	316	-9.443	138
ZINC000096112039	230	-8.23	376	-9.347	139
ZINC000096112056	225	-8.245	391	-9.324	140

ZINC000003842061	187	-8.315	436	-9.254	141
ZINC000008300622	408	-7.943	220	-9.618	142
ZINC000096112319	248	-8.206	384	-9.339	143
ZINC000012376462	479	-7.853	154	-9.777	144
ZINC000004235426	384	-7.981	252	-9.551	145
ZINC000096112344	339	-8.049	304	-9.466	146
ZINC000014651078	399	-7.96	248	-9.554	147
ZINC000001095821	62	-8.795	589	-9.086	148
ZINC000004235821	387	-7.974	269	-9.524	149
ZINC000006017925	115	-8.542	542	-9.136	150
ZINC000096112221	247	-8.208	410	-9.293	151
ZINC000096112239	346	-8.034	315	-9.444	152
ZINC000096112300	83	-8.682	582	-9.09	153
ZINC000096112298	163	-8.381	503	-9.182	154
ZINC000014779271	107	-8.558	561	-9.116	155
ZINC000096112107	94	-8.633	575	-9.097	156
ZINC000096112389	249	-8.206	425	-9.272	157
ZINC000096112377	394	-7.965	281	-9.509	158
ZINC000001588038	256	-8.197	424	-9.273	159
ZINC000096112329	510	-7.826	174	-9.722	160
ZINC000004222862	504	-7.831	184	-9.7	161
ZINC000008635858	556	-7.791	136	-9.854	162
ZINC000005412197	350	-8.024	359	-9.366	163
ZINC000096112041	120	-8.529	590	-9.086	164
ZINC000096112369	398	-7.96	312	-9.447	165
ZINC000004293351	308	-8.108	404	-9.307	166
ZINC000096112058	486	-7.847	232	-9.591	167
ZINC000096112323	610	-7.747	108	-9.971	168
ZINC000096112371	238	-8.218	489	-9.196	169
ZINC000008299933	359	-8.013	369	-9.353	170
ZINC000096112393	208	-8.27	525	-9.159	171
ZINC000096112069	85	-8.661	653	-9.034	172
ZINC000096112385	307	-8.11	447	-9.238	173
ZINC000004235420	226	-8.242	540	-9.137	174
ZINC000096112374	664	-7.699	102	-9.984	175
ZINC000096112292	511	-7.825	264	-9.53	176
ZINC000096112178	315	-8.083	461	-9.217	177
ZINC000096296996	227	-8.237	553	-9.124	178
ZINC000008635362	468	-7.864	323	-9.422	179
ZINC000096112341	417	-7.935	379	-9.345	180
ZINC000096112026	118	-8.532	680	-9.009	181
ZINC000096112282	285	-8.14	519	-9.165	182
ZINC000012603333	596	-7.76	208	-9.643	183
ZINC000096112332	155	-8.402	651	-9.035	184
ZINC000096112034	150	-8.412	657	-9.027	185
ZINC000096112243	616	-7.744	194	-9.682	186
ZINC000004222865	520	-7.82	293	-9.483	187
ZINC000096112251	77	-8.717	739	-8.955	188

ZINC000030881843	647	-7.711	173	-9.723	189
ZINC000096112315	326	-8.065	500	-9.185	190
ZINC000096112386	342	-8.038	490	-9.195	191
ZINC000008623875	582	-7.767	255	-9.547	192
ZINC000008623222	441	-7.912	398	-9.312	193
ZINC000005410189	720	-7.655	140	-9.822	194
ZINC000015672358	255	-8.2	608	-9.077	195
ZINC000030881268	555	-7.795	328	-9.416	196
ZINC000008635918	681	-7.682	202	-9.654	197
ZINC000096269328	216	-8.259	669	-9.016	198
ZINC000096112229	612	-7.746	273	-9.515	199